

Plate shell structures of glass

Studies leading to guidelines for structural design



Anne Bagger

PhD Thesis

**Department of Civil Engineering
2010**

DTU Civil Engineering Report R-221 (UK)
April 2010

Plate shell structures of glass

Studies leading to guidelines for structural design

Anne Bagger

Ph.D. Thesis

Department of Civil Engineering
Technical University of Denmark

2010

Plate shell structures of glass
Studies leading to guidelines for structural design
Copyright ©, Anne Bagger, 2010
Printed by DTU-Tryk
Department of Civil Engineering
Technical University of Denmark
ISBN: 9788778773005
ISSN: 1601-2917

Preface

This thesis is submitted as a partial fulfilment of the requirements for the Danish Ph.d. degree. The study has taken place at the Department of Civil Engineering at the Technical University of Denmark (DTU Byg), in the period from August 2006 to October 2009. Professor Jeppe Jönsson has been the project's principal supervisor, and associate professor Henrik Almegaard has been co-supervisor, together with professor Kristian Dahl Hertz (from November 2008). All three are affiliated to DTU Byg. Professor Werner Sobek from the Institute for Lightweight Structures and Conceptual Design (ILEK) at Stuttgart University has been external co-supervisor. In the summer 2007, professor Sobek hosted a three month research stay at ILEK, in connection with the study.

The thesis is written as a monograph. A list of relevant papers prepared during the study is included, but this work is not a part of the thesis.

Kgs. Lyngby, October 2009

Anne Bagger

Preface to published version of thesis

The thesis was defended at a public defence on Friday the 9th of April 2010. Official opponents were Professor Henrik Stang, Technical University of Denmark, Dr. Switbert Greiner, Dr.-Ing. Switbert Greiner / ArtEngineering GmbH, and Dr. Mauro Overend, University of Cambridge. Subsequently the Ph.D. degree was awarded from the Technical University of Denmark.

Compared to the original submitted version of the thesis a number of minor editorial corrections have been implemented.

Kgs. Lyngby, April 2010

Anne Bagger

Acknowledgements

First of all, I wish to thank my group of supervisors. This project would not have been realized if not for professor Jeppe Jönsson and associate professor Henrik Almegaard. I am very grateful to Professor Kristian Hertz who has offered invaluable support along the way.

Professor Werner Sobek has been a tremendous inspiration during the project; he has infused my work with a love of the game, and for that I am very grateful. Working at ILEK was an exceptional experience.

I would also like to thank a number of people for their support and contributions to the project. My dear hardworking students, the late Ture Wester, Benedict Verhegghe, Jan Belis, Lucio Blandini, Heiko Trumpf, Gabriela Metzger, Stefan Neuhäuser, Matthias Rippmann, Günther Witek, Ingo Stelzer, Leif Otto Nielsen, John Forbes Olesen, Jens Gravesen, Andreas Bærentzen, Natalie Mossin, Søren Hansen, Jakob Knudsen, Claes Bockhoff, prof. Vamberský, prof. Rots, Andrew Borgart, Pierre Hoogenboom and Nicholas Gurieff.

I wish to thank Lars Ostenfeld Riemann and John Flemming Jensen from Rambøll for their support.

I thank HILTI, 3M, DuPont, DELO, Scanglas, Pilkington, bo-glas and Betech Seals, who have all contributed generously with time, knowhow and products. I also thank the Siemens Foundation, the Oticon Foundation, the Larsen and Nielsen Foundation, Alexandre Haynman and wife Nina Haynman's Foundation and the Otto Mønsted Foundation, who have all contributed to the financing of experiments and my travels abroad.

I also thank the opponents at the defence of this thesis, Dr. Switberg Greiner, Dr. Mauro Overend and Professor Henrik Stang, for their comments and the fruitful discussions that followed.

Last, but not least, I am very grateful for the loving support of my dear family, Lars, Pernille and Annika.

Abstract

This thesis is a study of plate shell structures – a type of shell structure with a piecewise plane geometry, organized so that the load bearing system is constituted by distributed in-plane forces in the facets. The high stiffness-to-weight ratio of smoothly curved shell structures is mainly due to their curved shape. A plate shell structure maintains a high stiffness-to-weight ratio, while facilitating the use of plane structural elements.

The study focuses on using laminated glass panes for the load bearing facets.

Various methods of generating a plate shell geometry are suggested. Together with Ghent University, a script has been developed for an automated generation of a given plate shell geometry and a corresponding finite element (FE) model.

A suitable FE modelling technique is proposed, suggesting a relatively simple method of modelling the connection detail's stiffness characteristics. This modelling technique is used to model a plate shell structure with a span of 11.5 meters in the FE software ABAQUS. The structure is analyzed with six different connection details with varying stiffness characteristics, to investigate the influence of these characteristics on the structural effects. Based on these investigations, and FE analysis of other plate shell models, the structural behaviour is described.

Possible methods of estimating the stresses in a given plate shell structure are proposed.

The non-linear behaviour of a plate shell structure is investigated for varying parameters, such as facet size, imperfections, and connection characteristics. The critical load is compared to that of a similar, but smoothly curved, shell structure.

Based on the investigations throughout the study, a set of guidelines for the structural design of plate shells of glass is proposed.

Resumé

Denne afhandling omhandler skive-skaller. Dette er en type skalkonstruktion, der består af plane elementer, hvor geometrien er organiseret således, at det primære bærende system udgøres af fordelte membrankræfter i facetterne. Det høje stivheds/vægt forhold for jævnt krumme skalkonstruktioner skyldes primært deres krumme form. Skive-skaller har ligeledes et højt stivheds/vægt forhold, men har yderligere den fordel at de er konstrueret af plane konstruktionselementer.

I denne afhandling fokuseres på at bruge laminerede glas-elementer som de lastbærende facetter.

En række metoder, der kan anvendes til at danne skive-skallers geometri, præsenteres. I samarbejde med Ghent Universitet er der udarbejdet et script, der kan generere en given skive-skals geometri, og en tilhørende finite element (FE) model.

En metode til at modellere en given skive-skal i et FE program præsenteres. Denne metode anvender en forholdsvis simpel modellering af en given samplingsdetaljes stivhedsegenskaber. Metoden er anvendt til at modellere en skive-skal med et spænd på 11,5 meter, i FE programmet ABAQUS. Konstruktionen er analyseret for seks forskellige samplings-designs med varierende stivhedsegenskaber, for at undersøge hvilken indflydelse disse egenskaber har på konstruktionens virkemåde. Andre skive-skaller er ligeledes analyseret i Abaqus. Med udgangspunkt i disse resultater er konstruktionstypens virkemåde beskrevet.

Metoder til at estimere spændinger og nedbøjninger i en given skive-skal foreslås.

Den ikke-lineær opførsel af skive-skaller undersøges for varierende parametre, såsom facet størrelse, imperfektioner og samlingens stivhedsegenskaber. Den beregnede kritiske last sammenlignes med den kritiske last for en lignende, men jævnt krum, skalkonstruktion.

Baseret på de præsenterede undersøgelser foreslås en række retningslinier for design af skive-skaller.

Table of Contents

| | | |
|----------|------------------------------------------------------------|-----------|
| 1 | Introduction | 1 |
| 1.1 | Background | 1 |
| 1.1.1 | Shell structures | 1 |
| 1.1.2 | Glass structures | 2 |
| 1.1.3 | Plate shell structures | 4 |
| 1.2 | Statement of problem | 5 |
| 1.3 | Scope of this study | 6 |
| 2 | Plate shell geometry | 9 |
| 2.1 | Creating plane-based facettet geometry | 10 |
| 2.1.1 | Mapping a plane pattern | 11 |
| 2.1.2 | Mapping a spatial pattern | 14 |
| 2.1.3 | Using multiple layer patterns | 17 |
| 2.2 | pyFormex script | 18 |
| 3 | Modelling plate shells | 23 |
| 3.1 | Connection stiffness parameters | 24 |
| 3.2 | FE modelling technique | 27 |
| 3.2.1 | Modelling of connections | 27 |
| 3.2.2 | Description of plate shell FE model | 31 |
| 3.2.3 | Convergence of stresses | 32 |
| 4 | Shell action in plate shells | 35 |
| 4.1 | Shell structures | 35 |
| 4.2 | In-plane forces in plate shell structures | 36 |
| 4.2.1 | Linear FE study of plate shell | 38 |
| 4.2.2 | Comparison to shell action in smooth shell | 43 |
| 4.2.3 | Estimating in-plane forces in a plate shell | 49 |
| 5 | Bending moments in plate shells | 51 |
| 5.1 | Local plate bending in plate shell facets | 51 |
| 5.1.1 | Plate bending in a polygonal plate | 52 |
| 5.1.2 | Linear FE study of plate shell | 55 |
| 5.1.3 | Estimating bending moments in plate shell facets | 57 |
| 5.2 | Other bending moments in plate shells | 61 |

| | | |
|----------|---------------------------------------------------------------------------------|------------|
| 6 | Non-linear investigations | 65 |
| 6.1 | Buckling of shell structures | 65 |
| 6.2 | Non-linear behaviour of plate shells | 67 |
| 6.2.1 | Basis of FE analysis | 67 |
| 6.2.2 | Bending of the facets | 69 |
| 6.2.3 | Imperfections | 72 |
| 6.2.4 | Connection stiffness | 76 |
| 6.2.5 | Modelling technique variations | 78 |
| 6.2.6 | Summary of non-linear study | 79 |
| 7 | Design of connection detail | 81 |
| 7.1 | Functional requirements for the connection detail | 81 |
| 7.2 | Glued-in plate connection | 84 |
| 7.3 | Friction connection | 86 |
| 7.4 | Glued butt joint | 88 |
| 8 | Guidelines for design of plate shell structures | 91 |
| 8.1 | Geometry | 91 |
| 8.2 | Determining stresses and displacements | 91 |
| 8.2.1 | Facets | 92 |
| 8.2.2 | Connections | 93 |
| 8.2.3 | Buckling | 93 |
| 8.3 | Supports | 94 |
| 8.4 | Construction | 94 |
| 8.5 | Fire strategy | 94 |
| 8.5.1 | Glass plate shell structures and fire | 95 |
| 8.6 | Other design aspects | 96 |
| 8.6.1 | Support settlements | 96 |
| 8.6.2 | Temperature movements | 96 |
| 8.6.3 | Glass fracture | 97 |
| 8.6.4 | Final remarks | 97 |
| 9 | Conclusion | 99 |
| 9.1 | Future work | 102 |
| A | Description of Abaqus models | 105 |
| B | In-plane forces in three plate shells and their equivalent smooth shells | 107 |
| C | Test of approximate expressions for plate bending in facets | 109 |
| | Bibliography | 111 |
| | List of Symbols | 115 |
| | List of Figures | 117 |

Publications (not included in the thesis)

- [1] Anne Bagger, Jeppe Jönsson, Henrik Almegaard and Ture Wester. Facetted Shell Structure of Glass. In *Proceedings of Glass Processing Days 2007*, Tampere, Finland, 2007.
- [2] Henrik Almegaard, Anne Bagger, Jens Gravesen, Bert Jüttler and Zbynek Sir. Surfaces with piecewise linear support functions over spherical triangulations. In *Proceedings of Mathematics of Surfaces XII*, Sheffield, England, 2007. Springer-Verlag.
- [3] Anne Bagger, Jeppe Jönsson and Ture Wester. Investigation of stresses in facetted glass shell structures. In *Shell and Spatial Structures – Structural Architecture: Towards the future looking to the past*, Venice, Italy, 2007. International Association for Shell and Spatial Structures (IASS)
- [4] Anne Bagger, Jeppe Jönsson and Henrik Almegaard. Bending stresses in Facetted Glass Shells. In *Proceedings of Challenging Glass 2008*, Delft, Holland, 2008.
- [5] Jaap A.M. Aanhaanen, Anne Bagger and N.J.A. Vamberský. The stability of a facetted glass dome structure. In *New Materials and Technologies – New Designs and Innovations*, Acapulco, Mexico, 2008. International Association for Shell and Spatial Structures (IASS)
- [6] Anne Bagger, Benedict Verheghe and Kristian D. Hertz. Modeling plate shell structures using pyFormex. In *Evolution and trends in design analysis and construction of shell and spatial structures*, Valencia, Spain, 2009. International Association for Shell and Spatial Structures (IASS)

Chapter 1

Introduction

This thesis is a study of *plate shell structures of glass* – a type of shell structure that consists of plane elements of glass, and no additional load bearing structure.

1.1 Background

1.1.1 Shell structures

A *shell structure* is a structural surface, which is shaped and supported so that it can carry load primarily by in-plane forces [24] [49]. Both in-plane compression and in-plane tension forces can develop in a shell structure. A structural surface where only in-plane tension forces are present is termed a *tension structure*. Pre-stressed cable nets and membrane structures belong to this category [40].

The stiffness of a shell structure is highly dependent on the shape of the surface and the support conditions, and not so much on the thickness of the surface. Efficient shell structures (i.e. appropriately shaped and supported) can span 500 to 1500 times the surface's thickness. This facilitates large spans, since the self weight of the structure is very low. Figure 1.1 shows two examples of shell structures, both of them concrete shells.

Reinforced concrete is a building material well suited for smooth shell surfaces, since it is directly moldable and can be cast on-site, creating a continuous surface. For concrete shells, the major challenges lie in the scaffolding and formwork during construction [19].

For other building materials such as steel, wood or glass, creating a curved, continuous shell surface is troublesome. For building purposes, these materials are traditionally available in straight (1D) or plane (2D) elements of limited size. It is therefore of interest to approximate the smoothly curved shell surface by using straight or plane elements.

Figure 1.2 shows two examples of shell structures with a piecewise plane surface – the geometry is built up by plane triangles. In these two structures, the glass panes have no load bearing role, other than carrying load to the panes' support lines. The structure primarily carries load to its supports by concentrated axial forces in the triangulated lattice structure. More information on lattice shell structures can for example be found in [41].



(a) Deitingen Raststätte, Deitingen, Switzerland, by Heinz Isler. Photo: de.wikipedia.org.



(b) Los Manantiales Restaurant, Mexico City, by Félix Candela. Photo: Dorothy Candela.

Figure 1.1: Examples of shell structures.



(a) Great court at British Museum, by Foster and Partners. Illustration from [50].



(b) BG Bank courtyard, Berlin, by Frank Gehry. Photo: travel.webshots.com

Figure 1.2: Examples of faceted shell structures with triangulated geometry.

1.1.2 Glass structures

The shell structures in Figure 1.2 use glass as a cladding material. However, the high stiffness and compressive strength of glass, and the continuous improvement of glass manufacturing techniques, allow for a broader use of the material.

Load carrying glass structures are seen in modern buildings in a growing number of varieties – glass beams, glass fins in facades transferring horizontal loads, glass columns,

shear transferring glass panes, glass floors, and other applications. Figure 1.3 and Figure 1.4 illustrate two examples of new applications of load carrying glass structures. Figure 1.3 shows glass columns at the headquarters of Danfoss in Denmark. Figure 1.4 shows the glass dome at the Institute for Lightweight Structures and Conceptual Design (ILEK) at Stuttgart University.



Figure 1.3: Load bearing glass columns at the headquarters of Danfoss, Denmark, by Schmidt, Hammer & Lassen. Each column carries a vertical load of $250kN$. Photo: Rambøll.



Figure 1.4: Glass dome at ILEK [16]. The glass segments are doubly curved laminated glass with a total thickness of $10mm$, connected by glued butt joints with a width of $10mm$. The diameter of the shell structure is $8.5m$. Photo: ILEK.

Glass is a material which displays no plastic deformation before failure. Small flaws in the glass surface causes stress concentrations at the crack tips when the surface is loaded in tension, and this reduces the tensile strength considerably compared to the compressive strength.

Common for the design of various structural glass elements are that they are designed to meet these specific properties of glass; a high compressive strength, a relatively low tensile strength, and brittle behaviour. For information about the material components in glass, specific material properties, manufacturing techniques (such as toughening, lamination

etc.), the reader is referred to some of the existing publications on glass in building [13] [26] [48] [60].

1.1.3 Plate shell structures

A shell structure with a triangulated faceted geometry primarily carries load by concentrated tension and compression forces in the edges and vertices of the geometry, i.e. in the bars and nodes. Research done primarily at the Royal Danish Academy of Fine Arts, School of Architecture, has shown that for any given stable¹ triangulated faceted structure, a *dual faceted structure* exists, which primarily carries load by distributed in-plane forces in the facets [12] [55] [57] [58]. Such a system is termed a *plate shell structure* in the following. Principally, every vertex in the triangulated system has been replaced by a plane. As every facet in a triangulated system is triangular, every vertex in a plate shell system will connect three facet corners.

Two dual faceted systems are shown in Figure 1.5.

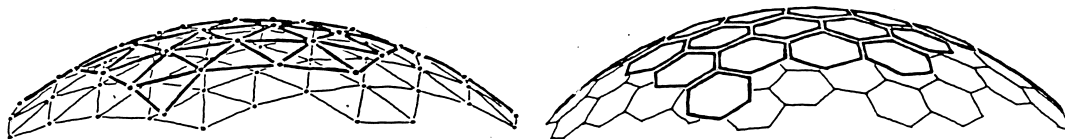


Figure 1.5: Dual faceted systems. Left: triangulated system. Right: plate shell system. Illustration from [56].

Statically, the three-way vertices in a plate shell structure has the consequence that the vertices are irrelevant for the stability of the system; the stability of the system is based on distributed in-plane forces in the facets, which are transferred along the facet edges. This means that the geometry of a plate shell structure is organized so that *the facets* constitute the primary load bearing structure. This eliminates the need for structural components other than the facets themselves.

Plate shell structures appear in nature in many different scales [59]. Figure 1.6 shows a few examples. The three-valence vertices are clearly recognizable. The non-continuous surface enables growth in the connection lines.

At the Danish Building Research Institute in Denmark, a Ph.D. study on spatial stability of shell structures [9] resulted in the realization of a plate shell structure in plywood, with a span of about 9m. Built in 1993, the model is still intact (2009), apart from some material deterioration of the facets. The structure is shown in Figure 1.7.

¹The term “stable” as used in this context refers to the structure’s statical determinacy. A stable structure is not a mechanism, and is either statically determinate or indeterminate.

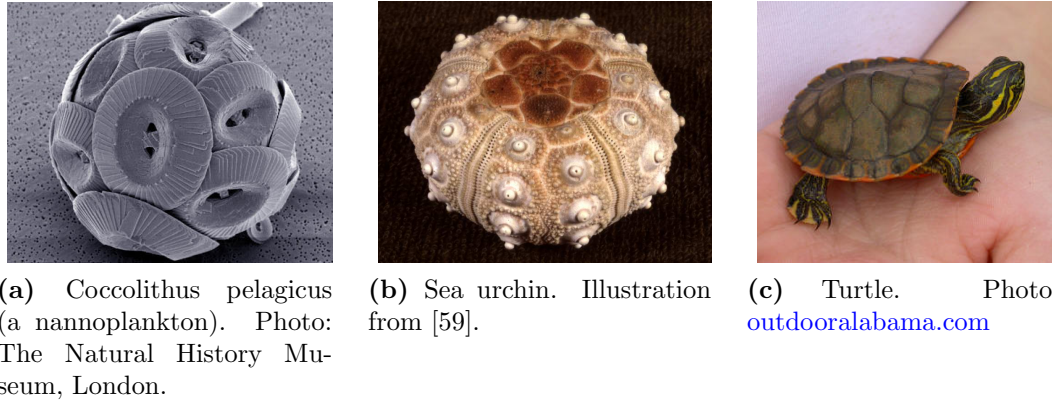


Figure 1.6: Plate shell structures in nature.



Figure 1.7: Full scale model of plate shell structure in 19mm plywood, located at the Danish Building Research Institute, Denmark. Designed by Henrik Almegaard. Illustration from [9].

1.2 Statement of problem

Based on the background information in Section 1.1, the possibility of designing a plate shell structure with glass facets is an appealing idea; a plate shell structure of glass combines a light-weight structural concept (the shell), and manageable production methods (plane elements of limited size), with the unique aesthetic qualities of glass.

Since the geometry of a plate shell is organized so that the stabilizing forces are distributed in the facets, this structural principle is especially well suited for glass, where stress concentrations should be avoided due to the brittleness.

The main goal of this thesis is to facilitate the design and construction of plate shell structures, particularly with glass facets. The research in plate shells conducted at the Danish Architectural School primarily focused on the principal stability of faceted structural systems, and the concept of duality. Based on the results from that research, the intention of the present study is to develop more specific knowledge about the structural behaviour of plate shells, leading to guidelines for the design of physical plate shell structures. This goal is approached by addressing the following questions:

- What is a plate shell structure? What are the basic characteristics, and how can

the geometry be generated?

- How does the structure work? What are the relevant design parameters, and how do these influence the result?
- How can such a structure be realized?

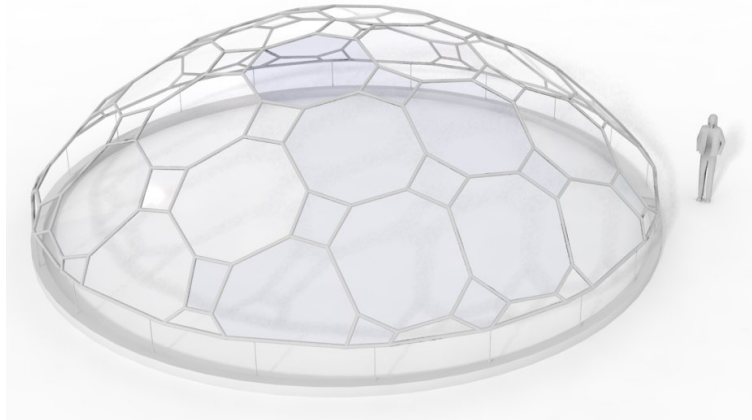


Figure 1.8: Visualization of a plate shell structure with glass facets. Prepared by M. Rippman, ILEK.

1.3 Scope of this study

The questions above are addressed by a combination of academic research and practical engineering. Correspondingly, the thesis is organized so that it can be read in two levels; the main text aims to present information which is relevant for the design engineer. Elaborations on methods and results, certain theoretical aspects and other issues relevant for a continuation of the research, are placed in footnotes.

Possible methods of creating the geometry are suggested in **Chapter 2**. Generating the geometry for a plate shell structure can be troublesome with existing CAD tools. The reason for this is that the position of the faceted shape's edges and vertices is not explicitly defined in space (as they are for a triangulated geometry); they are implicitly defined as the intersection lines and points between the facet planes (which *are* explicitly defined). The suggested methods for generating the geometry are illustrated by a series of examples.

To facilitate easy generation of the plate shell geometry, and transformation of the geometry into a finite element (FE) model, a *Python*-script for the free software tool *pyFormex* has been developed in cooperation with Ghent University. The script can generate a plate shell geometry based on user input in the form of a list of points. The script can adapt the geometry to a user defined structural height and span, create connection lines with

user defined stiffness parameters, and export this information as a FE model to ABAQUS², including information about materials, element type, element meshing, boundary conditions and loads.

In **Chapter 3** a modelling technique for FE analysis of plate shells is suggested. Specifically, modelling of the connections is focused upon.

The structural behaviour of plate shells is investigated in **Chapters 4 and 5**, assuming geometrically linearity (i.e. no large displacements and no buckling). This investigation is divided into two parts. The first part (Chapter 4) deals with in-plane forces in the structure. The second part (Chapter 5) deals with bending moments in the facets. In both parts, emphasis is on describing the different structural effects *physically*, in order to provide the design engineer with an intuitive understanding of the structure's behaviour. Based on this explanation, FE analysis in ABAQUS is used to verify the structural effects, and to quantify the consequences in terms of stresses, displacements etc. Finally, based on the findings of the FE analysis, simple approximate calculation methods are developed, to facilitate a fast and easy estimation of stresses and displacements for a given plate shell design. These tools are developed to provide the designer with an overview of the structure in a preliminary design phase.

The behaviour of plate shell structures when including effects from geometrically non-linearity is studied in **Chapter 6**. This potential area of research is very large, and the study in Chapter 6 should be seen as an introductory investigation into the topic, with the aim to provide a general feel for the structure's non-linear behaviour. Design parameters such as faceting pattern, overall facet size, imperfections and connection characteristics are varied, and the results are compared. Also, the results for the plate shells are compared to the non-linear behaviour of a similar *smooth* shell structure.

The question of how to design the detail that connects the facets is addressed in **Chapter 7**. The functional requirements and wishes for the connection detail are discussed; based on this discussion, three different detail designs are suggested. Two of these designs have been tested experimentally.

The findings throughout the study are collected into a set of proposed design guidelines in **Chapter 8**. Topics that have not been studied in the thesis are brought up, and a design approach for these is suggested.

Chapter 9 sums up the main conclusions of the thesis, and suggests a direction for further research.

²ABAQUS is a general-purpose finite element analysis program for mechanical and structural engineering [5].

Chapter 2

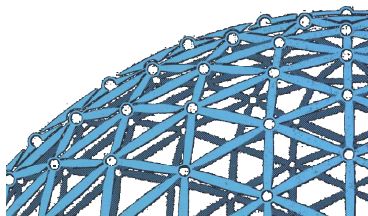
Plate shell geometry

This chapter aims to provide some practical tools for the generation of plate shell geometry.

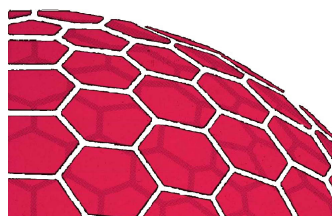
A smooth curved surface is characterized by its Gaussian curvature, which can be positive (convex shape), negative (non-convex/saddle shape) or zero (developable, for example a cone segment) [9]. Surfaces of non-zero Gaussian curvature are termed doubly curved. In the present study, only doubly curved shapes of positive curvature, i.e. *convex shell shapes*, are considered.

A smooth convex shell surface can be approximated by a faceted surface. The relevant methods of determining such a faceted geometry can be divided into two principally different approaches: *Point-based faceting* (triangulation) and *plane-based faceting* (plate shell geometry).

In a point-based faceted geometry three points are used to define each plane (facet). By distributing points on a smoothly curved surface and connecting these points with straight lines (while obeying certain rules), a triangulated geometry of piecewise plane triangles can be defined (as in [9]). Figure 2.1a shows an example of a point-based triangulated geometry. More information about triangulating a smooth surface can for example be found in [45].



(a) Point-based geometry



(b) Plane-based geometry

Figure 2.1: The two basic types of faceted convex geometry. (Illustration: Ture Wester.)

In a plane-based faceted geometry the smooth convex surface is approximated by a num-

ber of planes, meaning that the position and orientation of each plane is defined in space, and the facets' boundaries are produced by determining the intersection lines and points of these planes [28]. In such a system, three planes define a point, so three facets will meet in every vertex of the geometry [55]. Figure 2.1b shows an example of a plane-based faceted geometry. To illustrate this concept, imagine cutting off slices of an apple with plane, random cuts until all the peel is gone. The resulting geometry is a plane-based faceted geometry, and three planes/facets will meet in every vertex. It can be shown that as the number of facets on a given convex plane-based faceted surface increases, the average number of edges on each polygonal facet will approach six [55].

These two basic types of faceted geometry¹, point-based and plane-based, can principally be described as each other's *dual*. For more information about the geometric and structural duality between point-based and plane-based systems see for example [55]. A short introduction to the concept of duality was also given in Section 1.1.3.

As mentioned earlier, we will limit the present study to convex shell shapes².

While point-based systems are a common sight in shell structures, and geometrically studied in many contexts, plane-based faceted systems are less well known. For this reason, most CAD systems cannot handle a plane-based faceted geometry in an effective way. The first challenge in the design of a plate shell structure lies therefore in how to generate and manipulate a suitable geometry. Section 2.1 focuses on possible methods of generating a suitable pattern, and how to transform the pattern into a plane-based faceted geometry. Section 2.2 presents a *Python* script for the software tool *pyFormex* which can generate a finite element model of a plate shell, ready for export to ABAQUS. The script is written by Benedict Verheghe, Ghent University, in cooperation with the author [14].

2.1 Creating plane-based faceted geometry

In the following, a number of methods for producing plane-based faceted geometries are proposed. The focus is on collecting some practical tools to facilitate the faceting process, and to explore some possibilities of using, varying and expanding these tools.

Since the geometry is plane-based, we basically wish to define the position and orientation

¹A third family of faceted geometries have quadrangular facets. Geometrically and structurally, these are hybrids of plane-based and point-based systems. The possibility of patterning and the choice of "overall" shape, are constrained by certain geometrical conditions [10] [53]. Structurally, the system is a mix of a plate shell structure (with in-plane shell action in the facets) and a lattice structure (with concentrated forces in the edges and vertices).

²When performing a plate based faceting of a non-convex surface (i.e. with negative Gaussian curvature) special conditions apply [9]. The facets of such a geometry are hourglass-shaped, and the topology (i.e. which planes intersect each other) is not uniquely determined by the facets' position in space. Also, the hourglass-shaped facets have concave corners, and there will be large stress concentrations in these concave corner points, as shown analytically in [42]. For facets of glass this will result in cracks.

for the plane of each facet in space. This can be done by distributing points on a smoothly curved surface (in this case limited to being convex), and in each of these points determine the tangent plane to the smooth surface [28]. As described above, the intersection lines and points of these tangent planes determine the boundaries of the facets. Most of the methods described in Sections 2.1.1, 2.1.2 and 2.1.3 deal with how to distribute the tangent points on a smooth convex surface – these sections propose ideas about possible patterns, and how to manipulate these patterns.

Instead of defining tangent planes to a convex surface, other methods of defining the facets' position in space could be of interest. The facet planes could for example be determined by a dual-manipulation of a triangulated geometry [57], or determined by using the support function representation of a smooth surface and the resulting faceted geometry [11]. The present study only focuses on determination of the facets via tangent planes.

2.1.1 Mapping a plane pattern

Consider a pattern of points defined in a plane. We wish to map the points onto a convex surface, and determine the tangent planes to the surface in those points. This mapping inevitably distorts the pattern. Depending on the mapping method, we can maintain certain characteristics of the pattern, like certain lengths or angles, but all characteristics cannot be maintained simultaneously. The larger the difference between the original shape (here: a plane) and the surface, which we map the pattern onto, the more distorted the mapped pattern becomes.

Some different mapping methods are possible, see for example [45] and [34]. In the following, three simple procedures are suggested. (1.) Parallel projection, (2.) central projection and (3.) a mapping suggested by the author, which in the following is referred to as a “parametric” mapping. In Table 2.1 the three methods are illustrated by some examples in order to show the strengths and weaknesses of the different procedures in a given context. The example shows a regular pattern mapped onto a spherical dome with the ratio h/l , where h is the dome height and l is the span of the dome.

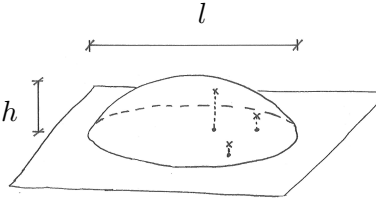
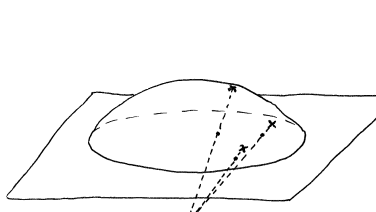
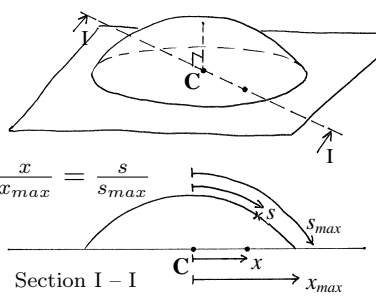
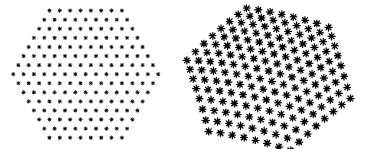
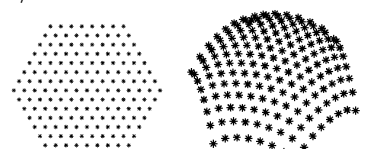
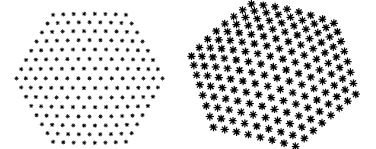

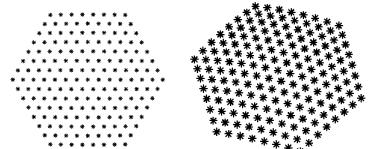
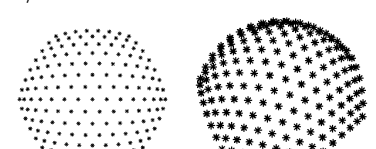
| <i>Parallel projection</i> | <i>Central projection</i> | <i>Parametric mapping</i> |
|-------------------------------------------------------------------------------------------------------------------------------------------------------------------------------------------------------------------------------------------------------------------------------------------------------------|---------------------------------------------------------------------------------------------------------------------------------------------------------------------------------------------------------------------------------------------------------------------------------------|-----------------------------------------------------------------------------------------------------------------------------------------------------------------------------------------------------------------------------------------------------------------------------------------------------------------------------------------------------------------------------------------------------------------------------------------------------------------------------------------------------------------------|
|  |  |  <p style="text-align: center;">Section I - I</p> |
| <p>The points are projected vertically onto the convex surface. (This is actually a special case of a central projection, where C is infinitely distant.)</p> | <p>The points are projected radially onto the convex surface with reference to an appointed origin, C.</p> | <p>The relative position of a point in the plane is kept as the relative position of the point on the convex surface, with respect to an appointed origin.</p> |
| <p>Plan and isometric view of the mapped pattern: $h/l = 0.1$</p>  <p>$h/l = 0.4$</p>  | <p>Plan and isometric view of the mapped pattern: $h/l = 0.1$</p>  <p>$h/l = 0.4$</p>  | <p>Plan and isometric view of the mapped pattern: $h/l = 0.1$</p>  <p>$h/l = 0.4$</p>  |
| <p>This method is generally easy to implement. It can be used on a large variety of convex shapes, analytically determined as well as free form. The larger the angle between the original pattern plane and the convex surface's tangent plane, the larger the distortion of the pattern in that area.</p> | <p>This projection can be used on a large variety of convex shapes, analytically determined as well as free form. In the example above, this method yields a large distortion of the pattern when the curvature of the convex surface is large.</p> | <p>This mapping method yields a relatively smooth distribution of the original pattern onto the convex surface in the example above - for small curvature as well as large curvature. It is limited to surfaces where the smallest distance between any given point on the surface and an appointed origin on the surface can be determined (i.e. the length of the geodesic curve). A section of a sphere and a paraboloid of revolution (where the appointed origin is the centre of rotation) are such shapes.</p> |

Table 2.1: Three methods used to map a regular pattern onto a section of a sphere.

Figure 2.2 shows a series of examples, where a pattern in a plane has been mapped onto a smooth convex surface, and the tangent planes to the surface have been used to construct a plane-based facettled geometry. All three examples use the parametric mapping technique, and they have been generated using first a MATLAB script³ written by the author, and after that the *pyFormex* script presented in Section 2.2.

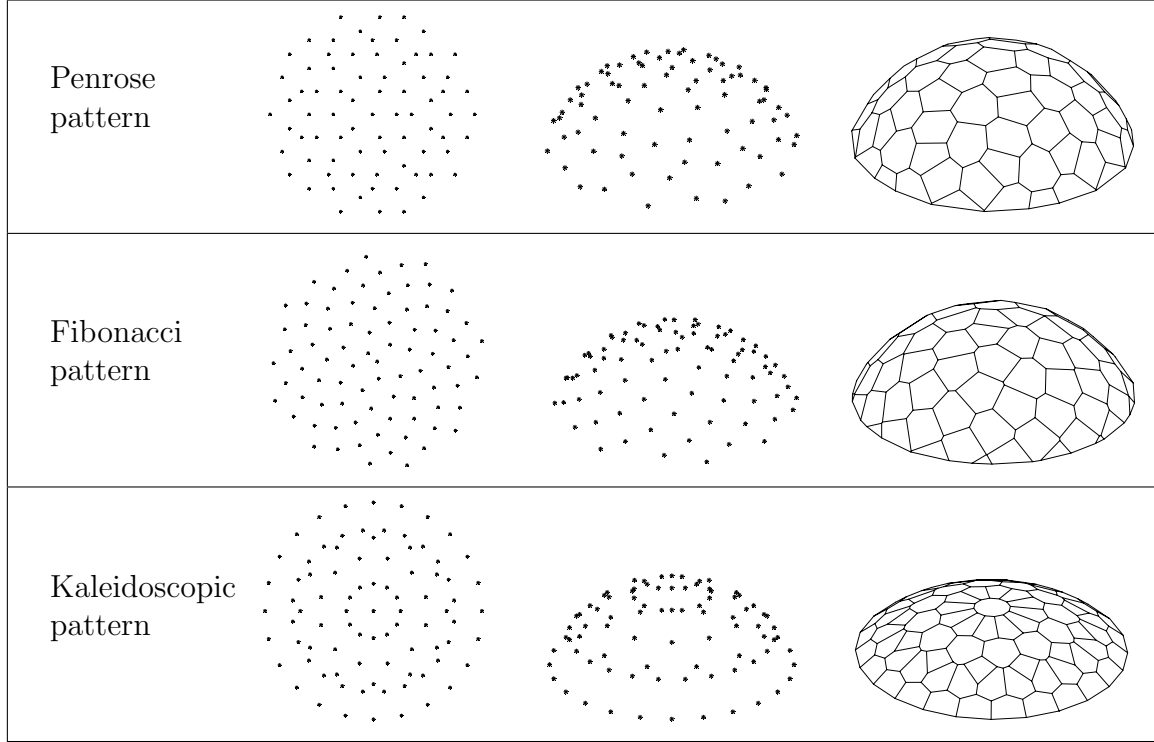


Figure 2.2: Three examples of a plane-based facettled geometry, generated by mapping a plane pattern onto a section of a sphere, and determining the tangent planes to the sphere in these points.

The first example in Figure 2.2 uses a five-fold symmetry as plane pattern. The intersection points of a Penrose tiling (rhombus version) define the points in the pattern.⁴

The middle example in Figure 2.2 uses a pattern of points based on the Fibonacci sequence.⁵

³The MATLAB script can map an array of points in the plane onto either a spherical dome or a paraboloid of revolution (both of varying span and height), using either parallel, central or parametric mapping. The script also supports the mapping of a pattern defined on a cone, as illustrated in Figure 2.7 (page 16). Besides generating an array of points which can be used as input to *pyFormex*, the script can produce input to the software *Nydrool*, written by Klavs Feilberg Hansen [27]. *Nydrool* can, among other features, generate a plane-based facettled geometry, based on a group of defined planes in space. The MATLAB script can be attained by contacting the author.

⁴The resulting plane-based facettled geometry is merely a different version of the original five-fold symmetry. A certain facet shape belongs to each possible “cluster” of tiles in the original Penrose tiling. Therefore, the number of possible facet shapes is finite – even quite small (9 shapes in total). Depending on the curvature of the smooth shape (here a spherical shape of relatively high curvature), the original pattern is distorted to a certain degree.

⁵The points are determined by $(r; \theta)_n = (\sqrt{n}; 2\pi\varphi n)$, where $(r; \theta)_n$ is the n^{th} point in polar coordinates

In the third example in Figure 2.2 a more or less random pattern of a rotational symmetry has been defined, mapped onto a spherical dome and used to construct a plane-based faceted geometry.

Another possibility for the construction of a plane pattern is shown in Figure 2.3. Some of the points in a regular pattern (with three principal directions) have been slightly adjusted, so that they sketch up a certain desired shape⁶. (The example shown here is most likely too finely faceted to be feasible as a structure.)

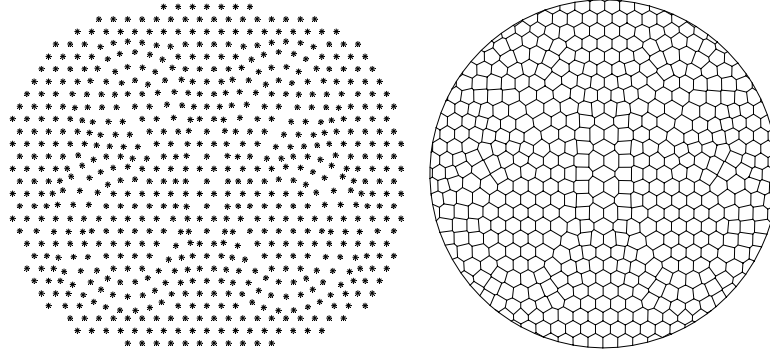


Figure 2.3: A plane regular pattern is adjusted to outline a butterfly, and used to produce a plane-based faceted geometry.

2.1.2 Mapping a spatial pattern

A large difference in shape between an original pattern basis (which in Section 2.1.1 was a plane) and the convex surface onto which the pattern is mapped, yields a certain distortion of the original pattern. Generally, the larger the difference, the larger the distortion. We now wish to explore the possibility of defining the original pattern on a surface which is *not* a single plane – a surface which serves as a better approximation to the mapped pattern. This is partly to have a smaller geometric difference between the original pattern and the mapped pattern, and partly to extend the possibilities for different patterning schemes.

and φ is the Golden number, $\varphi = \frac{1+\sqrt{5}}{2}$, [36]. Since the nature of the Fibonacci sequence is crossing spirals (a two-way pattern), and the nature of a randomly produced plane-based geometry is polygons with six edges in average (a three-way pattern), the plane-based geometry in Figure 2.2, middle image, is a mix of these two tendencies. Therefore, a given spiral can be found by following a limited number of neighbouring facets, where after it dissolves as the hexagonal nature of the facets take over.

⁶The original, regular pattern is defined by the corner points of a pattern of equilateral triangles. The best result comes from keeping the pattern adjustments so small that the topology of the original hexagonal faceted shape is kept, meaning that all facets remain hexagonal. Generally, the further the points are moved from their initial location, the more the length of the resulting facet edges are influenced. Small edge lengths may be difficult to connect with a physical connection detail. An appealing feature about the shown geometry is that the outlined image does not reveal itself directly. The image is sketched up by facet edges which are perpendicular to the image contour, which is much more subtle than if the image had been directly outlined. For the same reason, if the “hidden image” is too complex, the meaning is more or less lost in the faceted geometry.



Figure 2.4: Construction of the Zeiss Planetarium in Jena, Germany, designed by Walther Bauersfeld in 1923 [29].

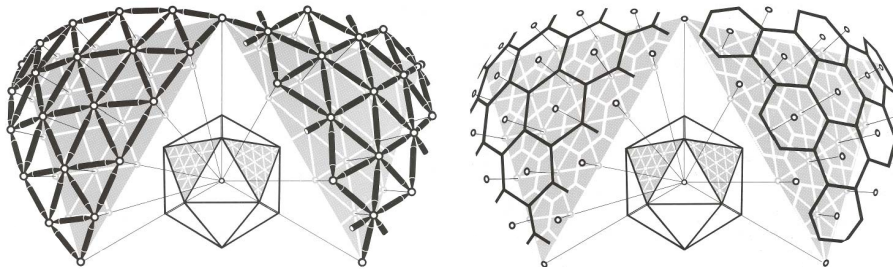


Figure 2.5: Geodesic triangulation of sphere (left), and the dual plane-based geometry (right). Illustration from [55].

Figure 2.4 shows a geometry that in the 1950'ies became known as a *geodesic sphere*, when Buckminster Fuller patented the geometric layout [25]. The geodesic sphere is generated as shown in Figure 2.5, where the faces of an icosahedron⁷ are subdivided into smaller triangles. The corner points of these triangles are mapped onto an enveloping sphere, and connected with straight lines, thereby forming a triangulation of the sphere. A plane-based geometry, dual to the geodesic sphere, can be generated by determining the tangent planes to the corner points of the triangles, and letting these planes intersect each other. The triangulation and the dual plane-based geometry are shown in Figure 2.5.

The geometry in Figure 2.5 uses an icosahedron as basic polyhedron, but the two other regular polyhedra with triangular faces (the tetrahedron⁸ and the octahedron⁹) can also serve as basis for a geodesic shape, see Figure 2.6. The icosahedron serves as a better approximation to the sphere than the octahedron and especially the tetrahedron – the facets are much more homogenous when based on the icosahedron.

⁷The icosahedron is a regular polyhedron with 20 equilateral triangles and 12 vertices.

⁸The tetrahedron is a regular polyhedron with 4 equilateral triangles and 4 vertices.

⁹The octahedron is a regular polyhedron with 8 equilateral triangles and 6 vertices.

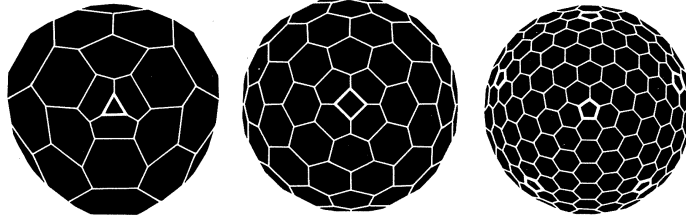


Figure 2.6: Three examples of plane-based geodesic domes, based on a tetrahedron, an octahedron and an icosahedron respectively. Illustrations from [55].

The number of subdivisions of the original polyhedron's faces can be varied, thereby producing a finer or coarser geodesic faceting.

Non-regular polyhedra can also be used as basis for a pattern, thereby facilitating a wide variety of different faceted layouts.¹⁰

Another possibility for defining a spatial pattern is to define the pattern on a cone. This is especially relevant for a pattern of a repetitive rotational symmetry. The procedure is illustrated in Figure 2.7. Consider a plane pattern that repeats itself n times in a polar rotation around a centre. The fact that the pattern is repeated makes it possible to remove a part of the pattern without changing the local topology of the pattern. One or more repetitions are therefore removed, and the remaining plane pattern is “gathered” into a cone shape. From this cone shape, the pattern is mapped onto a convex shape, ideally with a height-to-span ratio similar to that of the cone.¹¹

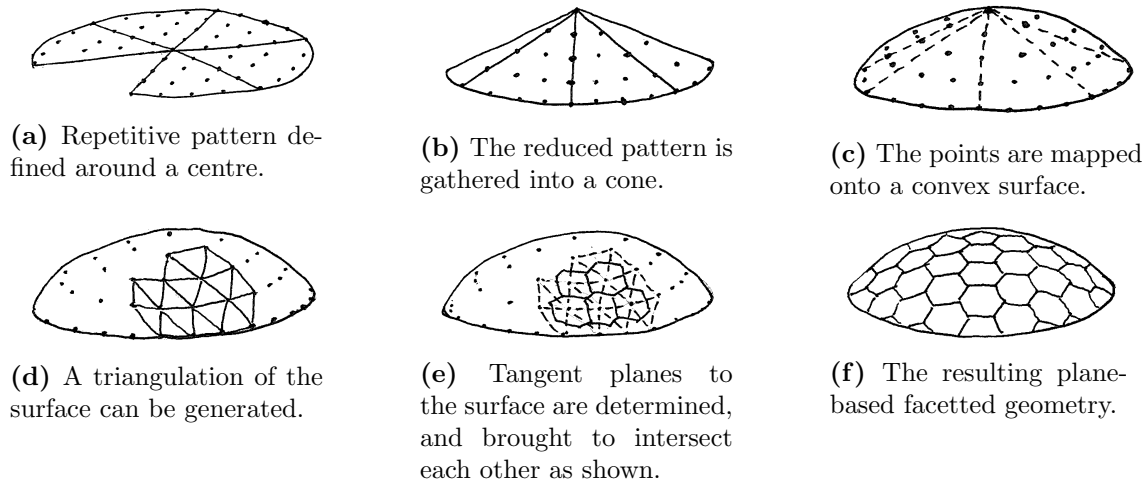


Figure 2.7: Generation of a plane-based faceted geometry from a pattern on a cone.

¹⁰Polyhedra can be a very useful basis for describing a pattern, since they are piecewise plane and therefore easy to handle analytically and/or in CAD. Also, if the smooth surface that the pattern is mapped onto is not of rotational symmetry, choosing a non-regular polyhedron for the pattern basis can be a way of avoiding too large difference between the original pattern and the mapped pattern.

¹¹This feature is implemented in the MATLAB script mentioned in footnote 3 in this chapter.

This method can yield a result which is a variation of the geodesic dome, but it can also be used for other geometries. Some examples are shown in Figure 2.8. To the left is a regular pattern of points (with 3 principal directions), where varying parts of the geometry are cut away. To the right is a Penrose pattern, generated as described on page 13, also with varying parts cut away.

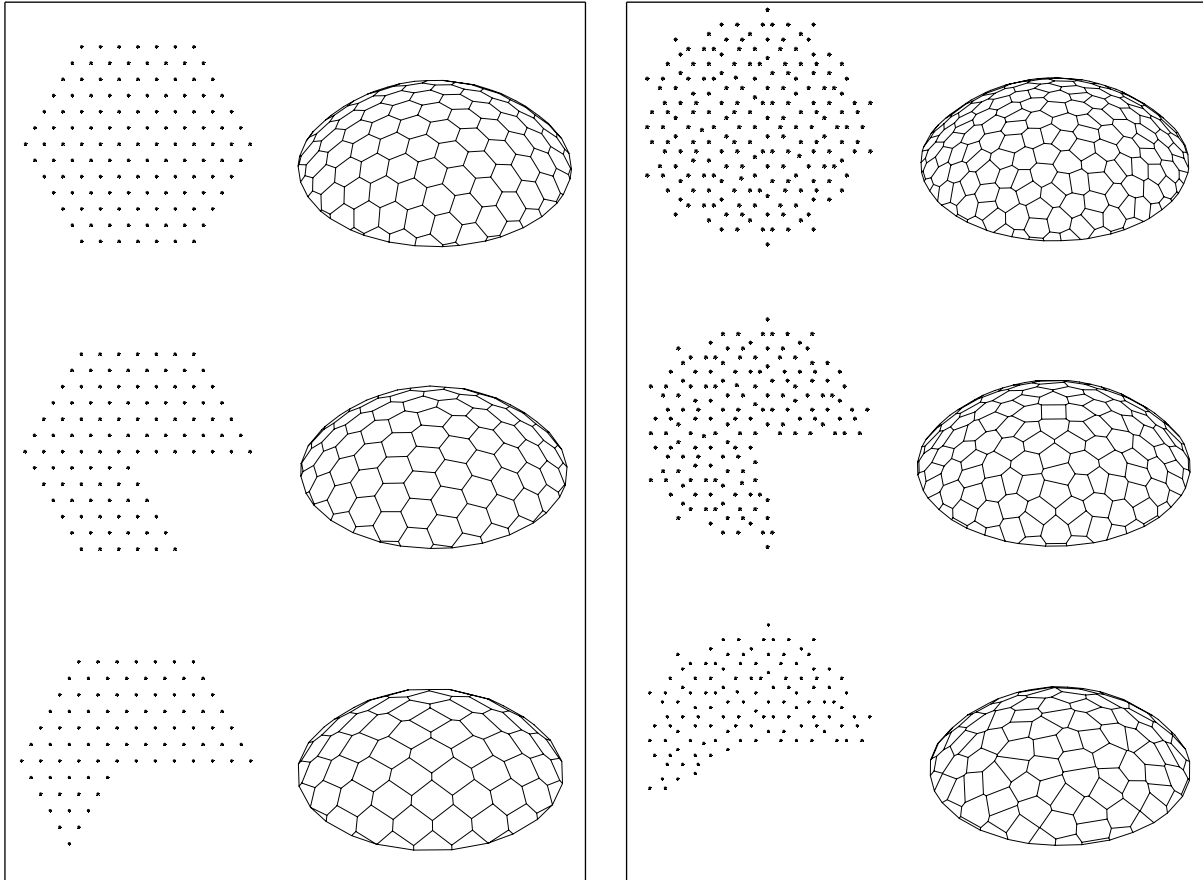


Figure 2.8: Mapping of two different patterns defined in a cone. To the left a regular pattern with 3 principal directions. To the right a Penrose pattern.

2.1.3 Using multiple layer patterns

Consider a pattern of points in a plane, or in space. The points can be divided into two groups (or more). The first group of points is mapped onto a smooth convex surface. The second group is mapped onto a surface with the same shape, but a slightly different size. The result is two “layers” of points. By using these points to produce a plane-based faceted geometry, the relative size of the facets can be manipulated. If the scaling of the two surfaces are too different from each other, some facets will disappear from the resulting faceted geometry¹². The principle of the concept of multiple layer patterns is

¹²Generally, the scaling of the different layers of the smooth surface should be almost alike. In most cases, a 1-15‰ difference in scale is appropriate. The suitable span of difference in scale depends on the curvature of the geometry, and the relative size of the facets. For a geometry of low curvature or a fine faceting, the difference in scale should be in the low end of the of the suggested range.

illustrated in Figure 2.9; in the image to the left three points are defined on the same surface (illustrated by a section through the surface). In the image to the right one point is mapped onto a surface with a slightly different (larger) scale than the other two points. As a consequence, the relative size of the facets change. Some examples using the two-layer concept are shown in Figure 2.10.

Naturally, the points can be divided into more than two groups, if so desired.

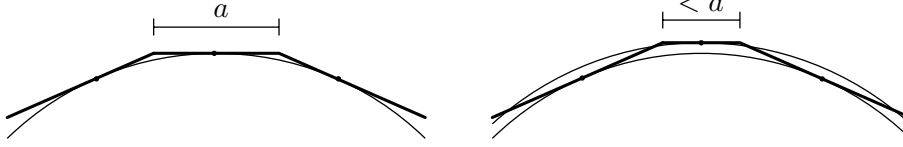


Figure 2.9: Principle sketch of the multiple layer patterns.

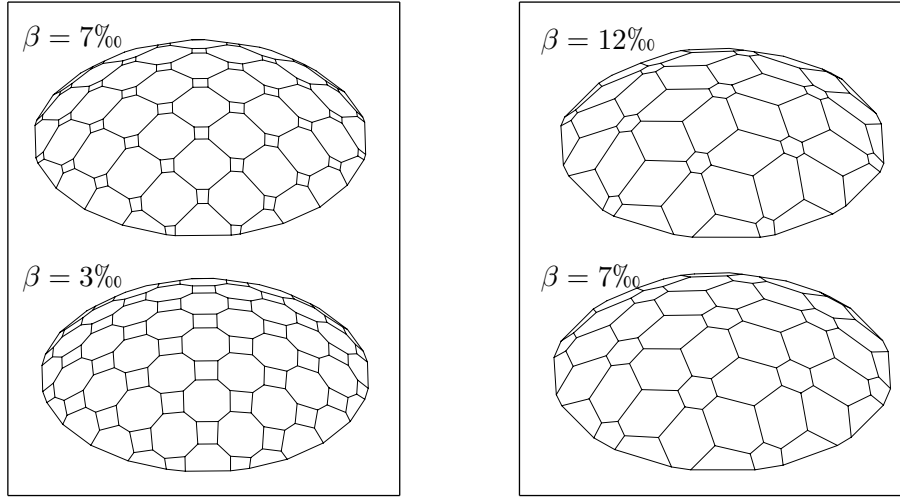


Figure 2.10: Four examples of the use of two layers of points. β refers to the applied difference in scale between the two surfaces.

2.2 *pyFormex* script

To facilitate an automated generation of the plane-based geometry of a plate shell structure, and a finite element (FE) model to run in ABAQUS, a script has been developed for the software tool *pyFormex*. *pyFormex* is a powerful free software currently under development by B. Verheghe *et al.* at Ghent University [4]. *pyFormex* contains a *Python* implementation of Formex algebra pioneered by H. Nooshin [43] and was developed for the automated design of spatial structures by means of sequences of mathematical transformations [4] [54].

In the following, the *pyFormex* script is presented from the design engineer's point of view. For a more thorough technical description of the programming procedures in the script, the reader is referred to [14].

The *pyFormex* script is written by B. Verheghe, based on requests from and discussions with the author.

Table 2.2 and 2.3 gives an overview of the user defined input, and the script's output. Figure 2.11 illustrates the different steps in the geometry generation.

As previously described in this chapter, a plane-based faceted geometry is generated by determining the position of each facet's plane in space. In the *pyFormex* script, this is achieved by loading a text-file with a list of points, all of which are points on a convex surface (an example is illustrated in Figure 2.11(a)). Such a file can be generated by one of the procedures suggested in Sections 2.1.1, 2.1.2 and 2.1.3.

The *pyFormex* script generates a triangulated convex surface based on the loaded list of points (Figure 2.11(b)). The facets' normals are determined for each point, either analytically from a known expression of the surface (for example a spherical surface), or from the triangulation (using the mean normal of the triangles surrounding the point). Using the facets' normals, the facet planes are constructed and brought to intersect each other, creating the plane-based faceted geometry, as illustrated in Figure 2.11(c). The geometry is then cut by a plane at a specified ground level (Figure 2.11(d)), and is scaled to meet a specified span size and height¹³.

The script prepares the basic faceted geometry for the modelling of the connections (the modelling technique is described in detail in Section 3.2.1, page 27) by offsetting the facet edges in the facet plane, towards the facet centre (Figure 2.11(e)), and the joint areas are defined (Figure 2.11(f)).

Material properties (glass facets), boundary conditions (supported against translations along the boundary) and load (self weight) are defined by the script, as well as a number of geometry sets to facilitate an efficient handling of the model in ABAQUS.

Finally, the *pyFormex* script exports all data, including mesh seeds and element type, in the format of an ABAQUS/CAE *Python* script. Running the exported script in ABAQUS will create the model, including element mesh, and prepare the analysis job for submission. For non-linear analysis some adjustments must be made before job submission¹⁴.

¹³This is possible without warping the facets, since points in a plane will remain in a plane after scaling in one or more directions.

¹⁴The predefined step, where load is defined, is changed into "Static, Riks", and geometrically nonlinearity is switched *on* in the step definition. The non-linear parameters are chosen suitably. *Imperfections* can for example be added in the form of $\Delta z = f(x, y)$ (an imperfection value is added to the vertical position of each node, depending on the nodes position in the ground plane, as described in Chapter 6). However, running the necessary algorithm for the nodes is problematic, since the nodes are described in relative coordinates for each facet and joint, and a list of nodes is therefore not directly extractable from the ABAQUS input-file. The following is a description of how the model is modified, so that all nodes are listed in absolute coordinates in one single list in the input-file (which can also be useful in other situations): 1. Save the model under a different name. 2. Mesh the structure as desired. (This mesh cannot be altered later.) 3. Delete all sets, boundary conditions, steps and constraints. 4. Use "Display Group" to view facets only. 5. Use "Create Mesh Part" (mesh module) to gather all facet elements into one part. 6. Repeat step 4 and 5 for joint elements. 7. Suppress all instances. 8. Create instance consisting of the two new parts. 9. Assign section to the two new parts (part module). 10. Merge mesh (assembly module). 11. Define steps, loads, boundary conditions, output requests and job.

| | |
|------------------------|---------------------------------------------------------------------------------------------------------------------------------------------------------------------------------------|
| Point array | The user creates and uploads a file containing a list of points (in cartesian coordinates) on a convex surface. |
| Ground plane | The user states the position of the ground plane, at which the geometry will be cut and the structure will be supported. |
| Span and height | The basic geometry can be stretched to meet a given size in the ground plane and in the height. |
| Connections | The user specifies the geometric layout of the joint strips, which will model the connections. (The connection modelling technique is described in detail in Section 3.2.1, page 27.) |
| Mesh | The general element size, or the number of elements along certain edges, is specified. The element type is chosen among a list of shell elements. |

Table 2.2: User defined input to the *pyFormex* script.

Table 2.2 lists the key input elements for the *pyFormex* script, defined interactively by the user. Table 2.3 lists the output (the FE model), when the resulting *Python* script is run in ABAQUS.

| | |
|----------------------------|---------------------------------------------------------------------------------------------------------------------------------------------------------------------------------------------------------------------------------------------------------------------------------------------------------------------------------------------------------------------------------------------------------------------|
| Python script | The output of the pyFormex script is a <i>Python</i> script, ready to run in ABAQUS, which results in an ABAQUS/CAE FE model with the features described below. |
| Geometry | Facets and joint strips are defined as surfaces. Each facet or joint strip is an individual ABAQUS <i>part</i> , and the coinciding edges of the parts are connected by <i>tie constraints</i> ¹⁵ . |
| Material parameters | The facet material is defined as glass; a linear elastic, isotropic material, with E-modulus 70GPa , Poisson's ratio 0.22 and density $25\text{kN}/\text{m}^3$. The joint strip material is also linear elastic and isotropic. The material parameters can be adjusted by the user in ABAQUS, so that the joint strips represent the stiffness of a given connection detail, see Section 3.2.1 (page 27). |
| Mesh | The structure is meshed by ABAQUS according to the element size specified by the user in the script. |
| Sets | Geometric sets (surface sets and line sets) are defined by the script for convenient handling of the geometry in ABAQUS. The sets are useful if the user wishes to specify other element sizes in certain areas (for example a finer mesh in all facet corners), or when applying loads to the structure. |
| Loads | Gravity load is applied to the structure by the script. Other loads must be applied by the user in ABAQUS ¹⁶ . |
| Boundary conditions | The structure's boundary in the ground plane is supported against translation. |
| Analysis output | A request for analysis output is defined by the script, requesting stress components in upper, middle and lower surface of the shell elements, translations, rotations, section forces and section moments. |
| Job | A job is defined by the script, ready to be submitted for analysis in ABAQUS. |

Table 2.3: Output of the *pyFormex* script.

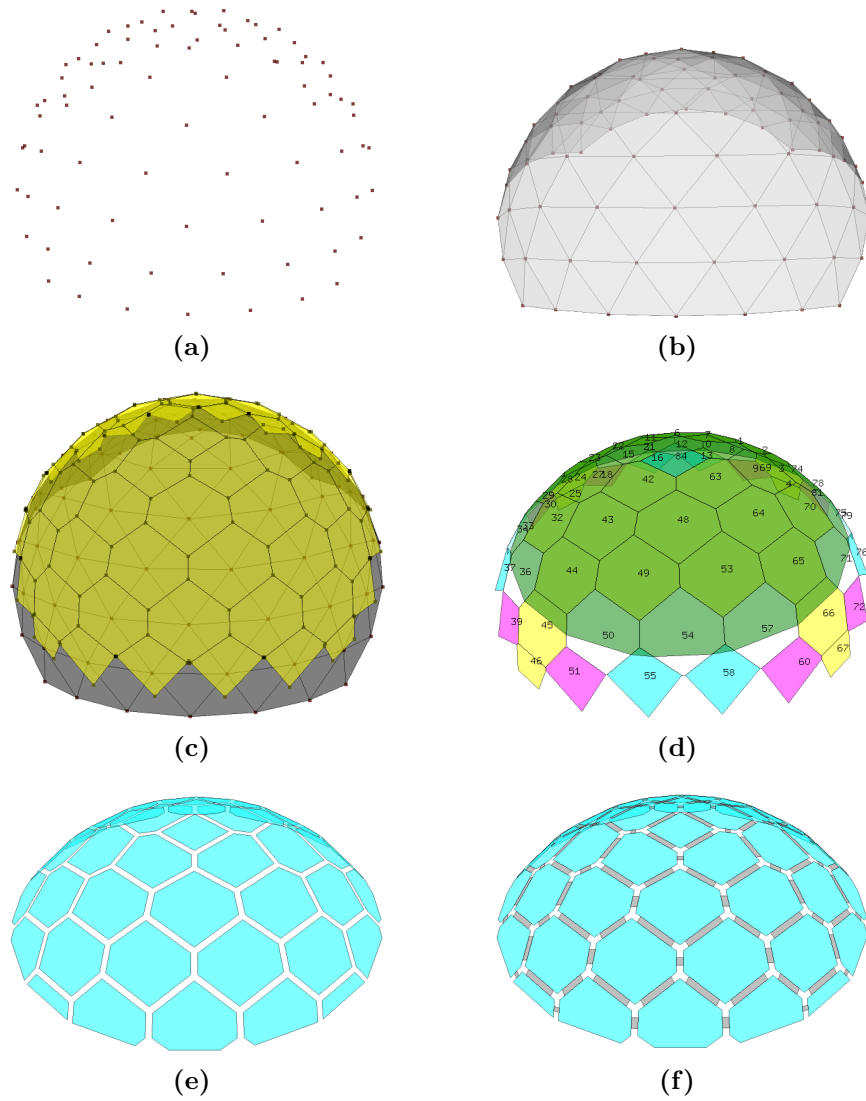


Figure 2.11: Illustration of the stepwise plate shell geometry generation in the *pyFormex* script.

¹⁵In ABAQUS, *parts* are the building blocks of an ABAQUS/CAE model. Parts are put together to create an *assembly* that can then be meshed and analyzed. A *tie constraint* is a method to define a fixed link between two parts [3]. In this case, that coinciding edges of two parts must have identical displacements.

¹⁶There are plans for a further development of the script, to apply snow and wind load in *pyFormex*.

Chapter 3

Modelling plate shells

This chapter aims at developing an appropriate method for creating a FE model of a plate shell. The intention is to develop a modelling technique which is as simple as possible, while reproducing the most important structural aspects of the structure.

Particularly, a simple representation of the physical connection detail is in focus, since modelling the actual detail with every geometric feature, and using “exact” material properties would be unrealistically cumbersome. It is deemed more valuable to use a simpler model, the limitations of which are well known.

In the following, the structural behaviour of plate shells is briefly described, so that it can serve as basis for choosing an appropriate modelling technique. The description is based on the research presented in the subsequent chapters.

Consider a plate shell structure, sufficiently supported to behave as a shell structure (see Sections 4.1 and 4.2). When the facets are loaded by out-of-plane load, they will be subjected to bending (see Section 5.1). Via bending the load is carried to the edges of the facets. Because of the angle between adjacent facets, and because the structure is supported so that in-plane forces can develop, the out-of-plane load is transformed into in-plane forces at the facet edges [12] (see for example the illustrations in Table 4.1, page 37). This transformation results in in-plane forces which are perpendicular to the connection lines. In addition to these, in-plane forces parallel to the connection lines may also develop.

These in-plane forces can be described as the structure’s *shell action*. The high structural efficiency (i.e. high stiffness to weight ratio) of plate shells is a result of this shell action.

Each facet can be seen as supported out of their own plane on the surrounding facets. Since the surrounding facets have a finite stiffness, and since the physical connection detail also has a finite stiffness, each facet is supported along its edges by supports of finite stiffness. If the connection detail behaves as a hinge (a line hinge, allowing rotations about the facet edge direction), the facet edges are free to rotate. For a connection detail of larger stiffness against rotations, the facet edges are more restrained against rotation. In that case, the connection detail will be loaded by bending moments from the facet edges.

3.1 Connection stiffness parameters

Since the stiffness characteristics of the physical connection detail have a significant role in the local support of each plate shell facet, these stiffness characteristics must be reproduced with adequate precision in the FE model.

Since we wish to have a relatively simple description of the stiffness components, a linear correlation is assumed to exist between the various types of movement in the connection and its resistance, so that the connection detail's stiffness components can be described by linear springs – translational and rotational. The consequences of a possible non-linear stiffness behaviour (for example load-dependent stiffness, creep, and changes due to wear) will be discussed where relevant in the subsequent chapters.

The most important stiffness components are shown in Figure 3.1. They are

- a *rotational stiffness* k_m , linking the bending moment m_{22} to the rotation of the plate edge φ , and
- an *axial stiffness* k_n , linking the in-plane force n_{22} to the plate's movement in its own plane, perpendicular to the edge.

These two stiffness components will be discussed more into detail further down in this section.

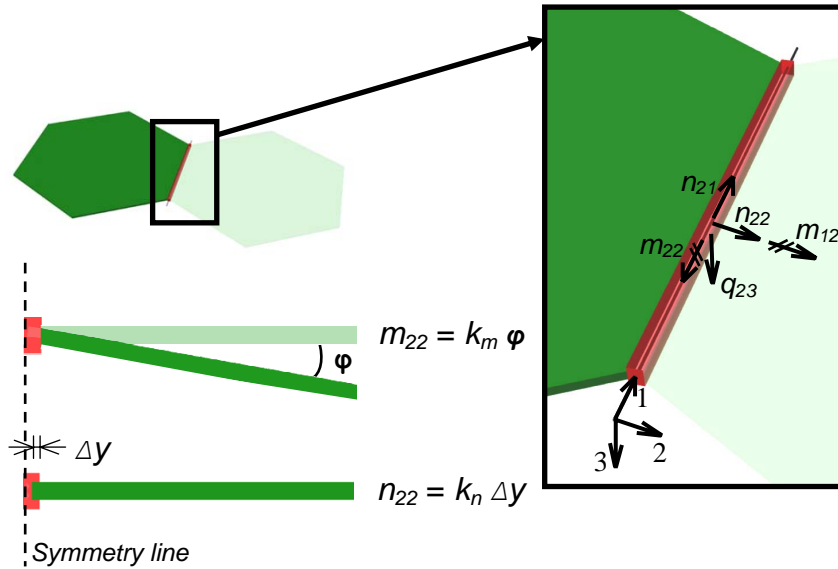


Figure 3.1: Definition of the two most significant stiffness components in the connection; rotational stiffness k_m and axial stiffness k_n . The red block represents the physical connection detail. The terms refer to *local directions*, relative to the regarded facet edge.

In addition to the rotational stiffness k_m and axial stiffness k_n the connection will also have a finite stiffness against other deformations.

- A stiffness in the connection detail against curvature of the plate edge (primarily associated to m_{11}). Depending on the connection design, this is most likely negligible compared to the stiffness of the plates themselves.

- A stiffness against in-plane shear displacements in the connection $k_{v,i}$.
- A stiffness against out-of-plane shear displacements in the connection $k_{v,o}$.

On page 29 in Footnote 3 a comparative study suggests that an imprecise reproduction of the shear stiffness parameters in a FE model of a plate shell, results in relatively small errors on the stresses and buckling load.

The two key stiffness parameters are assumed to be the rotational stiffness k_m , and the axial stiffness k_n .

Rotational stiffness k_m

As illustrated in Figure 3.1 the rotational stiffness k_m links the bending moment m_{22} to the rotation of the plate edge φ . If k_m is small, the plates will act as if connected to each other by a line hinge, and almost no bending moment m_{22} will be transferred between the plates. If k_m is large, a certain amount of bending moment m_{22} will be present in the connection.

If k_m is so large that the connection attracts significant bending moments, the detail must also be strong enough to be able to transfer them.

Referring to the definition of k_m (in Figure 3.1), this parameter ties the bending moment m_{22} in a connection to *half* of the sum of the connected plates' edge rotations. It has been defined this way because in a design load case two adjacent plates will most likely have similar edge rotations. If the plates do not rotate similarly, for instance if one of the plates is smaller than the other or affected by a smaller load, the connection detail will rotate, so that both plates have similar rotations relative to the connection.

Axial stiffness k_n

As illustrated in Figure 3.1, the axial stiffness k_n ties the normal force n_{22} in a connection to half of the sum of the connected plates' in-plane movement, perpendicular to the connection.

The axial stiffness k_n primarily has influence on two behavioral issues: (1.) the in-plane movements when straight plate edges transfer axial in-plane forces from the overall shell action, and (2.) the tendency of straight plate edges to deform (curve).

The first issue has little effect on the stress distribution in a linear calculation of the structure. In a non-linear analysis, however, the stiffness against in-plane movements of the plates seems to have an effect on the buckling load. This effect is studied in Chapter 6.

The second of the two issues is clarified in the following: when the edge of a facet curves out of the facet plane, the distance to the edge of the neighbouring plate will vary along the edge, because of the geometric conditions. The principle is illustrated in Figure 3.2. This means that if the plate edge curves, the connection detail will be affected by in-plane deformations perpendicular to the edge. Therefore, if the connection detail has a large stiffness against these deformations (i.e. axial stiffness k_n), the plate edge will be somewhat restrained from curving.

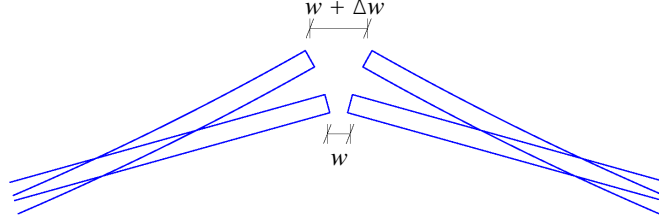


Figure 3.2: The distance between the facet edges change when the edge deforms out of the facet's plane.

Parameter values

In Chapter 7 three different connection details are suggested, each of them with advantages and drawbacks. There are two variants of each detail. The stiffness parameters of these six details are estimated and discussed in Chapter 7. The parameters are summarized in Table 3.1. These values are used in the FE analysis of plate shells throughout the thesis. (The order in which the connection details are listed in the table is determined by certain aspects of their structural behaviour – it thereby differs from the order in which the details are described in Chapter 7.)

An additional variant has been added in Table 3.1 for comparison purposes: a butt joint of glass, with the same geometry as the listed glued butt joints (i.e. with a joint thickness of 15mm , and a joint width of 10mm – see page 90 in Section 7.4).

Illustrations of the three connection details, taken from Chapter 7, are shown in Figure 3.3.

| Connection detail | k_m (kN) | k_n (kN/mm^2) | $k_{v,i}$ (kN/mm^2) | $k_{v,o}$ (kN/mm^2) |
|-------------------------------|-------------------|------------------------|----------------------------|----------------------------|
| Glued-in line hinge | 0.6 | 5 | 1 | 6 |
| Glued-in plate (3mm aluminum) | 16 | 5 | 1 | 6 |
| Glued butt joint | | | | |
| – $E_{adhesive} = 1kN/mm^2$ | 71 | 3.8 | 1.0 | 1.0 |
| – $E_{adhesive} = 2.5kN/mm^2$ | 176 | 9.4 | 2.6 | 2.6 |
| Friction connection | | | | |
| – Klingsil | 100 | 0.5 | 0.08 | 1 |
| – EPDM | 5 | 0.02 | 0.02 | 0.1 |
| Glass joint | 4.1×10^3 | 220 | 86 | 86 |

Table 3.1: Estimated stiffness parameters for six variants of connection details, plus a pure glass joint. The values are summarized from Chapter 7.

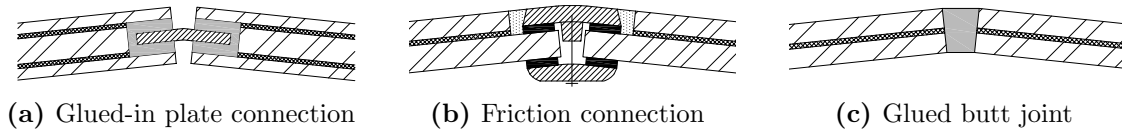


Figure 3.3: Three connection details suggested in Chapter 7.

3.2 FE modelling technique

The plate shell facets are modelled by surface elements, characterized by a mid-plane and a thickness. Strains are thereby assumed to vary linearly through the plate thickness. Since the facets are subjected to bending as well as in-plane forces, it is appropriate to model them by *shell elements* (an element type which includes both types of behaviour).

The connection detail's stiffness parameters are implemented in the FE model by reducing the size of each facet, so that a small gap exists between the facet edges, and then adding a strip of elements which connects the facets. The width, thickness and material characteristics of the connecting strip of elements are chosen, so that the strip represents the stiffness of the connection detail. This procedure is described in detail in Section 3.2.1.

The plate shell models' boundary conditions are modelled as infinitely stiff supports (against translations but not rotations). The physical supports of an actual plate shell will have finite stiffness against movements. However, it has not been found necessary to model these, as the structure's maximum stresses are typically not located near the ground plane. If necessary, the same procedure as the modelling of connections can be applied to model the supports; a strip of elements can connect the external support with the structure, and the characteristics of these elements can be chosen so that they represent the physical support detail.

In Section 3.2.2 the FE model of a specific plate shell is described in detail. This model is used for FE analysis throughout the report.

The convergence of the resulting stresses is discussed in Section 3.2.3. This discussion leads to general suggestions about element size.

3.2.1 Modelling of connections

In all FE calculations in the present study the connection stiffness parameters are implemented in the FE model by adding a thin strip of elements between the glass facets, illustrated by the grey areas in Figure 2.11f (page 22). This element strip is referred to as a *joint strip* in the following. The width, thickness and material characteristics of the joint strip are chosen, so that the joint strip represents the requested stiffness. The connection stiffness parameters were introduced in Section 3.1.

In this section the following issues are addressed:

- How the parameters of the joint strip are chosen, so that the joint strip represents the desired connection stiffness parameters.

- The accuracy of this representation of the connection stiffness.
- The parameters used in this thesis.

The rotational stiffness, k_m , of the joint strip can be shown to be given by¹

$$k_m = \frac{1}{6} \frac{t_j^3}{w} E_j \quad (3.1)$$

where k_m is defined as given in Figure 3.1 (page 24), t_j is the thickness of the joint strip elements, w is the width of the joint strip (i.e. distance between the plate edges), see Figure 3.4. E_j is the E-modulus of the joint strip elements.

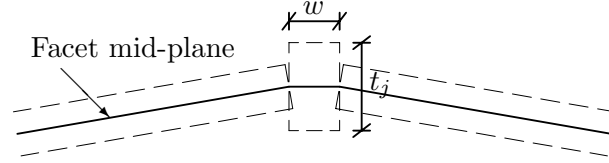


Figure 3.4: Section perpendicular to a joint line.

In (3.1) a plane stress distribution is assumed, so Poisson's ratio for the joint strip elements, ν_j , should be set to zero. The joint material is modelled as linear elastic and isotropic.

The axial stiffness, k_n , of the joint strip is given by²

$$k_n = \frac{2t_j}{w} E_j \quad (3.2)$$

The shear stiffness parameters are found correspondingly:

$$\begin{aligned} \text{In-plane shear stiffness:} \quad k_{v,i} &= \frac{2t_j}{w} G_{j,12} \\ \text{Out-of-plane shear stiffness:} \quad k_{v,o} &= \frac{2t_j}{w} G_{j,13} \end{aligned} \quad (3.3)$$

In (3.3) $G_{j,12}$ and $G_{j,13}$ are the shear-moduli for in-plane and out-of-plane displacements respectively, for an orthotropic material (in a shell element). If the joint strips are modelled with an isotropic material, we have

$$G_{j,12} = G_{j,13} = G_j = \frac{E_j}{2(1 + \nu)} \quad (3.4)$$

For a connection design with given stiffness parameters, the joint strip width, thickness and material parameters can be chosen so that the connection's stiffness parameters are represented by the joint strip elements.

¹This is shown by considering the resistance in a plane section of the element strip against a small mutual rotation of the connected plates. Effects from the initial angle between the connected plates is considered negligible. A plane stress distribution is assumed.

²This is shown by considering the resistance in a section of the element strip against a small in-plane movement of the connected plates, perpendicular to the plate edge/joint.

If the modelled joint material is *isotropic*, only two of the four stiffness parameters can be correctly reproduced. The remaining two parameters will be implicitly given. In section 3.1 it was argued that the rotational and axial stiffness parameters (k_m and k_n) were the key parameters in determining the structural behaviour. By choosing a joint strip width w , and using (3.1) and (3.2) we get for an isotropic joint

$$t_j = \sqrt{12 \frac{k_m}{k_n}} \quad (3.5)$$

and

$$E_j = k_m \frac{6w}{t_j^3} \quad (3.6)$$

The resulting shear stiffness parameters are then implicitly given by (3.3), where $G_{j,12} = G_{j,13} = \frac{E_j}{2}$ since Poisson's ratio is set to zero.

If the joint strips are modelled with an *orthotropic* material, the in-plane and out-of plane shear-moduli can be chosen independently of the E-modulus, so that $k_{v,i}$ and $k_{v,o}$ can be reproduced explicitly. From (3.3) we get

$$\begin{aligned} G_{j,12} &= k_{v,i} \frac{w}{2t_j} \\ G_{j,13} = G_{j,23} &= k_{v,o} \frac{w}{2t_j} \end{aligned} \quad (3.7)$$

Comparative numerical tests have been run on two plate shell models with isotropic and orthotropic joint strip material respectively (and otherwise identical properties), show a maximum error of 5% on linear stresses, and 4% on the buckling load when using the isotropic material³. A maximum error of 5% is considered negligible. The joint strips are therefore modelled by an *isotropic* material in all analysis in this thesis. (Some combinations of connection stiffness parameters *may* result in larger errors.)

The parameters listed in Table 3.2 can be used in a FE model to represent the connection details given in Table 3.1 (page 26). w has been set to 10mm. ν is set to zero to model a plane stress distribution (except for the *glued butt joint*, see below). t_j and E_j are determined using (3.5) and (3.6) respectively. (The pure glass joint is left out.) The joint material is isotropic.

For the *glued butt joint*, the modelled joint strip resembles the actual connection detail, and therefore the joint strip is given the stiffness parameters of the adhesive directly.

³ The plate shell models used for the comparison are **FacC_ImpA_Nonuni** and **FacC_ImpA_Nonuni_Ort** – both models are described in detail in Appendix A. These models apply the *glued-in plate* connection detail (see Section 7.2, page 84). The isotropic joint material models the shear stiffness parameters with relatively large errors. (The actual *glued-in plate* connection: $k_{v,i} = 1kN/mm^2$, $k_{v,o} = 6kN/mm^2$. The isotropic representation of the connection yields: $k_{v,i} = 2.5kN/mm^2$, $k_{v,o} = 2.5kN/mm^2$.) A non-uniform load is chosen as the load applied to the structure, since a non-uniform load results in larger shear forces in the connections than a uniform load, thereby “activating” the shear stiffness more. A linear calculation has been carried out, and the principal stresses have been compared in 3 different locations; at a facet mid-point, at a facet edge mid-point, and at a connection end-point. This comparison showed a maximum error of 5% on the stresses (the largest error was located at a connection end-point). Also, a geometrically non-linear calculation has been carried out on the two models. The buckling load of the models were compared; the difference was 4% (see also page 79).

The joint strips are interrupted at a small distance (80-100mm) from the facet corners, so that the corner areas are not connected (see the detail to the left in Figure 3.5). The reason for this is discussed in Sections 4.2 and 5.1.

| Connection detail | w (mm) | ν (-) | t_j (mm) | E_j (kN/mm ²) |
|--------------------------------------|-------------|--------------|---------------|--------------------------------|
| Glued-in line hinge | 10 | 0 | 1.2 | 20.8 |
| Glued-in plate (3mm aluminum) | 10 | 0 | 6.15 | 4.07 |
| Glued butt joint | | | | |
| – $E_{adhesive} = 1\text{kN/mm}^2$ | 10 | 0.45 | 15 | 1.0 |
| – $E_{adhesive} = 2.5\text{kN/mm}^2$ | 10 | 0.45 | 15 | 2.5 |
| Friction connection | | | | |
| – Klingsil | 10 | 0 | 49 | 0.051 |
| – EPDM | 10 | 0 | 55 | 0.0018 |

Table 3.2: Values to be used in a FE model of a plate shell, to model the connection stiffness parameters summarized in Table 3.1 (page 26). w and t_j are defined in Figure 3.4.

Precision of the joint modelling technique

The precision of the joint modelling technique described above has been investigated by running simple tests in ABAQUS: two rectangular glass plates were connected by a joint strip with a given width, thickness and material parameters, and via the plates, the joint was subjected to uniform bending and uniform tension. These tests showed that the joint strip provides the expected rotational and axial stiffness⁴. A coarse element mesh in the joint, even with poorly shaped elements (i.e. with large side-length ratio), provides good precision for the rotational and axial stiffness. For linear FE analysis, one element across the joint width is therefore regarded as sufficient.

While the joint strips serve as a good representation of the connection stiffness parameters, the *sectional forces* are calculated with less precision⁵. Especially near the ends of the joint strips, the sectional forces in the joint strip may be too erratic to be of use. In this case, the sectional forces in the glass edge can be used instead.

Naturally, the *stresses* in the joint strip elements should not be used, as the thickness of the elements has no direct physical meaning.

⁴The following parameters were varied in the tests. Joint width (10mm and 20mm). Thickness and E-modulus (chosen according to the six sets of parameters in Table 3.2). Number of element over the width (1, 2 and 4 elements). Number of elements along the joint (10 and 100 elements). All the tests showed errors of less than 2% on the expected stiffness.

⁵In a FE calculation, sectional forces are derived from the structural displacements/strains, and are therefore always equally or less precise.

3.2.2 Description of plate shell FE model

The plate shell structure shown in Figure 3.5 has been modelled in ABAQUS, and used for structural analysis repeatedly throughout the thesis. The model is referred to by the name **FacC**. This model, and other models referred to in this thesis, are described in detail in Appendix A.

Model **FacC** is a convex plate shell structure, where all facets are tangent planes to a paraboloid of revolution. The structure's height is 1.9 meters, and the maximum span is 11.5 meters. The facets measure roughly 2 meters diagonally. The angle between neighbouring facets is approximately 12 degrees.

The facets are all 15mm monolithic glass plates⁶, modelled by a linear elastic, isotropic material with an E-modulus of 70GPa, and Poisson's ratio of 0.22.

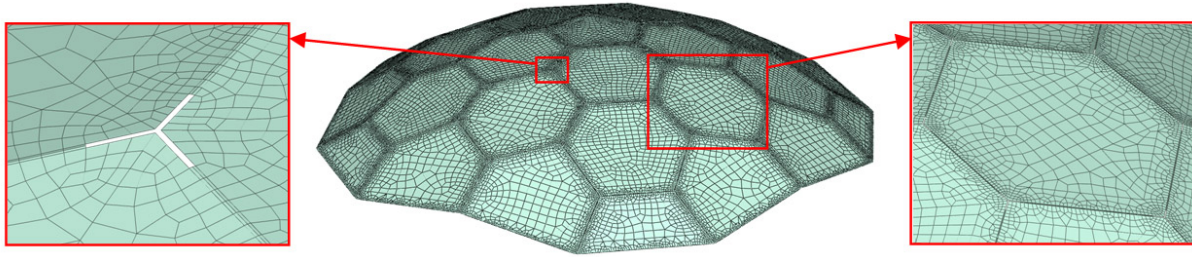


Figure 3.5: Plate shell model **FacC**, modelled in ABAQUS.

The structure is supported against translations in all directions along the boundary.

In the performed *linear analysis* (see Chapters 4 and 5), the structure is loaded by two load cases; a uniform load case, where a uniform pressure load of $1.0kN/m^2$ (directed inwards) is acting on the entire structure, and a non-uniform load case, where the same load is acting on half of the structure.

In the performed *non-linear analysis* (see Chapter 6), the structure is also loaded by both a uniform load case and a non-uniform load case. The uniform load case is a uniform distributed vertical load of $100kN/m^2$ (directed downwards). In the non-uniform load case, the same load is acting on half of the structure, and the other half is loaded by a vertical load of $25kN/m^2$ (directed downwards).

All structural parts are modelled with S4 shell elements, which is a general-purpose shell element in ABAQUS⁷. All calculations are linear, corresponding to small deformations, unless something else is mentioned.

The model **FacC** in Figure 3.5 was produced by a student, T. Isgreen [31], before the completion of the *pyFormex* script (see Section 2.2, page 18). The supported boundary of the structure is not lying in one single plane⁸, and the joint strips are modelled a little

⁶For a discussion of the modelled glass thickness, see Section 8.2.1.

⁷S4 is a finite-membrane-strain element, which uses thin shell theory (i.e. ignoring out-of-plane shear deformations) for small shell thickness, and thick shell theory (i.e. including out-of-plane shear deformations) for larger shell thickness. ABAQUS decides whether a thickness is small or large, compared to a typical geometric length of the structure [2].

⁸Comparative studies indicate that this has negligible effect on the shell action in the structure, and

differently than the modelling procedure described in Section 3.2.1⁹. All other plate shell models in the thesis have been generated using the *pyFormex* script, and therefore have the supported boundary lying in one single plane, and joint strips defined as described in Section 3.2.1. The effects of the above mentioned differences in modelling are considered negligible.

3.2.3 Convergence of stresses

The discretization of real, continuous, structural parts into finite elements causes discretization errors. Generally, the smaller elements, the smaller discretization error [20].

To keep the number of nodes, and thereby the calculation time, as low as possible, we wish to use finite elements which are as large as possible, while giving a stress response of an adequate precision. Especially areas of large stress variations need a fine mesh (i.e. small elements compared to the geometric dimensions) for the stress response to be well described.

A model of a plate shell may have many areas with large stress variations – the corner areas of each facet may be exposed to stress concentrations near the end of the joint strips. However, the number of nodes will become far too large if all these stress concentrations are to be analyzed with high accuracy. Instead, a relatively coarse mesh can be used in general (8-12 elements per facet edge – see Figure 3.6, left), and a few facet corners can be meshed with very small elements (Figure 3.6, right). A preliminary analysis with a semi-fine mesh (Figure 3.6, middle) can identify which corners are most likely to have the largest stress concentrations, and these corners can be meshed with small elements.

The procedure described above is possible, because even a very coarse mesh (of 6-8 elements per facet edge) has converged in terms of deformations¹⁰, with errors of less than 2%. The structural parts around an area with a fine mesh will therefore give the correct structural resistance, even with a relatively coarse mesh.

In the present study, convergence of stresses has been verified in the studied models by re-running a given analysis with a finer mesh in the area of focus, and checking that the stresses have not changed more than 5% when the element side length is halved. In cases where the stresses have not converged, this is explicitly mentioned in connection with the referred results.

only influences the bending stresses to the extent that the lowest facets are smaller or larger, given an alternative boundary cut.

⁹The joint strips in the model in Figure 3.5 are divided into two parts along the joint centre line, and each half is in the same plane as the adjacent facet. Comparative studies indicate that this has negligible effect on the resulting stiffness of the joint strip. The choice of joint parameters is made using the modelling technique described in Section 3.2.1.

¹⁰This has been tested using the following plate shell models: **FacC_Plate**, **FacC_hinge**, **FacF_Plate** and **FacStar** (a description of the models can be found in Appendix A). A linear analysis has been run on each model, using a relatively coarse mesh (6-8 elements per facet edge). Subsequently, a linear analysis has been run on the same model, but with a relatively fine mesh (26-30 elements per facet edge). The calculated deformations and rotations have then been compared for the two mesh densities. The maximum difference found in any of these test was 1.5%.

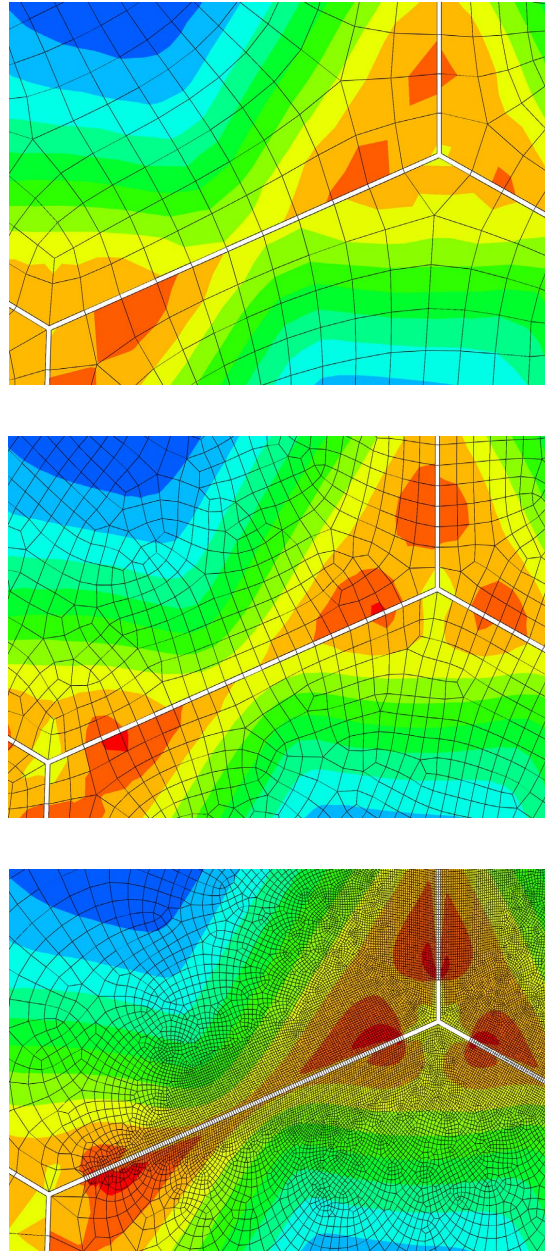


Figure 3.6: Stress distribution in a detail of a model, for varying element sizes. Stress component: Largest principal stress S_1 in the upper surface. The stress contour scale is identical in the three plots.

Chapter 4

Shell action in plate shells

In this chapter and Chapter 5 the structural behaviour of plate shells is studied, assuming small displacements. The present chapter focuses on shell action (i.e. in-plane forces) in the structure, and Chapter 5 focuses on bending moments.

Section 4.1 sums up some information about shell structures in general.

In Section 4.2 the shell action in plate shell structures is studied. Initially, the different structural effects are described *physically*, in order to provide the design engineer with an intuitive understanding of the structure's behaviour. Section 4.2.1 presents FE analysis results of a plate shell model for 6 different sets of connection stiffness parameters. In Section 4.2.2 these results, and results from other plate shell FE analysis, are compared to the shell action in similar smooth shells. Finally, in Section 4.2.3 a method is suggested for estimating in-plane forces in a plate shell. This method is developed to facilitate an overview of the shell action in a plate shell structure in a preliminary design phase, without the need for a full FE analysis of the structure.

4.1 Shell structures

Consider a curved structural surface. The surface is structurally effective if the curvature and support conditions enables efficient in-plane forces to develop in the surface [49]. In this case, the structural surface is termed a *shell structure*. The in-plane stiffness of a thin-walled structural surface is many times greater than the bending stiffness, and therefore the displacements of a shell structure are very small, given the amount of structural material.

The thickness of a shell structure is typically determined by its buckling behaviour (see Section 6.1), and in some cases also by bending moments near supports or free edges.

The direction and magnitude of forces in a shell structure depend on the structure's shape and support conditions. It is generally difficult – if not impossible – to predict the flow of forces by hand calculations. For some simple shell shapes, such as spherical domes, analytical expressions exist for a few simple load cases (see for example [49] and [52]), but generally, FE analysis tools are necessary in order to determine the structural response of a shell structure.

4.2 In-plane forces in plate shell structures

A plate shell structure is a structural “hybrid”, carrying load by both shell action and bending action. The overall structural behaviour of a plate shell structure shares an important characteristic with a shell structure: the load is transformed into in-plane forces, and is thereby carried to the supports by shell action. This entails a high structural efficiency, which can be observed by comparing the shell displacements¹ of a plate shell to the displacements of an equivalent smooth shell²; the shell displacements of a plate shell is typically just 2-3 times larger than the displacements of an equivalent smooth shell³. If a vertical load on a given plate shell were to be taken to the supports by a single, plane plate with the same span as the plate shell (i.e. same span, but pure bending action), the plate thickness would have to be 40-60 times larger than the facet thickness, to have the same deflection⁴.

Locally, the facets in a plate shell structure are subjected to plate bending, carrying the load to the facet edges. At the facet edges, the load can be transformed into in-plane forces, *if* the structure’s in-plane stiffness is sufficient. This transformation is statically indeterminate, since the out-of-plane forces at the facet edges can also be balanced by out-of-plane forces in the adjacent facets, corresponding to an overall bending behaviour of the structure. This behaviour leads to much larger displacements in the structure. Section 5.2 describes this behaviour more into detail. In the following, the structure’s in-plane stiffness is assumed to be so much larger than the overall bending stiffness that no overall bending behaviour occurs, meaning that all out-of-plane shear forces are transformed into in-plane forces at the facet edges.

The transformation of out-of-plane load into in-plane forces is described in Table 4.1.

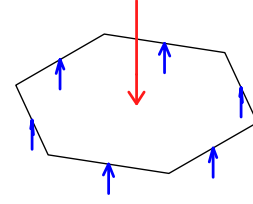
¹The term “shell displacements” refers to the displacement of the mid-point of a facet edge in the plate shell. This area gives the best account of the structure’s shell action, as it is an area only slightly affected by plate bending in the facets, or the tendency to uplift in the facet corners, as it will be explained later on.

²“Equivalent smooth shell” in this context means that the shell geometry is similar, but smooth instead of faceted, and that the thickness, material, support conditions and loads are the same.

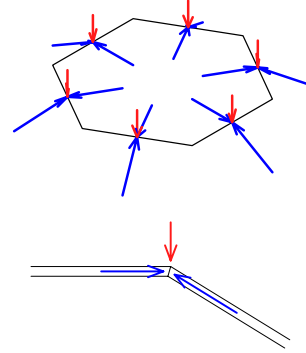
³This comparison has been made on three plate shell models and their equivalent smooth shells. The models are **FacC_plate**, **FacF_plate** and **FacStar**. The models **FacC_plate** and **FacF_plate** have the same equivalent smooth shell; the model **Smooth**. The equivalent smooth shell to **FacStar** is the model **Smooth_FacStar**. The models are described in detail in Appendix A. The load is a uniform distributed pressure load of $1kN/m^2$, directed inwards. The maximum deflection of the facet edge mid-points in each plate shell is compared to the maximum deflection of the equivalent smooth shell. The maximum deflections are: $u_{max,FacC} = 0.096mm$, $u_{max,Smooth} = 0.044mm$. $u_{max,FacF} = 0.13mm$. $u_{max,FacStar} = 0.059mm$. $u_{max,Smooth_FacStar} = 0.031mm$.

⁴This can be realized by comparing the deflections stated in Footnote 3 to the linear deflections of a circular plate, using the expression $u_{max} = \frac{(5+\nu)qR^4}{64(1+\nu)D}$, where q is the load, ν is Poisson’s ratio, R is the plate radius and D is the flexural rigidity of the plate, $D = \frac{Et^3}{12(1-\nu^2)}$. E is the E-modulus of the plate material and t is the thickness. [52]

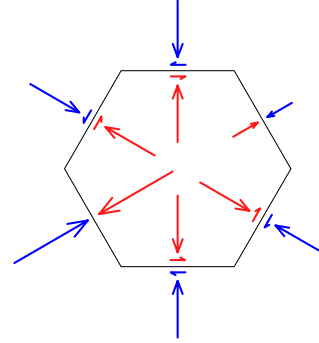
Out-of-plane load on a facet causes bending in the facet. Via plate bending, the load is transferred to the facet edges as out-of-plane shear. The bending moments are described more into detail in Section 5.1. The principle sketch to the right shows the load resultant (red for action) and the out-of-plane shear force resultant for each facet edge (blue for reaction). (Illustration from [12].)



The out-of-plane shear forces at the facet edges are transformed into in-plane forces in the facet and the neighbouring facets⁵. These in-plane forces are perpendicular to the facet edges, and are referred to as the *axial in-plane forces*. The out-of-plane shear forces (and the balancing axial in-plane forces) are not uniformly distributed along the facet edges. (Illustration from [12].)



When the axial in-plane forces in a facet are not in equilibrium, the resulting in-plane force in the facet will be transferred to the supporting plates by in-plane shear along some of the edges⁶. A plate shell structure can be shaped and designed so that these in-plane shear forces are negligible for certain loading situations, for example for the structure's self weight.



When a facet is subjected to bending, the facet edges will deform (curve), since the connection detail and supporting plates have a finite stiffness. As an edge deforms out of the facet's plane, the distance to the neighbouring edge will change, because the plates have a mutual angle (see the sketch to the right). Since the connection detail has a stiffness against this movement (strains perpendicular to the longitudinal direction of the connection), in-plane forces will develop at the facet edges, perpendicular to each edge, adding to the axial in-plane forces described above. The resultant of these forces (summed up over an edge) is zero, but locally they can become significant if the stiffness in the connection detail is large.

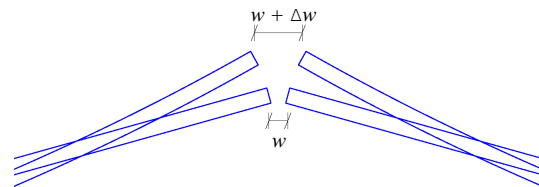


Table 4.1: Transformation of external load into shell action in a plate shell.

As it appears from Table 4.1, the in-plane forces are distributed in the facets (as opposed to a triangulated lattice structure, where the shell action is constituted by concentrated forces in the bars and nodes). At the facet edges of a plate shell facet, in-plane axial forces (i.e. perpendicular to the edge) and in-plane shear forces are acting, balanced by the external load and the neighbouring facets.

Because the facet corners have a tendency to lift, and the connection detail opposes this movement, concentrated in-plane forces will develop in the corner areas, near the ends of the connected part of an edge (referred to as a *connection end*). These in-plane stress concentrations are reduced if the connections are shorter than the facet edges, leaving an area in the corner zones unconnected and free to lift, see Figure 4.1. The reason for the facet corners' tendency to uplift, and the consequences in terms of the bending moments in the facets, are studied in Section 5.1.

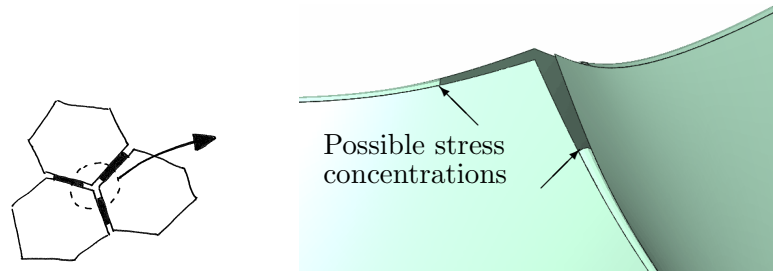


Figure 4.1: Deformed plot of a vertex in a plate shell. In-plane stress concentrations will develop at the ends of the connections.

The axial stiffness k_n of the connection detail is defined in Section 3.1 (page 24). The stress concentrations at the connection ends depend on the size of k_n ; larger k_n -values result in larger resistance against uplift of the corners, and thereby larger in-plane stress concentrations.

4.2.1 Linear FE study of plate shell

The plate shell model in Figure 4.2, model **FacC**, has been analyzed in ABAQUS for six different sets of connection stiffness parameters. A detailed description of the model and its six variants can be found in Appendix A. The six variants use the six connection details in Table 3.1 (page 26).

The in-plane forces along the facet edge marked in Figure 4.2 are in focus. That particular edge is chosen, because the largest in-plane forces in the structure for the applied load occur there.

⁵This is only possible if the structure is adequately shaped and supported to work as a shell structure

⁶The relative size of the axial in-plane force resultants depends on a number of factors. If the angle between the facet and the supporting plates is varying from plate to plate, the axial in-plane force resultant will also vary (because of the force equilibrium shown elsewhere in the table (Table 4.1)). Also, the axial force may vary because of the nature of the load. Finally, the relative size of the out-of-plane shear force resultants (and thereby the axial in-plane forces) is statically indeterminate, and is therefore dependent on the stiffness of the supporting plates, and the facet itself.

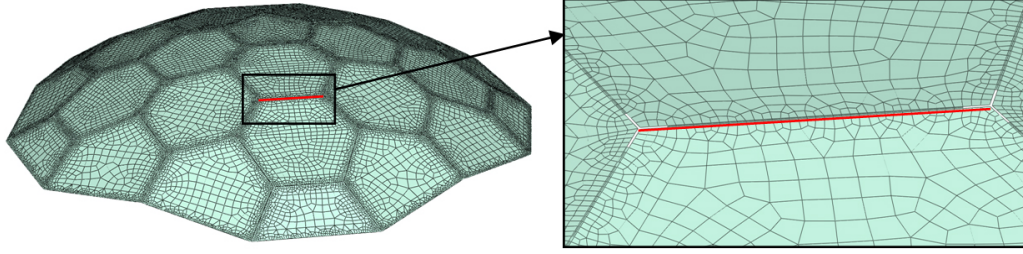
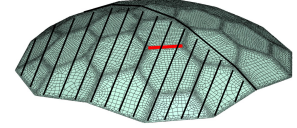


Figure 4.2: In-plane forces are examined along the marked (red) glass edge. Model: **FacC**.

The structure is subjected to two different load cases. The first load case (in the following termed the *uniform load case*) is a pressure load of $1kN/m^2$ directed inwards on the entire structure. In the second load case (the *non-uniform load case*), the same pressure load is acting on only half of the structure – the loaded part is marked in the image to the right.



The uniform load case is defined as a uniform pressure load because this results in similar bending action in facets of similar size, regardless of their orientation in space. It has been defined in this way, even though such a load is not physically realistic, because the intention of the investigation is to study the various structural effects of the plate shell system, rather than determine a specific degree of utilization. Likewise, the non-uniform load case is defined so that it represents a asymmetric loading situation in general, and is not a physically realistic load case.

In model **FacC**, the joint element strips representing the connection detail, are interrupted $100mm$ from the facet corners, so that the corner areas are not connected (see Figure 4.2). Therefore, in the following graphs showing the in-plane forces along the marked glass edge, the first 3 and last 3 force values are from nodes on the free part of the facet edge, near the facet corners.

As described in Section 3.2.2, the maximum span of the shell is $11.5m$, the height is $1.9m$, the facets measure roughly $2m$ in diameter, and the facet thickness is $15mm$.

The axial and shear in-plane forces, n_{22} and n_{12} , along the marked glass edge (see Figure 4.2) are plotted in the graphs in Figure 4.3. The orientation of n_{22} and n_{12} relative to the studied edge is defined in Figure 3.1, page 24. The rotational stiffness k_m and axial stiffness k_n of the connection as well as the dimensionless factor $\frac{k_m}{k_n t^2}$ are listed in the graph legend in Figure 4.3.

The force resultants, N_{22} and N_{12} , are found by integration of the in-plane forces along the studied edge, and given in Table 4.2.

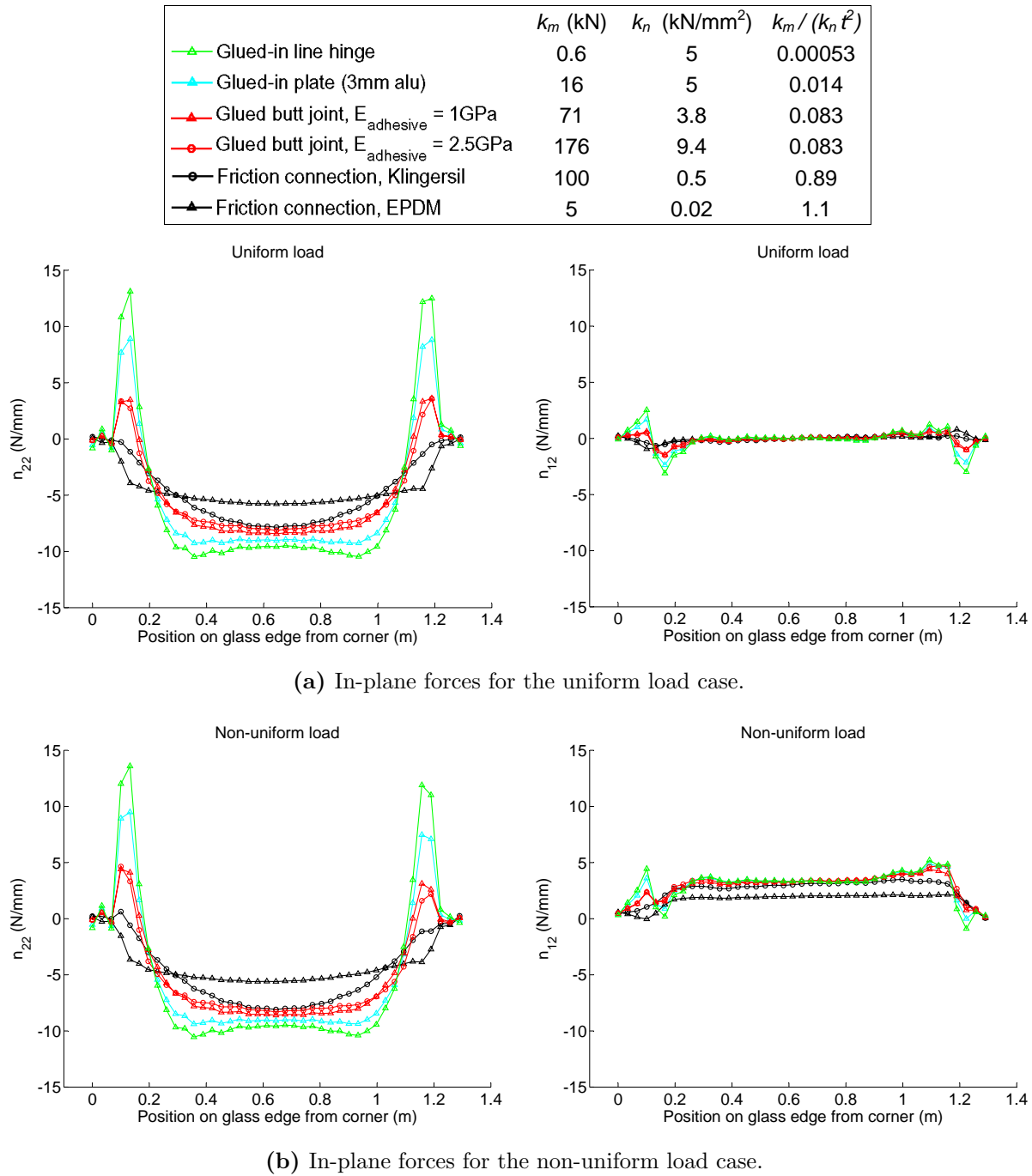


Figure 4.3: Comparison of axial and shear in-plane forces along the glass edge marked in Figure 4.2, for six different connection details.

| Connection detail | Uniform load | | Non-uniform load | |
|-------------------------------|------------------|------------------|------------------|------------------|
| | N_{22} (kN) | N_{12} (kN) | N_{22} (kN) | N_{12} (kN) |
| Glued-in line hinge | -6.6 | -0.12 | -6.5 | 3.9 |
| Glued-in plate (3mm aluminum) | -6.4 | -0.10 | -6.5 | 3.9 |
| Glued butt joint | | | | |
| – $E_{adhesive} = 1kN/mm^2$ | -6.2 | -0.06 | -6.4 | 3.8 |
| – $E_{adhesive} = 2.5kN/mm^2$ | -6.1 | -0.06 | -6.4 | 3.9 |
| Friction connection | | | | |
| – Klingsil | -6.0 | -0.04 | -6.1 | 3.4 |
| – EPDM | -5.7 | -0.03 | -5.4 | 2.2 |

Table 4.2: In-plane force resultants N_{22} and N_{12} , found by integration of the in-plane forces n_{22} and n_{12} plotted in Figure 4.3.

Discussion of the axial in-plane force, n_{22}

When comparing n_{22} for the uniform and the non-uniform load case in Figure 4.3, the distributions can be seen to be very alike. As argued in Table 4.1, n_{22} at a connection depends on the load on the two connected facets. In this case, they are the same in the two load cases, hence the similar n_{22} distribution.

As it appears from the n_{22} distributions in Figure 4.3, the size of the n_{22} peaks at the connection ends is related to the size of the dimensionless factor $\frac{k_m}{k_n t^2}$; the smaller $\frac{k_m}{k_n t^2}$, the larger n_{22} peak. As explained in Table 4.1, these peaks are caused by the connection details' resistance to curving of the facet edges. Larger k_n values result in larger resistance against curving, while larger k_m values results in less tendency for the facet edge to curve, and thereby less resistance. Section 5.1 goes more into detail with this effect.

The axial in-plane force resultant N_{22} (see Table 4.2) is largely independent of the connection stiffness parameters. Therefore, larger n_{22} peaks values at the connection ends results in larger n_{22} forces at the middle of the edge.

The n_{22} peak forces in the two models with the largest peak values (the models with the *glued-in plate* connection and the *glued-in line hinge* connection respectively) have not converged fully. However, based on the experimental data on a physical *glued-in plate* connection (referred to in Section 7.2), it is estimated that load dependent creep will cause the large stress peaks to reduce somewhat. For this reason, in the present context the n_{22} peaks are merely recognized as being present for these types of connection designs, and their actual value must be looked into by additional studies taking the creep into account.

The distance from the connection ends to the facet corners influences the n_{22} distribution. This is not investigated into detail in this context, but work with various plate shell models has indicated that the n_{22} peak is *reduced* when the free edge length at the corners is increased. This is also in concordance with the expectations, since a larger free edge

length permits more movement of the facet corner, and thereby less restraint of the edge. However, at the same time the force resultants must be transferred between the facets over a smaller connected length, and this may affect the general stress level.

Discussion of the in-plane shear force, n_{12}

In the uniform load case, the in-plane shear force resultant N_{12} is almost zero (see Table 4.2). There are relatively small n_{12} peaks at the connection ends, the value of which depends on the connection stiffness parameters. These n_{12} peaks stem from the turning of the large tension forces at the connection ends (see the n_{22} distribution in Figure 4.3 and the vector plot in Figure 4.4 below).

In the non-uniform load case, the in-plane shear force resultant N_{12} is not zero. The value is about 60% of the axial in-plane force resultant N_{22} . N_{12} is smaller for the model with very low k_n value – the *EPDM friction connection* – most likely because the lower stiffness allows the shear forces to become more evenly distributed among the facets' edges.

Illustration of the in-plane forces

Vector plots of principal in-plane forces in the model **FacC_adh1** (this is model **FacC** with the glued butt joint with $E = 1GPa$) are shown in Figure 4.4 for the uniform load case (left) and the non-uniform load case (right).

As the plots illustrate, in the uniform load case, where no resulting in-plane shear force is present, the principal directions of the in-plane forces are parallel and perpendicular to the edge line, except near the tension peaks at the connection end. The maximum and minimum principal in-plane forces are almost equal (except near the the connection end), meaning that the plate is under uniform compression in that area. The vector plot is almost entirely symmetric around the mid-point of the edge line (not visible in the plot).

In the non-uniform load case, the principal axes form an angle of 45 degrees with the edge line. This is because the state of almost uniform compression (where the principal directions are easily turned) is superposed by pure shear (where the principal directions are 45 degrees to the edge loaded by shear). The vector plot is no longer symmetric, but repeats itself when rotated about the mid-point of the edge line (not visible in the plot).

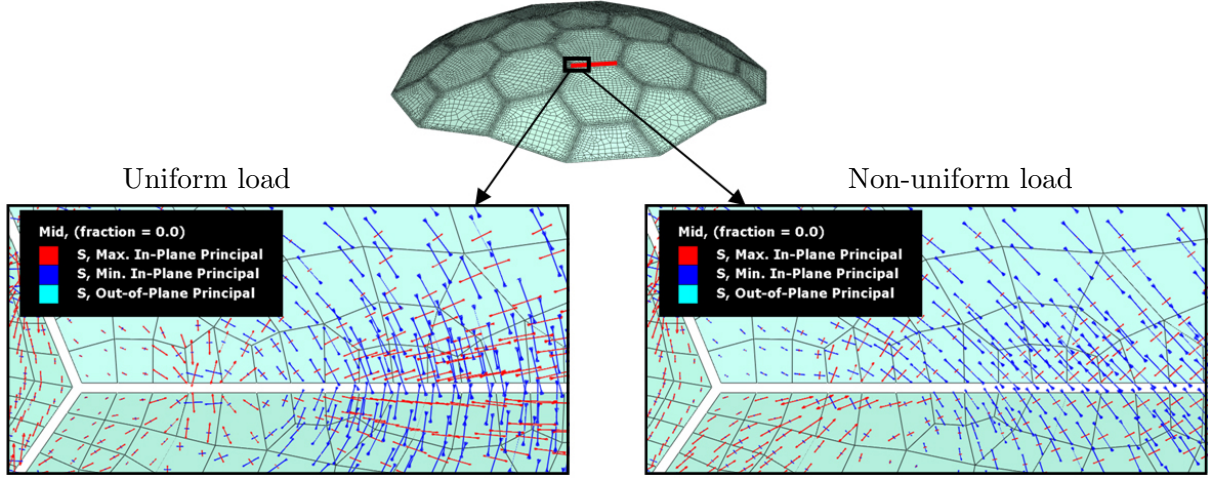


Figure 4.4: Vector plots of in-plane forces near a corner of the studied facet.

4.2.2 Comparison to shell action in smooth shell

In this section, the results presented in Section 4.2.1 (model **FacC**), are compared to the in-plane forces in the equivalent smooth shell structure, model **Smooth**. (For a definition of the term “equivalent smooth shell” see footnote 2.) Also other plate shell models are compared to their respective equivalent smooth shells in the present section.

Table 4.3 sums up some key values for the shell action in the plate shell edge, subject to investigation in Section 4.2.1. These values can be compared to the results in Table 4.4, which states the in-plane forces in the equivalent smooth shell, at a similar⁷ location on the structure.

In Table 4.3, $n_{ij,nom}$ is the nominal value of n_{ij} , found by dividing the force resultant N_{ij} by the edge length, 1.29m. $n_{ij,peak}$ is the largest value of n_{ij} at the edge. $n_{ij,edge}$ is the value of n_{ij} at the edge mid-point.

In Table 4.4, $n_{1,smooth}$ and $n_{2,smooth}$ are the principal in-plane forces (maximum and minimum respectively). $n_{12,smooth}$ is the maximum in-plane shear force, determined by $n_{12,smooth} = \frac{n_{1,smooth} - n_{2,smooth}}{2}$.

The following correlations can be deduced by comparing the results in Tables 4.3 and 4.4:

- The nominal axial in-plane force at the plate shell connection, $n_{22,nom}$, is comparable to the minimum principal force $n_{2,smooth}$ (i.e. largest compression) in the smooth shell.
- The axial in-plane force at the edge mid-point, $n_{22,edge}$, is 1.0 to 2.0 times larger than the minimum principal force $n_{2,smooth}$ in the smooth shell. This ratio depends on the peak-value, $n_{22,peak}$.

⁷The principle stresses are found in model **Smooth** at a point with the same coordinates in the ground plane as the mid-point of the investigated facet edge in model **FacC**.

- For the uniform load case, where the in-plane shear force is negligible in the smooth shell, the nominal in-plane shear force $n_{12,nom}$ in the plate shell is also negligible.
- For the non-uniform load case, the in-plane shear force is non-negligible in both the smooth shell and the plate shell. The in-plane shear force at the facet edge mid-point, $n_{12,edge}$, is 1.4 to 2.4 times larger than the shear force in the smooth shell, $n_{12,smooth}$. This ratio is smallest for the model with very low k_n value – the *EPDM friction connection* – most likely because the lower stiffness allows the shear forces to become more evenly distributed among the facets' edges. $n_{12,edge}$ is independent of the peak value, $n_{12,peak}$ (since the peaks in the two ends cancel each other).

| Connection detail | $n_{22,nom}$ (N/mm) | $n_{22,peak}$ (N/mm) | $n_{22,edge}$ (N/mm) | $ n_{12,nom} $ (N/mm) | $ n_{12,peak} $ (N/mm) | $ n_{12,edge} $ (N/mm) |
|-------------------------------|------------------------|-------------------------|-------------------------|--------------------------|---------------------------|---------------------------|
| <i>Uniform load</i> | | | | | | |
| Glued-in line hinge | -5.1 | 13.1* | -10.0 | 0.1 | 3.1* | 0.1 |
| Glued-in plate (3mm alu) | -5.0 | 8.9* | -9.0 | 0.1 | 2.4* | 0.1 |
| Glued butt joint | | | | | | |
| – $E_{adhesive} = 1kN/mm^2$ | -4.8 | 3.5 | -8.3 | 0.1 | 1.0 | 0.1 |
| – $E_{adhesive} = 2.5kN/mm^2$ | -4.7 | 3.4 | -8.0 | 0.1 | 1.5 | 0.1 |
| Friction connection | | | | | | |
| – Klingsil | -4.7 | –** | -7.7 | 0.0 | –** | 0.1 |
| – EPDM | -4.4 | –** | -5.7 | 0.0 | –** | 0.1 |
| <i>Non-uniform load</i> | | | | | | |
| Glued-in line hinge | -5.0 | 13.5* | -10.0 | 3.0 | 5.2* | 3.4 |
| Glued-in plate (3mm alu) | -5.0 | 9.5* | -9.2 | 3.0 | 4.9* | 3.4 |
| Glued butt joint | | | | | | |
| – $E_{adhesive} = 1kN/mm^2$ | -5.0 | 4.4 | -8.6 | 2.9 | 4.4 | 3.3 |
| – $E_{adhesive} = 2.5kN/mm^2$ | -5.0 | 4.6 | -8.2 | 3.0 | 4.7 | 3.4 |
| Friction connection | | | | | | |
| – Klingsil | -4.7 | –** | -8.0 | 2.6 | –** | 3.3 |
| – EPDM | -4.1 | –** | -5.6 | 1.5 | –** | 2.0 |

Table 4.3: In-plane forces at a glass edge in model **FacC**. The glass edge is marked in Figure 4.2. The used terms are defined in the text above. * This peak value has not converged in the FE model (see page 41). ** No peak value.

| $n_{1,smooth}$ (N/mm) | $n_{2,smooth}$ (N/mm) | $ n_{12,smooth} $ (N/mm) |
|--------------------------|--------------------------|-----------------------------|
| <i>Uniform load</i> | | |
| -4.7 | -5.0 | 0.2 |
| <i>Non-uniform load</i> | | |
| -2.9 | -5.7 | 1.4 |

Table 4.4: In-plane principal forces in model **Smooth** (equivalent smooth shell to model **FacC**).

Figure 4.5 shows a contour plot of the minimum principal stress (i.e. largest compression) in the surface mid-plane of model **FacC_plate** (left) and the equivalent smooth shell, model **Smooth** (right). The structures are loaded by the non-uniform load case (the left half of each structure is loaded by $1kN/m^2$ pressure load, as described in Section 4.2.1). Since the force peaks at the connection ends are not in focus in this plot, the contour scale is adjusted so that only compression forces are shown. The scale is identical in the two plots.

The stresses in the smooth shell can generally be recognized in the middle of the facets in the plate shell. Stresses at the connections are larger, partly because of the developed stress peaks, partly because of the shortened load transfer length, and partly because the stresses are forced to follow certain “paths” (i.e. have certain orientations at the edges – this is studied more closely later in this section). At some edges in the loaded (left) half of the structure, the n_{22} force is superposed by in-plane shear, adding to the principal stress, and forming the dark blue “compression bands” visible in the plot. In the left part of the structure there is no out-of-plane load on the facets, and therefore there are no n_{22} forces at the connections. The only in-plane forces that are transferred across these connections are n_{12} forces.

If a given edge in the plate shell is parallel/perpendicular to a principal force in the smooth shell, that edge will not transfer any n_{12} forces.

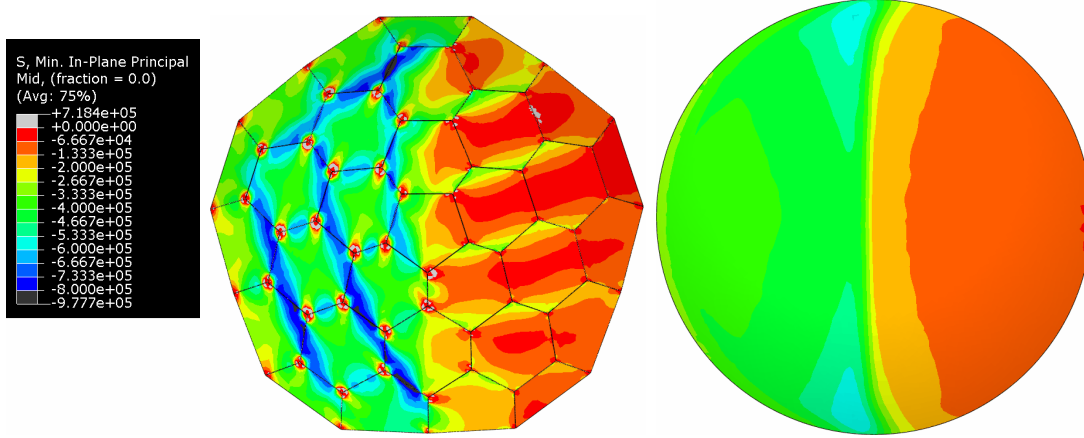


Figure 4.5: Left: Model **FacC_plate**. Right: the equivalent smooth shell, model **Smooth**. Minimum principal stress (i.e. largest compression) in the surface mid-plane (units: $N/m^2 = 10^{-6}N/mm^2$). The contour scale is identical in the two plots.

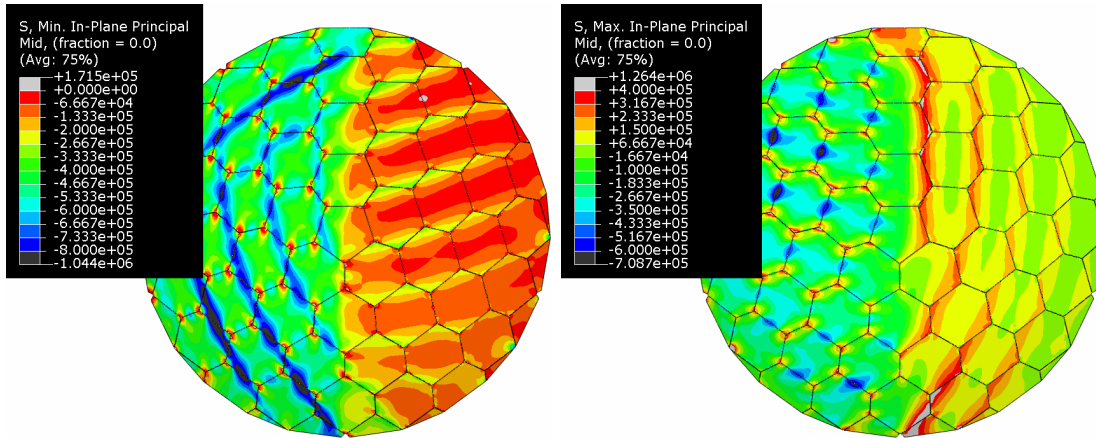


Figure 4.6: Model **FacF_plate**. Minimum (left) and maximum (right) principal stress in the surface mid-plane (units: $N/m^2 = 10^{-6}N/mm^2$).

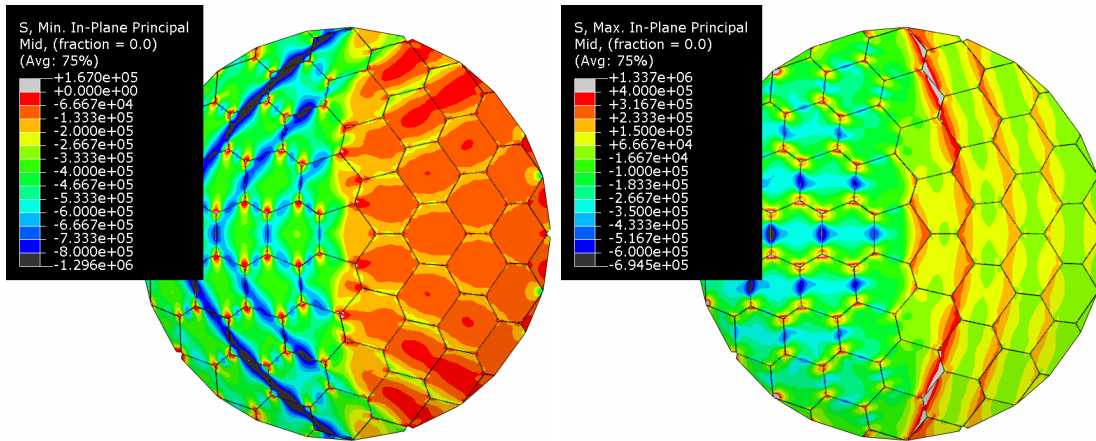


Figure 4.7: Model **FacF_plate**. Minimum (left) and maximum (right) principal stress in the surface mid-plane (units: $N/m^2 = 10^{-6}N/mm^2$). The load is rotated 18 degrees relative to the load case in Figure 4.6.

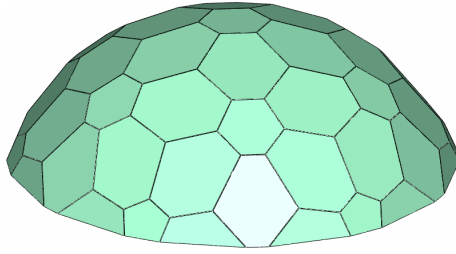
Figures 4.6 and 4.7 show similar plots for model **FacF_plate** – a plate shell structure with the same “average” geometry as model **FacC_plate** in Figure 4.5. The load is also the same, as well as the connection detail and boundary conditions. Only the faceting differs; the principal pattern is the same (geodesic type), but the facets are smaller in model **FacF_plate**. The angle between neighbouring facets is approximately 9 degrees – in model **FacC_plate** the angle is about 12 degrees. (Model **FacF_plate** is described in detail in Appendix A.) The contour scale for the minimum principal stress is the same in Figures 4.5, 4.6 and 4.7. The “compression bands” and “tension bands” are visible on both the left and right half of the structures.

A tabulated overview of the in-plane forces at a chosen edge in model **FacF_plate**, and the in-plane forces in the equivalent smooth shell, can be found in Appendix B.

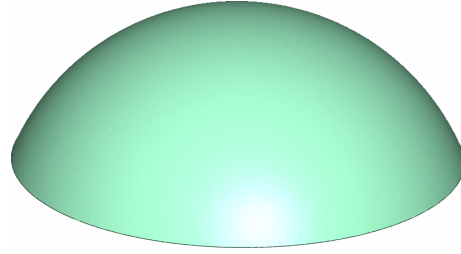
The shell action in a different plate shell layout, model **FacStar**, is illustrated in Figure 4.8, along with the shell action in the equivalent smooth shell, model **FacStar_Smooth**. The smooth shell shape is a section of a sphere. The size of the facets is more uneven than in the examples above. The angle between neighbouring facets is approximately 18 degrees. The connection detail is the same as above (the *glued-in plate* connection). The maximum span is 10.0m, the maximum height is 3.3m, and the facet thickness is 15mm. The load is a distributed vertical load of $1kN/m^2$, acting on the left half of the structure. A detailed description of the two models can be found in Appendix A.

Figure 4.8e and 4.8f are vector plots of the principal stresses in the surface mid-plane of the areas marked in 4.8c and 4.8d. The presence of shear at the connections is evident from the angle (about 45 degrees) between the principal stresses and the connection lines; the orientation of the connection lines guides the orientation of the principal stresses. This increases the stress level, since the stress flow becomes less optimal than in the smooth shell. Also, as the flow of stresses is interrupted at the corner areas, the stress level at the middle parts of the connections increase, since the same force resultant must pass over a smaller length. In the middle of the facets, the stress flow is very similar to the smooth shell.

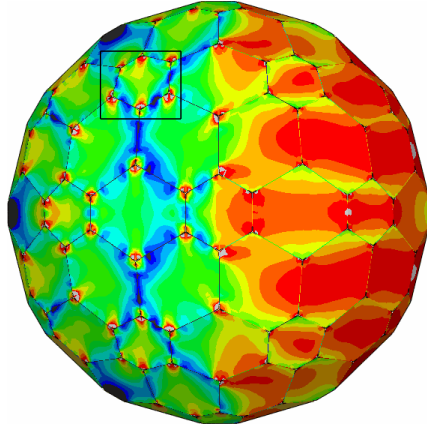
A tabulated overview of the in-plane forces at a chosen edge in model **FacStar**, and the in-plane forces in the equivalent smooth shell, can be found in Appendix B.



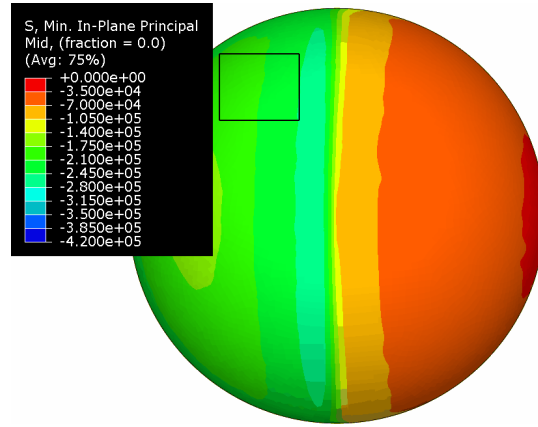
(a) Plate shell geometry



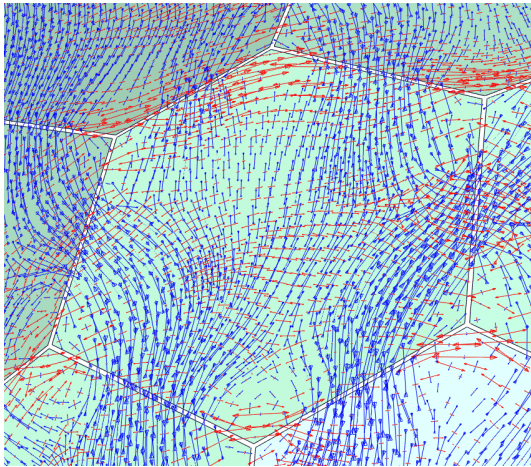
(b) Equivalent smooth shell geometry



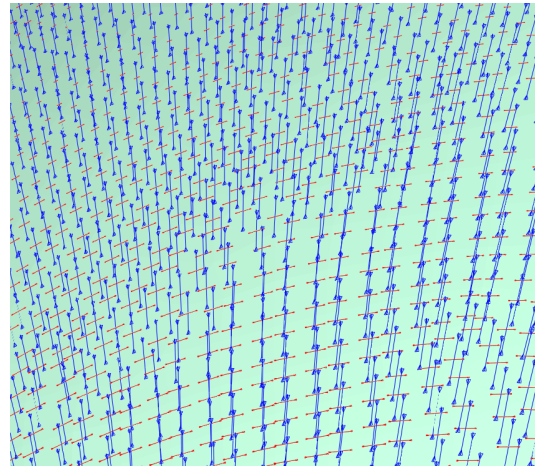
(c) Minimum principal stress (i.e. largest compression) in the surface mid-plane.



(d) Minimum principal stress in the surface mid-plane.



(e) Vector plot of mid-plane principal stresses at the area marked in (c).



(f) Vector plot of mid-plane principal stresses at the area marked in (d). The vector scaling is different than the plot in (e).

Figure 4.8: Plate shell model **FacStar** and its equivalent smooth shell, model **FacStar_Smooth**. The contour scale is the same in (c) and (d) (units: $N/m^2 = 10^{-6}N/mm^2$).

4.2.3 Estimating in-plane forces in a plate shell

Based on the investigations in the previous sections, a simple method for estimating the in-plane forces in a plate shell is suggested in this section.

It may be a very time consuming task to generate a FE model of a plate shell structure, if a suitable generation tool – for example the *pyFormex* script presented in Section 2.2 – is not directly applicable (or available). It will therefore be of practical value to be able to estimate the stresses in a plate shell by simple approximate calculations, at early stages of the design. This section deals with how to estimate the *in-plane forces* in plate shell facets. Section 5.1.3 focuses on estimating the *bending moments*.

Note the basis for the estimation method: results from the models **FacC**, **FacF** and **FacStar** have been used to develop the method. For plate shells with a different overall shape and/or other geometric parameters and stiffness characteristics, the estimation method may be unsuitable⁸.

The estimation method should only be used for *preliminary design*.

As we have seen, the in-plane forces in the analyzed plate shells are closely related to the in-plane forces in their equivalent smooth shells. Therefore, when we wish to estimate the in-plane forces in a given plate shell, we can start by determining the in-plane forces in its equivalent smooth shell. (For a definition of the term “equivalent smooth shell” see footnote 2.) A smooth shell structure is relatively simple to model and analyse in suitable FE software⁹. When the in-plane force distribution is known in the smooth shell, the in-plane forces in the plate shell connections at a given location may be estimated as follows:

$$\begin{aligned}
 n_{22,peak} &= -n_{2,smooth} \cdot k_1 & \text{where } k_1 \approx 0 - 5 \\
 n_{22,edge} &= n_{2,smooth} \cdot k_2 & \text{where } k_2 \approx 1.0 - 2.1 \\
 |n_{12,peak}| &= |n_{12,edge}| + |n_{22,peak}| \cdot k_3 & \text{where } k_3 \approx 0.1 - 0.3 \\
 |n_{12,edge}| &= |n_{12,smooth}| \cdot k_4 & \text{where } k_4 \approx 0.5 - 4.0
 \end{aligned} \tag{4.1}$$

In (4.1) $n_{22,peak}$ and $n_{12,peak}$ are the peak values of the axial and shear in-plane forces at the plate shell connection. $n_{22,edge}$ and $n_{12,edge}$ are the axial and shear in-plane force, at the mid-point of a connection in the plate shell. $n_{2,smooth}$ and $n_{12,smooth}$ are the in-plane minimum principal force and maximum shear force in the equivalent smooth shell, at a similar location on the structure. The stress terms in (4.1) are illustrated in Figure 4.9.

$k_1 - k_4$ are factors, expressing the correlation between stresses in the plate shell and its equivalent smooth shell. The values have been determined using results from the investigations in Sections 4.2.1 and 4.2.2, by determining the maximum and minimum ratio between the observed stresses in the plate shells and the principle stresses in the

⁸The author expects other convex shell shapes to show a similar correlation between the behaviour of the plate shell and its smooth equivalent, but this should be looked more closely into by additional research.

⁹Also, for some simple smooth shell shapes with some simple load cases, analytical expressions exist for determining the in-plane stresses, see for example [49] and [52]. This method of determining the forces is naturally also applicable.

equivalent smooth shells. (The used results are tabulated in Appendix B.)

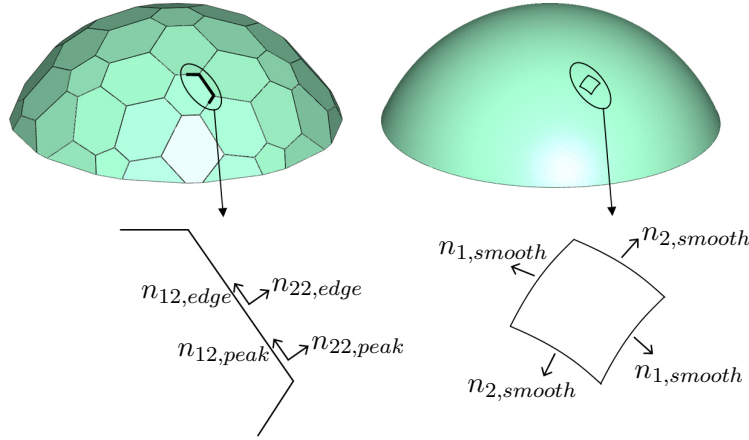


Figure 4.9: Illustration of the terms in (4.1).

The following discussion sums up the observed tendencies in the investigations in Sections 4.2.1 and 4.2.2, to help the designer estimate suitable values for $k_1 - k_4$ in a given design situation.

- k₁** The n_{22} peak value at a connection end, $n_{22,peak}$, mainly depends on two effects: the facet corners' tendency to lift, and the resistance in the connections against this movement. The facet corners' tendency to lift depends on the flexural stiffness of the plate and the rotational stiffness of the connection k_m . The resistance in the connections against lift of the facet corners depends on the axial stiffness of the connection k_n , and the angle between the facets. A combination of a large k_n -value and a low k_m -value may result in large $n_{22,peak}$ -values, depending on the stiffness of the plates, and the angle between the facets. Further studies must look into the size of $n_{22,peak}$ for other plate shell layouts than the ones tested in this thesis – until such results are available, the designer should estimate k_1 in (4.1) based on an assessment of the balance between the corner lift tendency and resistance, while contemplating the results shown in this work.
- k₂** The larger n_{22} peak value at the connection ends ($n_{22,peak}$), the larger n_{22} at the facet edge middle ($n_{22,edge}$). Therefore, if k_1 is large, k_2 should be chosen in the high end of the range given in (4.1).
- k₃** The shear force peak, $n_{12,peak}$, is a consequence of the axial force peak, $n_{22,peak}$ – a high $n_{22,peak}$ results in a high $n_{12,peak}$. Therefore, if k_1 is large, k_3 should be chosen in the high end of the range given in (4.1).
- k₄** The value of $n_{12,edge}$ – and thereby k_4 – depends on the orientation of the non-uniform part of the load, relative to the faceting pattern. It is recommended to use the maximum k_4 value, $k_4 = 4$.

Chapter 5

Bending moments in plate shells

In this chapter and Chapter 4 the structural behaviour of plate shells is studied, assuming small displacements. As stated in Section 4.2, a plate shell structure is a structural “hybrid”, carrying load by both shell action and bending action. In Chapter 4 shell action was studied, and the present chapter focuses on bending action in the structure.

Locally, the facets in a plate shell structure are subjected to plate bending, carrying the load to the facet edges as described in Section 4.2 (see for example Table 4.1, page 37). At the facet edges, the load is transformed into shell action, if the in-plane stiffness of the structure is sufficient. Section 5.1 describes this local plate bending behaviour, and how the local bending behaviour varies with the connection stiffness parameters.

If the structure’s in-plane stiffness is low or non-existing, the out-of-plane forces at the facet edges can also be balanced by out-of-plane forces in the adjacent facets, corresponding to an overall bending behaviour of the structure. This behaviour leads to much larger displacements in the structure. Section 5.2 focuses on such a non-local bending behaviour.

5.1 Local plate bending in plate shell facets

This section focuses on local bending behaviour in plate shell facets. The structure’s in-plane stiffness is assumed to be so much larger than the overall bending stiffness that no overall bending behaviour occurs, meaning that all out-of-plane shear forces are transformed into in-plane forces at the facet edges.

The largest local bending moment in a plate shell facet occurs in one of three possible locations (or nearby): the facet centre, an edge mid-point, or at a connection end. These three types of areas are indicated in Figure 5.1.

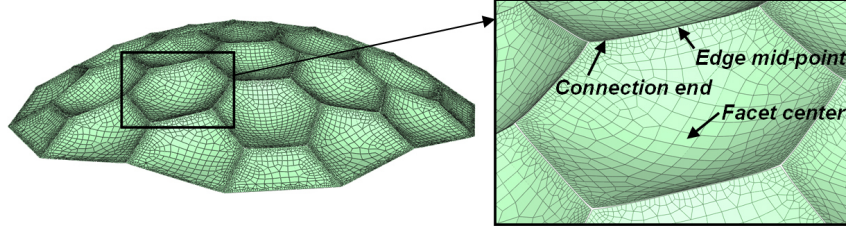


Figure 5.1: Deformed plot of plate shell, showing three types of areas on a facet where bending moments are in focus.

Section 5.1.1 describes the bending behaviour by first focusing on the behaviour of a polygonal plate, and then extending this description to the bending behaviour of a plate shell facet, by adjusting the boundary conditions. In Section 5.1.2, the effects of the local bending behaviour in plate shell facets is illustrated numerically, using FE analysis of plate shells. Finally, in Section 5.1.3 a method is suggested for estimating the local bending moments in a plate shell.

The relevant bending moment terms and their orientation are illustrated in Figure 5.2. As was the case in the study of in-plane forces, the terms refer to *local directions*, relative to the regarded edge.

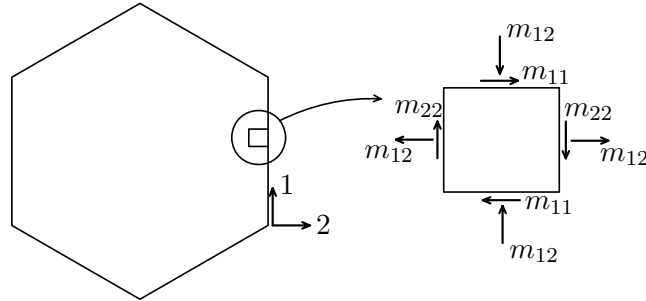


Figure 5.2: Local orientation of bending moment terms at a facet edge.

5.1.1 Plate bending in a polygonal plate

To describe the plate bending behaviour of a plate shell facet, we will first focus on a simply supported plate of convex polygonal shape¹. When it is loaded by a uniformly distributed out-of-plane load, the plate centre will deflect in a shape that resembles the deflection of a circular plate as much as possible, as this is the energetically most efficient. If the translational support has a finite stiffness, the plate edges will therefore tend to curve, and the plate corners will tend to lift. If the translational support is of infinite stiffness (i.e. the edges are simply supported), the edges are forced to remain straight when the plate is loaded; torsional bending moments will develop at the edges, and a bending

¹A convex polygonal plate has straight edges, and all corner angles are less than 180 degrees. In this thesis, only convex facets are considered, see the introduction to Chapter 2, and footnote 2 in Chapter 2.

moment singularity will occur in all corners with an angle of more than 90 degrees [42].² Now consider the same plate, but supported against rotations as well as translations along the boundary (clamped). In such a plate, no singularity will develop, regardless of the size of the corner angles³.

In a plate shell facet (which is a plane, polygonal, convex plate like the plates described above), the boundary is supported by supports of finite stiffness, translational as well as rotational. The above mentioned singularity will therefore be reduced to a bending moment concentration, and a concentrated out-of-plane reaction force in the corner⁴. Because of the plate's support conditions, concentrated in-plane forces will develop in the facet corners as described in Section 4.2 (page 38). This in-plane stress concentration can be significantly reduced by shortening the connections, so that the connected lengths are shorter than the facet edges, and a part of each facet corner is free to lift. (This is for example illustrated in Figure 3.5, page 31.)

As described in Section 3.1 (page 25), the rotational stiffness of the connection detail, k_m , ties the bending moment m_{22} in the connection to the plate edge rotation (see Figure 3.1, page 24). If k_m is small, the plates will act as if connected to each other by a line hinge, and almost no bending moment will be transferred between the plates. If k_m is large, a certain amount of bending moment will be transferred through the connection. This means that the ratio between the bending moment at the facet centre and the bending moment at the facet edges depends on the value of k_m .

To illustrate the effects discussed in this section, Figure 5.3 shows deformed plots of a

²This footnote gives an explanation for the bending moment singularity in a simply supported plate corner of more than a 90 degree angle. According to the boundary conditions we have $m_{22} = 0$ along the boundary. The constitutive conditions for plate bending states that $m_{11} = D(\kappa_{11} + \nu\kappa_{22})$, $m_{22} = D(\kappa_{22} + \nu\kappa_{11})$ and $m_{12} = D(1 - \nu)\kappa_{12}$. (Here D is the flexural rigidity of the plate $D = \frac{Et^3}{12(1-\nu^2)}$, κ_{11} and κ_{22} are curvature in the 1- and 2-direction respectively, κ_{12} is the twist, ν is Poisson's ratio, E is the plate material's E-modulus and t is the plate thickness.) Therefore we have also $m_{11} = 0$ along the boundary. Since $m_{11} = m_{22} = 0$ at the boundary, only the torsional moment $m_{12} \neq 0$. In the plate corner, where torsional bending moments from two edges meet, a singularity will arise, since the existence of pure torsional bending moments from two sides is inconsistent, when the angle at which they meet is not 90 degrees; the principal directions (for the curvature and bending moments) are governed by the supported edges, and in the corner they are contradictory. In a 90 degree corner (for example in a rectangular plate) the singularity will not arise – the torsional bending moment will be in equilibrium with a finite concentrated reaction force in the corner, in accordance with ordinary Kirchhoff-Love plate theory [52]. This concentrated force is infinitely large when the corner angle is larger than 90 degrees [42]. The singularity also results in infinitely large bending moments at the corner.

³This footnote gives an explanation for the absence of bending moment singularity in a plate corner, regardless of the corner angle, when the plate boundary is clamped. According to the boundary conditions we have $m_{22} \neq 0$ along the boundary. We then have $m_{11} = -\nu m_{22}$, according to the constitutive conditions (see footnote 2). The curvature is defined as $\kappa_{11} = -w_{,11}$, $\kappa_{22} = -w_{,22}$ and $\kappa_{12} = -w_{,12}$. Since $w_{,2} = 0$ along each edge, we have $w_{,12} = 0$ and thereby $m_{12} = 0$ along each edge. Since there is no torsional bending moments along the boundary, there are no concentrated reaction forces in the corners, and hence no singularities [42].

⁴The singularity disappears because the plate edges are allowed to curve, thereby permitting coinciding principal directions (for the curvature and bending moments) in the corners.

facet from the plate shell model **FacC**. The deformed facet is shown from four different variants of the model, each with a different connection detail (see Appendix A). The deformation scale factor is the same in the four plots.

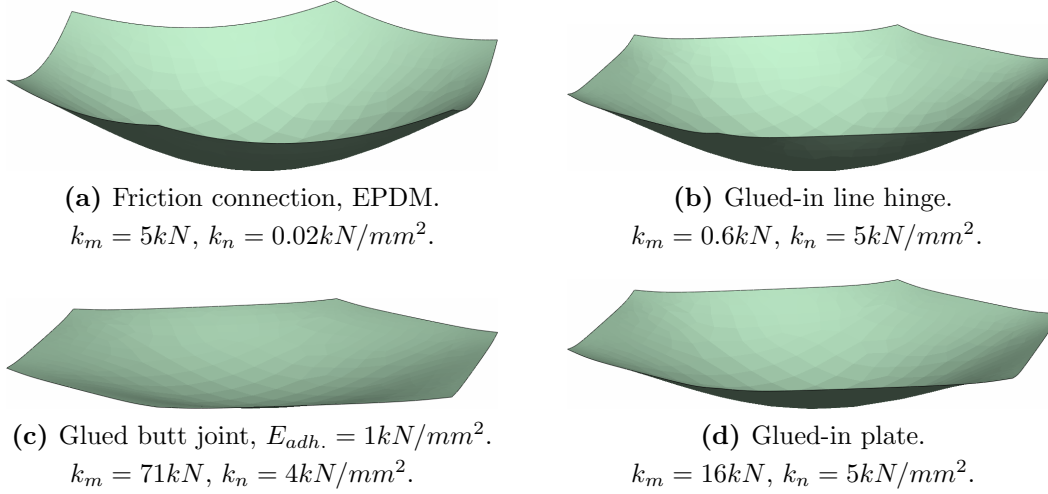


Figure 5.3: Deformed facet from the plate shell models **FacC_EPDM**, **FacC_hinge**, **FacC_adh1** and **FacC_plate** respectively.

The following details can be observed in Figure 5.3:

- When k_m is relatively small and k_n is very small (Figure 5.3a), the facet edges curve and the corners lift.
- When k_m is almost zero and k_n is large (Figure 5.3b), the edges are only slightly curved, (even though k_m is smaller than in 5.3a), because the large k_n -value restrains the edges against curving. Where the edges are free of the connection detail, the corners tend to lift. This may in some cases result in significant m_{11} bending moments at the connection ends.
- When k_m is very large and k_n is large (Figure 5.3c), the edges are almost straight since the plate edge is almost clamped (minimizing torsional bending moments along the edge). For the same reason, the deflection of the plate centre is significantly smaller than in 5.3b and 5.3a.
- When k_m is moderately large and k_n is large (Figure 5.3d), the plate edges curve slightly, but the tendency to corner uplift is smaller than in 5.3b. This is because k_m is larger in 5.3d than in 5.3b.

Depending on the connection stiffness parameters, the maximum bending moment in a plate shell facet will occur either in the facet centre, near an edge mid-point or at a connection end (as indicated in Figure 5.1). If k_m is large compared to the facet's bending stiffness (see Section 5.1.3, page 57) the maximum bending moment may occur at the facet edges. If k_m is small, the maximum bending moment will most likely occur at the facet

centre. As it will be shown by numerical examples in Section 5.1.2, for certain conditions (small k_m , large k_n , relatively large facets and relatively large angles between the facets) the largest bending moment may occur at a connection end.

5.1.2 Linear FE study of plate shell

In Section 4.2.1 (page 38) the in-plane forces in six variants of model **FacC** were studied at a chosen facet edge. In the present section, the same series of analysis is used to study the bending moments at the same edge in **FacC**. Only one of the two load cases studied in Section 4.2.1 is referred to in the present section, namely the *uniform load case*; the bending response is almost identical for the non-uniform load case⁵, and it is therefore left out.

The bending moments m_{11} and m_{22} along the studied edge are plotted in Figure 5.4. (The bending moment terms are illustrated in Figure 5.2, and the studied edge is marked in Figure 4.2, page 39.)

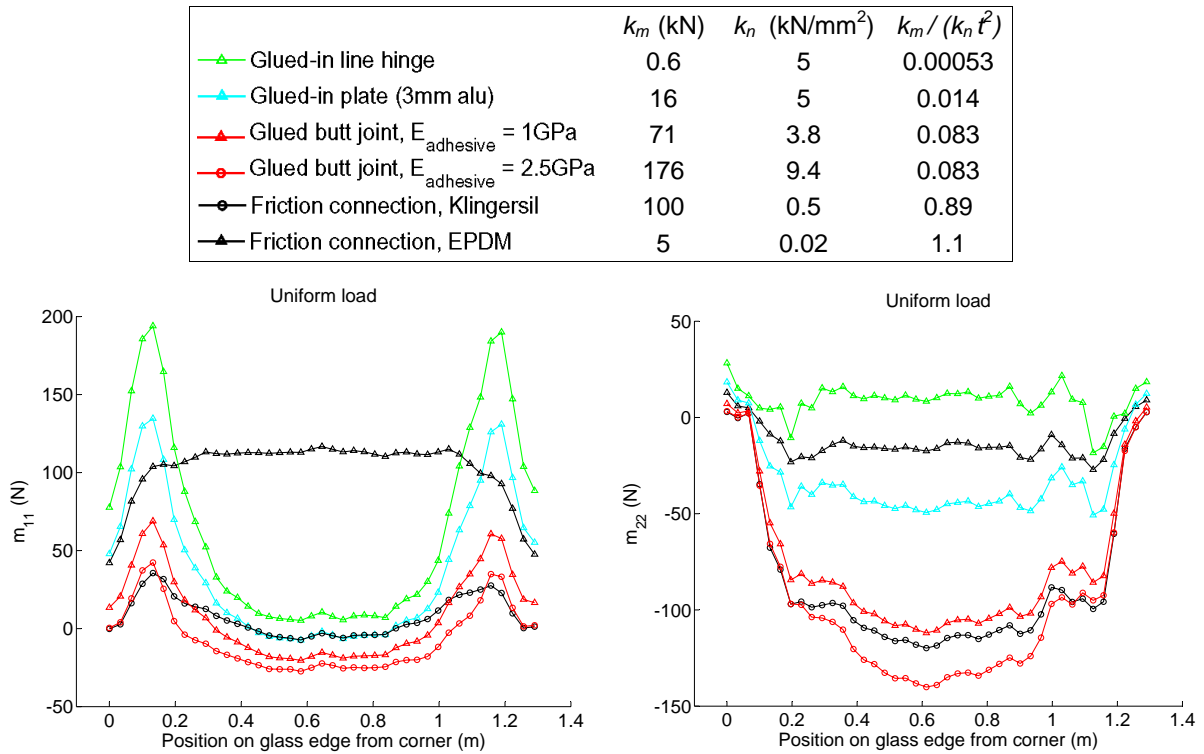


Figure 5.4: Bending response in the plate shell FE model described in Section 4.2.1, for the uniform load case.

The m_{22} bending moment (Figure 5.4, right) generally increases for connection details with larger rotational stiffness k_m . $k_m = 0$, corresponding to a hinged connection, will

⁵Local bending moments at a connection are almost entirely dependent of the *local* loading situation on the two connected facets. In the uniform load-case and the non-uniform load case referred to here and in Section 4.2.1, the external load on the two facets connected by the studied connection, is the same.

result in $m_{22} \approx 0$, and for $k_m \rightarrow \infty$, m_{22} will correspond to the facets being continuously connected. The m_{22} plot in Figure 5.4 shows that m_{22} has a small *positive* value⁶ along the edge of the hinged connection. This is because the bending moment is taken from the integration points of the edge elements, and thereby at a small distance from the actual facet edge. The smaller elements along the edge, the smaller distance between the integration points and the edge, and hence the smaller the positive m_{22} -value for a hinged connection. This “error” repeats itself for the other connection details also, but is only directly readable for the hinged connection, where m_{22} is known at the edge.

The m_{11} bending moment (Figure 5.4, left) does not load the connection detail directly – stresses from this bending term are internal in the facet. Like the n_{22} peak values, the m_{11} peak values increases for decreasing value of the dimensionless factor $\frac{k_m}{k_n t^2}$, except for model with the *EPDM friction connection* which has a very low axial stiffness k_n . For that model, the m_{11} distribution is smooth along the edge. m_{11} is primarily tied to the curvature of the edge⁷, and for a low k_n the edge curves smoothly.

For the connection details with larger k_n -values, the facet edges are more restrained from curving. At the connection ends, the facet corners can lift freely, causing a large local curvature of the edge in this area, and hence a large local m_{11} bending moment. Generally, the larger k_m the smaller local m_{11} at the connection ends, because of the reduced tendency to corner uplift. For connection details with large k_m and large k_n , m_{11} has *negative* values along the edge, because $m_{11} \approx \nu m_{22}$ when the edge curvature is almost zero⁷.

Table 5.1 lists the maximum bending moment near the middle of the studied edge ($m_{22,edge}$), near the edge’s connection ends ($m_{11,conn.end}$), and near the middle of the facet ($m_{fac.middle}$). For all combinations of connection stiffness parameters, the maximum bending moment will occur in one of these three types of locations on the structure.

As it appears from the table, the maximum bending moment does not occur near a connection end for any of the tested combinations of connection stiffness parameters. Of the six analyzed connection variants, the bending moment at a connection end is largest for the *glued-in hinge* connection, as expected from the discussion in Section 5.1.1. The analyzed structure is a relatively extreme case, combining a large k_n -value and $k_m \approx 0$ with a geometry with large facets and a relatively large angle between the facets.

⁶As it appears from the definition of the terms (Figure 5.2), a positive bending moment corresponds to a “sagging moment”, with compression in the upper surface, and tension in the lower surface of the plate.

⁷See the constitutive conditions in footnote 2.

| Connection detail | $m_{22,edge}$ (N) | $m_{11,conn.end}$ (N) | $m_{fac.middle}$ (N) |
|-------------------------------|----------------------|--------------------------|-------------------------|
| Glued-in line hinge | 12 | 194 | 218 |
| Glued-in plate (3mm aluminum) | -46 | 135 | 183 |
| Glued butt joint | | | |
| – $E_{adhesive} = 1kN/mm^2$ | -110 | 69 | 140 |
| – $E_{adhesive} = 2.5kN/mm^2$ | -138 | 43 | 120 |
| Friction connection | | | |
| – Klingersil | -120 | 35 | 135 |
| – EPDM | -12 | 93 | 232 |

Table 5.1: Comparison of maximum bending moments at the studied edge in model **FacC**.

5.1.3 Estimating bending moments in plate shell facets

Based on the investigations in the previous sections, a simple method of estimating the largest bending moments in a plate shell facet is developed, and presented in this section. The method should only be used for *preliminary design* of convex plate shells. In Section 4.2.3 (page 49) a similar method is presented for the approximation of *in-plane forces* in plate shell facets.

In most cases, the largest bending moment in a plate shell facet will occur in the facet centre, or near the middle of one of the facet's edges⁸. The bending moment in these two locations can be estimated by first determining the bending moments in a *circular plate*, supported by the same rotational stiffness, and then adjust the results to account for the polygonal geometry and the free corners. The following estimation method uses this approach.

Circular plate

Figure 5.5 shows a section through the centre of a circular plate, loaded by a uniform out-of-plane load, for three different support conditions: simply supported edge (left), clamped edge (middle), and the edge fully supported against translations and supported against rotations by a finite stiffness (right). The diagrams in the bottom of the figure show the corresponding bending moment (m_r in polar coordinates).

By use of ordinary Kirchhoff-Love plate bending theory for small displacements [52], expressions for the maximum plate deflection u , the bending moment at the plate edge m_{edge} (orientated like m_{22} in Figure 5.2), the bending moment at the plate middle m_{mid} , and the rotation of the plate edge φ , can be specified for the simply supported plate and the clamped plate respectively, see Table 5.2.

⁸As discussed on page 56, for structures with large facets, large angles between the facets, hinged connections ($k_m \approx 0$), and a large axial stiffness in the connections, the bending moment at a connection end may exceed the maximum bending moment at the facet middle.

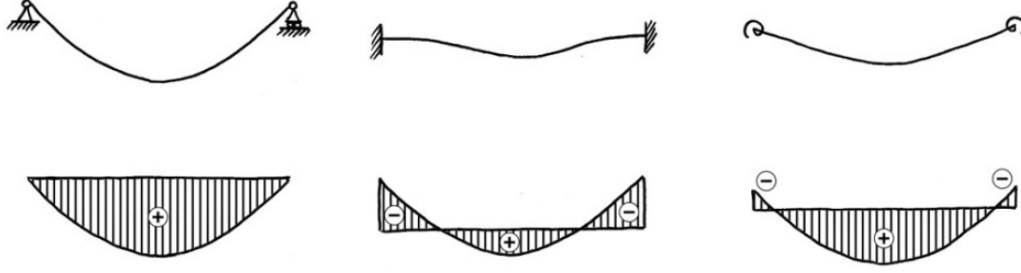


Figure 5.5: Section through centre of a circular plate, for three different support conditions. Top sketches: displacements. Bottom sketches: bending moment m_r . Illustration from [39].

| <i>Circular plate</i> | | | |
|------------------------|-------------------------------------------------------|---------------|-----------------------------------|
| Edges simply supported | | Edges clamped | |
| u_s | $= \frac{5+\nu}{1+\nu} \frac{1}{1024} \frac{qd^4}{D}$ | u_c | $= \frac{1}{1024} \frac{qd^4}{D}$ |
| $m_{edge,s}$ | $= 0$ | $m_{edge,c}$ | $= -\frac{1}{32} qd^2$ |
| $m_{mid,s}$ | $= \frac{1}{64} (3+\nu) qd^2$ | $m_{mid,c}$ | $= \frac{1}{64} (1+\nu) qd^2$ |
| φ_s | $= \frac{qd^3}{64D(1+\nu)}$ | φ_c | $= 0$ |

Table 5.2: Analytical expressions for u , m_{edge} , m_{mid} and φ for a circular plate.

In Table 5.2, the plate is loaded by a uniform load q , the plate diameter is d , the plate material is isotropic and linear elastic with Young's modulus E and Poisson's ratio ν . The plate thickness is t . $D = \frac{Et^3}{12(1-\nu^2)}$. Index s is used for the simply supported plate, and index c is used for the clamped plate.

When the plate edge is supported by a finite rotational stiffness, the value of u , m_{edge} , m_{mid} and φ will lie between the extreme values corresponding to a simply supported plate (a rotational stiffness of zero) and a clamped plate (infinite rotational stiffness). We wish to find the solution where the forces in the plate are in equilibrium, for a given linear rotational spring stiffness, k_m . The problem can be described by the following three correlations:

1. The clamped circular plate is subject to the same moment distribution as the simply supported plate, superposed by a uniform bending moment (uniform m_r in polar coordinates). The value of this superposing bending moment is just sufficient to cancel the edge rotation of the simply supported plate. If the circular plate's own resistance against edge rotation from a uniform moment acting at its edge is denoted k_p we have the correlation:

$$m_{edge,c} = k_p(\varphi_s - 0) \quad (5.1)$$

2. For the circular plate supported by a linear rotational stiffness k_m , the reaction bending moment at the edge m_{edge} is

$$m_{edge} = k_m \varphi \quad (5.2)$$

where φ is the rotation of the plate edge. The bending moment and rotation angle in (5.2), are *not* denoted with an index s or c , since it is a solution lying *between* the two extremes – $m_{edge,s} < m_{edge} < m_{edge,c}$ and $\varphi_c < \varphi < \varphi_s$.

3. For the circular plate supported by a linear rotational stiffness k_m , the reaction bending moment is balanced by the bending compliance of the plate:

$$m_{edge} = k_m \varphi = k_p (\varphi_s - \varphi) \quad (5.3)$$

(5.1) and (5.3) yield the following correlation:

$$m_{edge} = \alpha \cdot m_{edge,c} \quad (5.4)$$

where a *rotational restraint factor* α has been introduced, defined by

$$\alpha = \frac{k_m}{k_m + k_p}, \quad \alpha \in [0; 1[\quad (5.5)$$

When $\alpha = 0$ there is no rotational restraint, corresponding to a simple support (hinged). When $\alpha \approx 1$ the plate edge is fully clamped. α increases (thereby increasing the bending moment in the support) when

- the rotational support stiffness k_m increases
- the plate diameter d increases
- the plate thickness t decreases

The first term is self-evident. The second and third term state that the more flexible the plate is, the larger influence the connection stiffness will have.

The plate's stiffness against edge rotation from a uniform bending moment acting at its edge, k_p , is determined by (see for example [52]):

$$k_p = \frac{m_{edge,c}}{\varphi_s} = \frac{Et^3}{6d(1-\nu)} \quad (5.6)$$

We have now seen that the bending moment at the support of a circular plate with rotational spring support varies linearly with α . Also the bending moment at the plate middle m_{mid} , the plate edge rotation φ and the deflection of the plate u varies linearly with α . We have

$$u = (1 - \alpha)u_s + \alpha u_c \quad (5.7)$$

$$m_{edge} = \alpha m_{edge,c} \quad (5.8)$$

$$m_{mid} = (1 - \alpha)m_{mid,s} + \alpha m_{mid,c} \quad (5.9)$$

$$\varphi = (1 - \alpha)\varphi_s \quad (5.10)$$

Polygonal facet in plate shell

We now wish to adjust the expressions found above for the circular plate, so that they yield approximate values for the bending behaviour of a plate shell facet. The adjustment will be done so that the expressions estimate the bending moment in the facet middle m_{mid} , the maximum bending moment along the facet's edges m_{edge} , the out-of-plane deflection of the facet (relative to its edge mid-points) u and the maximum rotation of the facet's edges φ .

Naturally, the bending behaviour of a plate shell facet differs somewhat from that of a circular plate. The differences are caused by the different geometry, the un-supported corner zones and the finite translational support stiffness. Even so, a calibration process, where the expressions for the circular plate are adjusted by a factor, has resulted in expressions of sufficient precision for a preliminary design.

Table 5.3 shows the adjusted expressions for m_{mid} , m_{edge} , u and φ in a plate shell facet, in the two extreme situations corresponding to $k_m = 0$ and $k_m \rightarrow \infty$ respectively.

| Plate shell facet with 4, 6 or more edges (for pentagons: see below) | | | |
|-------------------------------------------------------------------------|-----------------------------------------------------------------|--------------------------------------------|---------------------------------------------|
| Edges hinged ($k_m = 0$) | | Edges clamped ($k_m \rightarrow \infty$) | |
| u_s | $= 1.1 \cdot \frac{5+\nu}{1+\nu} \frac{1}{1024} \frac{qd^4}{D}$ | u_c | $= 1.1 \cdot \frac{1}{1024} \frac{qd^4}{D}$ |
| $m_{edge,s}$ | $= 0$ | $m_{edge,c}$ | $= -1.4 \cdot \frac{1}{32} qd^2$ |
| $m_{mid,s}$ | $= 0.9 \cdot \frac{1}{64} (3 + \nu) qd^2$ | $m_{mid,c}$ | $= 1.3 \cdot \frac{1}{64} (1 + \nu) qd^2$ |
| φ_s | $= 1.1 \cdot \frac{qd^3}{64D(1+\nu)}$ | φ_c | $= 0$ |

Table 5.3: Approximate expressions for u , m_{edge} , m_{mid} and φ for a plate shell facet, for $k_m = 0$ and $k_m \rightarrow \infty$ respectively.

In Table 5.3 E and ν are Young's modulus and Poisson's ratio for the isotropic, linear elastic facet material, and t is the facet thickness. q is the uniform load perpendicular to the facet. $D = \frac{Et^3}{12(1-\nu^2)}$.

d is a measure for the *mean facet diameter*, determined as the mean value of the distance between opposing edge mid-points. For a *pentagon*, d is defined as the mean value of the distance between each edge mid-point and its opposing corner, multiplied by a factor 0.91. For polygons with a larger, uneven number of edges, d is defined in the same way as for the pentagon, but with no additional factor.

When the terms in Table 5.3 have been calculated, and α is determined by (5.5), m_{mid} , m_{edge} , u and φ can be found by using (5.7), (5.8), (5.9) and (5.10) respectively.

Precision of the estimated values

As explained earlier, the approximate expressions above should only be used for *preliminary design* of plate shells.

The adjustment of the approximate expressions has been performed by comparing FE

results of bending moments, deflections and rotations from 16 facets from analyzed plate shell models, to the same values determined using the approximate expressions. This comparison is documented in Appendix C. The deviations found between FE results and the estimated values are within the following margins:

| | |
|--------------|-------------|
| m_{edge} : | -10% to 20% |
| m_{mid} : | -10% to 20% |
| u : | -10% to 15% |
| φ : | -20% to 30% |

A positive error means that the estimated value is higher than the FE result.

The approximate expressions assume a similar edge rotation of the regarded facet and its surrounding facets. When this is not the case, for example if the size of the facets varies significantly, this will affect the precision of the estimate, and the deviations may exceed the values above.

For facets of irregular shape, the approximate expressions yield more conservative results than if the facet had been of regular shape (all other things being equal).

The ratio between connected edge length and total edge length is in the range of 0.75 and 0.85 for all the facets used in the adjustment of the expressions. The applicability of the expressions has not been tested for ratios outside this range.

5.2 Other bending moments in plate shells

As discussed earlier, when a facet in a plate shell structure is subjected to local bending by an external out-of-plane load, the facet carries the load to its edges, where it is transformed into shell action; the out-of-plane shear forces at the facet edges are balanced by in-plane forces in the facet itself, and in the neighbouring facets. However, the out-of-plane shear forces at the facet edges can also be balanced by out-of-plane shear forces in the neighbouring facets. This corresponds to a “non-local” bending action, where the structure carries the load to the supports by overall plate bending.

Since the structure is statically indeterminate (here meaning that it can carry the load by both shell action and non-local plate bending), the ratio between the two modes of functioning in a given plate shell structure is determined by the structure’s stiffness.

Deformations from bending action are generally much larger than deformations from shell action. Therefore, if the structure is shaped and supported so that it can carry the load effectively by shell action, the deformations will be small, and the non-local bending action will be negligible. If, on the other hand, the structure for some reason has large deformations, the non-local bending action will become active.

- If the plate shell (or a part of it) is shaped so that shell action involves relatively large deformations, non-local bending moments may become significant. This may be the case in areas where the structure has low curvature (small angles between neighbouring facets), or in the area near a free edge.

- If the plate shell is not sufficiently supported to develop in-plane forces, the structure will carry the load entirely by non-local plate bending [9]. This will result in large deformations. Such a case is illustrated in Figure 5.6. (The figure is presented more into detail further down in the text.)

The arguments above can also be used for a smooth shell, which like the plate shell is statically indeterminate, in the sense that it can carry load by both shell action and bending. The ratio between the two modes of functioning in a smooth shell structure is determined by the structure's stiffness and support conditions.

In a plate shell where non-local bending moments occur, these will primarily be in the form of torsional moments m_{12} at the connections. m_{22} at the connections will result in relatively large deformations, because of the reduced stiffness against rotations in the connection lines, whereas m_{12} is unaffected by this compliance. This appears from Figure 5.6, where two plate shell structures are compared (models **FacF_plate** and **FacF_3points**). The structures are identical, apart from their boundary conditions. The structure to the left is supported against translations along its entire boundary. The structure to the right is supported in 3 points, as indicated in the figure. The difference in scale of deformations is 1000.

The plots in the bottom of Figure 5.6 show the principle stresses in the upper surface of the structure. Stresses from the bending moments are superposed by stresses from the in-plane forces in the plots, so the vectors do not directly represent the bending moments. Nevertheless, it is apparent that in the structure to the right, where non-local bending moments are present and local bending moments are not, torsional bending moment is transferred across the connection.

Non-local bending moments in a plate shell must be determined by a FE analysis of the structure.

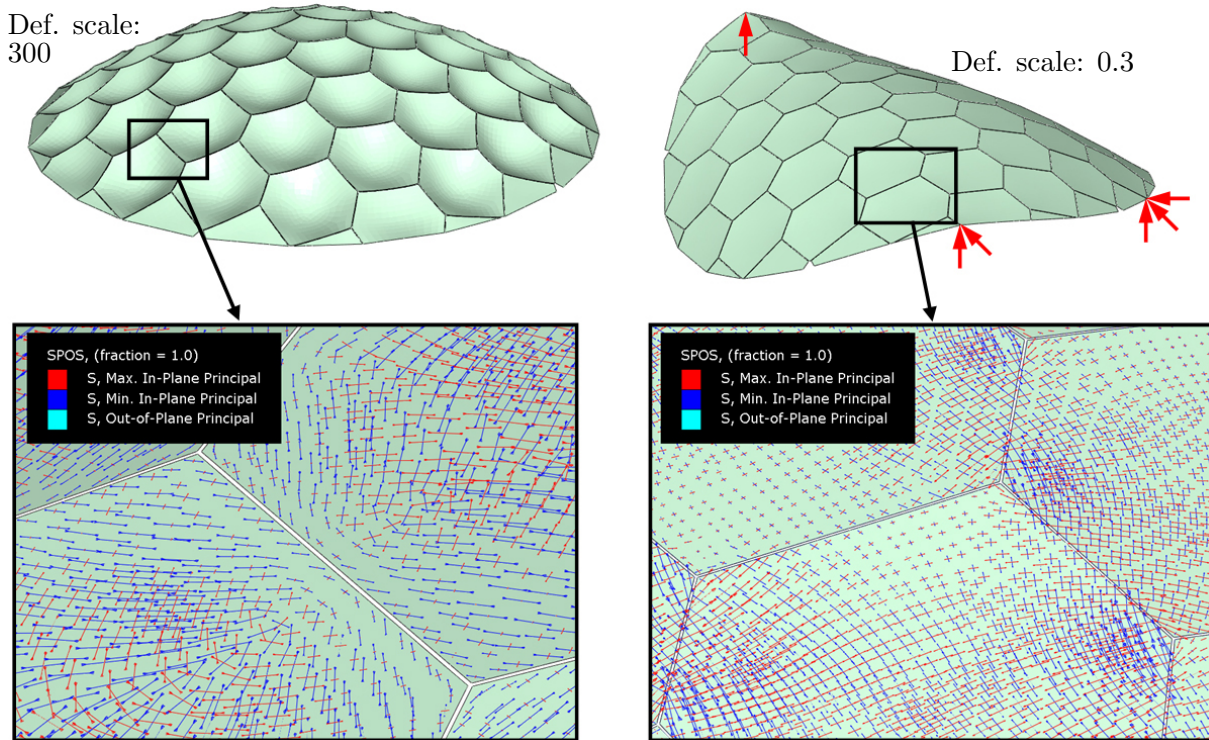


Figure 5.6: Two plate shells models: **FacF_plate** and **FacF_3points**. The models are identical except for their support conditions, see Appendix A. Scaled deformed plots, and details showing principle stresses in the upper surface.

Chapter 6

Non-linear investigations

This chapter focuses on the structural behaviour of plate shell structures when effects from geometrically non-linearity are included. This potential area of research is very large, and the study in the present chapter should be seen as an introductory investigation into the topic. The aim of the study is to promote an intuitive understanding of the non-linear behaviour of a faceted shell, in order to direct further research in the area, or (in a design situation) to help set up appropriate FE models for analysis.

Section 6.1 is a short summary of buckling of shell structures, taken from the literature. The non-linear behaviour of plate shells is addressed in Section 6.2.

6.1 Buckling of shell structures

This section summarizes established knowledge about buckling of shell structures, to the extent that it is relevant for the non-linear study of plate shells. The information can for example be found in [18], [24],[37], [38] and [51].

In a thin-walled shell structure, the membrane stiffness is many times greater than the bending stiffness, if the structure is shaped and supported appropriately.

Consider a shell structure loaded in compression by a given load of increasing magnitude. Until the load reaches a certain level, the shell carries the load mainly by membrane action. Energy is then stored in the structure mainly as membrane strain energy, and the corresponding displacements are small. This is referred to as the *prebuckling* state.

When the load level reaches a critical load, certain displacements can take place without adding any load. *Buckling* occurs at this load level, as membrane strain energy from compression is converted into bending strain energy, with large displacements as a consequence. The displacements that arise during buckling are referred to as the *bifurcation buckling mode*. The term *true bifurcation buckling* refers to a situation where the bifurcation buckling mode has zero amplitude until buckling occurs.

The structure's state after buckling, referred to as the *postbuckling* state, can be either *stable* or *unstable*¹. The postbuckling state is *stable* if the load-bearing capacity of the

¹Note that the term “stable” here is used in a different context than in Chapter 1.

structure increase with increasing amplitude of the bifurcation buckling mode. An example of a structure which is stable in its postbuckling state is a simply supported plate under compression in its own plane. The postbuckling state is *unstable* if the load-bearing capacity decreases with increasing amplitude of the bifurcation buckling mode. If a part of the load is not removed after the buckling has taken place, the structure will collapse. Spherical shell structures belong to this category. A *neutral* state, where an arbitrary size of the bifurcation mode is possible at the critical load level, can be formulated as an eigenvalue problem. This is a linearized model of the elastic stability of the structure, in which it is assumed that no (or negligible) displacements take place in the prebuckling state.²

In an ideal structure, where there are no geometric or material imperfections, and where the displacements in the prebuckling state are negligible, the linearized model of the elastic stability yields the critical load with a good approximation. In any real structure true bifurcation buckling does not exist, because no real structure is free of imperfections. Imperfections include geometric imperfections (for example from construction, support settlements and geometric changes due to creep and shrinkage), material imperfections (inhomogeneities etc.), residual stresses, temperature movements and/or stresses, and other effects. Imperfections reduce the critical load, compared to the linearized bifurcation load. The difference between the bifurcation load of the perfect structure, and the critical collapse load of the imperfect structure, depends on the amplitude of the imperfection.

The collapse load of a shell structure with imperfections can be determined by a geometrical non-linear FE-calculation, where imperfections have been assessed and implemented in the model. The load is applied in steps, each for which the displacements are calculated, and equilibrium is found for the deflected structure. The deflected structure is then basis of the following load step. Generally, the stiffness of the structure decreases with increasing load. FE software which can handle geometrically non-linear analysis, apply various methods for the stepwise attaining of the equilibrium state.

A dome shell structure is unstable in the postbuckling state. Since the load is not reduced on the structure when buckling occurs, the structure will collapse. The collapse happens almost instantly. For a shell structure, which has geometric and material imperfections, the actual load-bearing capacity can be $1/6^{th}$ or as little as $1/10^{th}$ of the critical load corresponding to bifurcation of the perfect structure [51]. Therefore, it is essential in a design process to assess possible geometric imperfections, and carry out geometrically non-linear FE calculations on the imperfect structure. In most cases, a linear combination of the lowest linear buckling modes for a shell structure are known to produce the worst possible imperfection shapes for the structure, given a certain maximum amplitude of deformation. The effect of imperfections of other types than geometric must also be assessed.

²For a simply supported column, the solution to this problem is the Euler load, and the corresponding bifurcation mode is a single or multiple sine arches.

6.2 Non-linear behaviour of plate shells

The general information about buckling of shells summarized in Section 6.1 is not directly applicable to plate shells, since a relatively large amount of bending action is present in such a structure. In this section we will study non-linear behaviour of plate shells under varying conditions, and compare the results to the behaviour of a similar, smooth shell.

Geometrically non-linear FE analysis have been carried out on the three structures shown in Figure 6.1 – two plate shells (models **FacC** and **FacF**) and a smooth shell (model **Smooth**). (See Appendix A for a detailed description of the models). Table 6.1 gives an overview of the analyzed model variants.

Section 6.2.1 describes the basis of the analysis. Section 6.2.2 addresses the non-linear behaviour of the facets, by describing how the local stiffness changes and internal forces are rearranged, as the load level increases.

The structural response of the analyzed structures under varying conditions are compared and discussed in Sections 6.2.3 to 6.2.5. As the results will show, failure due to buckling is unlikely to happen in the studied structures, since other design parameters will govern the load bearing capacity. A summary of the results is given in Section 6.2.6.

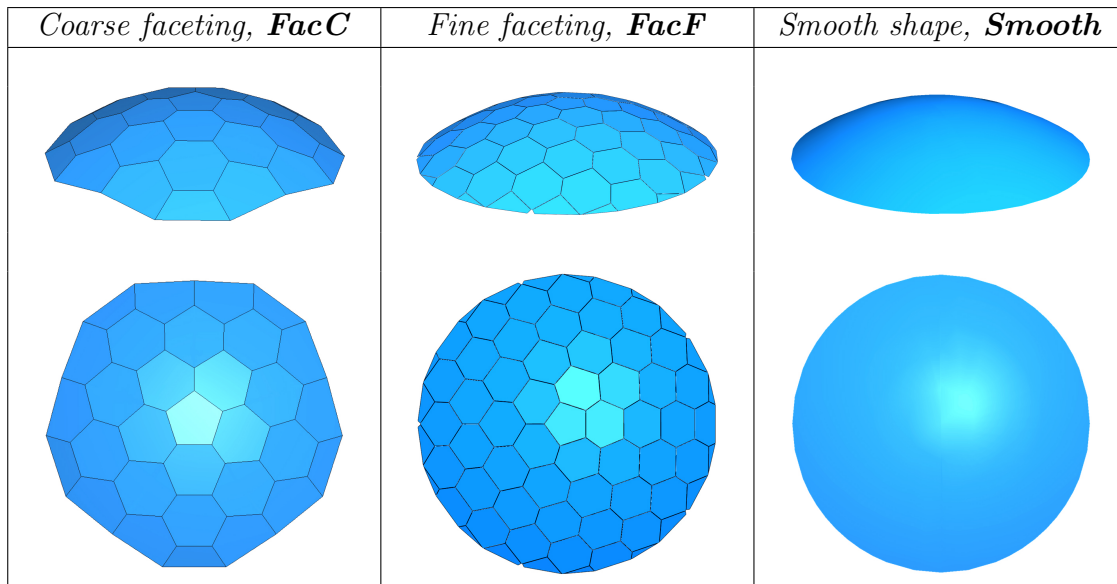


Figure 6.1: The three analyzed structures. The span of all three structures is 11.5m.

6.2.1 Basis of FE analysis

The three shell structures in Figure 6.1 have been subjected to geometrically non-linear FE analysis in ABAQUS³. All three structures have the same “average” geometry, same facet/shell thickness, uses the same connection detail (the *glued-in plate* connection) and

³In geometrically non-linear analysis, ABAQUS applies an Arc Length method [21] to obtain equilibrium for incremental load steps. The essence of the method is that the solution is viewed as the discovery of a single equilibrium path in a space defined by the nodal variables and the loading parameter. It is

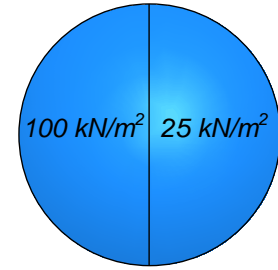
| Variation | FacC | FacF | Smooth | Section |
|----------------------------------------------------------------------------------------------------------------------------------------------------------------------------------------------------------------------------------------------------------------------------------------------------------------------------------------------------------------------------------------------------------------------------------------------------------------------------------------------------------------------------------------|--------------------------------------------------------------------------------------------------------------|-----------------------------------------------------------------------------------------------------------------------------|---------------------------------------|---------|
| Imperfections <ul style="list-style-type: none"> Perfect geometry <ul style="list-style-type: none"> – <i>uniform load</i> – <i>non-uniform load</i> Imperfection A <ul style="list-style-type: none"> – <i>uniform load</i> – <i>non-uniform load</i> Imperfection B (only uniform load) Imperfection C (only uniform load) | FacC_Perf_Uni FacC_Perf_Nonuni FacC_ImpA_Uni FacC_ImpA_Nonuni FacC_ImpB_Uni FacC_ImpC_Uni | FacF_Perf_Uni FacF_Perf_Nonuni FacF_ImpA_Uni FacF_ImpA_Nonuni FacF_ImpB_Uni FacF_ImpC_Uni | Smooth_Perf_Uni Smooth_Perf_Nonuni | 6.2.3 |
| Connection stiffness <ul style="list-style-type: none"> Rotational stiffness k_m reduced to 50% Rotational stiffness k_m reduced to 25% Axial stiffness k_n reduced to 50% Axial stiffness k_n reduced to 25% Axial stiffness k_n reduced to 5% k_m and k_n at 100% (standard) Joints extended to facet corners Joints end 80mm from corner (standard) | FacC_ImpA_Uni_Cor FacC_ImpA_Uni | FacF_ImpA_Uni_kn50 FacF_ImpA_Uni_kn25 FacF_ImpA_Uni_kn50 FacF_ImpA_Uni_kn25 FacF_ImpA_Uni_kn05 FacF_ImpA_Uni | | 6.2.4 |
| Modelling technique variations <ul style="list-style-type: none"> Element type: S4R Element type: S4 (standard) 5-7 elements per joint edge 8-10 elements per joint edge (standard) 11-13 elements per joint edge Orthotropic joint material Isotropic joint material (standard) | FacC_Perf_Uni_S4R FacC_Perf_Uni FacC_ImpA_Nonuni_Ort FacC_ImpA_Nonuni | FacF_Perf_Uni_S4R FacF_Perf_Uni FacF_Perf_Uni_Esmall FacF_Perf_Uni FacF_Perf_Uni_Elarge | | 6.2.5 |

Table 6.1: Overview of geometrically non-linear FE models.

have the same boundary conditions. The maximum span of the structures is $11.5m$, the height is $1.9m$, and the facet/surface thickness is $15mm$. The structures are supported against translations along the boundary.

Table 6.1 gives an overview of the analyzed models. The names used in the table for the different models are organized in three keys (some also have a fourth part), stating (1) the structure's geometry, (2) possible imperfection and (3) the applied load case. In the discussion of the results, the various FE models are referred to by their names given in Table 6.1.

As it appears in Table 6.1, two load cases have been studied – a uniform and a non-uniform. In the uniform load case, the reference load is a distributed vertical load of $100kN/m^2$ acting downward⁴. In the non-uniform load case, a distributed vertical load of $100kN/m^2$ is acting on half of the structure, and $25kN/m^2$ is acting on the other half (as in the sketch to the right).



All the analysis in Table 6.1 have been run several times, with varying parameters (initial load increment, maximum/minimum increment, number of increments), to verify the results⁵.

When referring to a *critical load* in the discussion of the FE results, it is the load level of the last load increment that did not yield negative eigenvalues in the search for equilibrium⁶.

6.2.2 Bending of the facets

This section focuses on the non-linear behaviour locally in the plate shell facets. Each facet is loaded by both in-plane loads (shell action) and out-of-plane loads (bending action). As the load level increases, the facet's in-plane stiffness and out-of-plane stiffness change, and this induces a rearrangement of the internal forces in the facets. A facet's response to in-plane load and out-of-plane load is described in the following.

assumed that the loading is proportional – i.e. all load magnitudes vary with a single scalar parameter. In addition, it is assumed that the response is reasonably smooth - that sudden bifurcations do not occur. The basic algorithm is the Newton-Raphson method. In the Arc Length algorithm, as it is implemented in ABAQUS, the increment size is limited by moving a given distance along the tangent line to the current solution point and then searching for equilibrium in the plane that passes through the point thus obtained and that is orthogonal to the same tangent line [2]. In each step the deformed structure serves as basis for the next load step, hence the geometric non-linearity.

⁴This load is not a realistic load, as it is about 40 times larger than a realistic design load on the structure. It serves only as a reference load.

⁵When more than one load path ends up at the same critical load (within 5%), and when the load step at the critical load is not too large (less than 3-5% of the total load), the results are considered verified.

⁶When the solution contains a negative eigenvalue, the load may have overstepped a point of bifurcation, and the resulting load-displacement path cannot be fully trusted without a more in-depth analysis what happens at that load level.

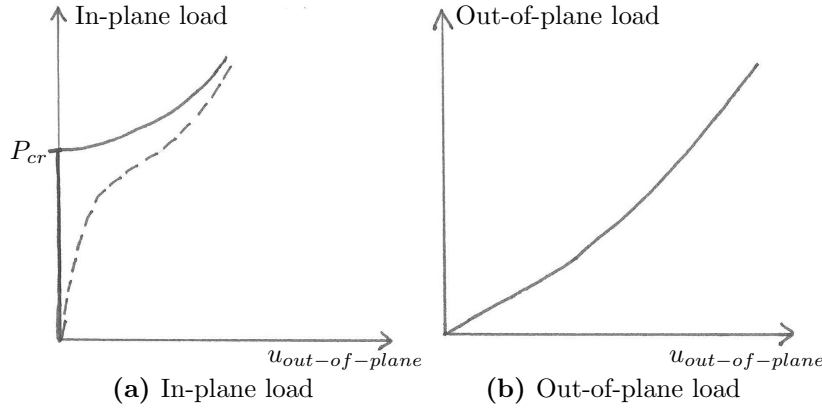


Figure 6.2: Principle sketches of non-linear out-of-plane deflection of plate.

In-plane load

A plate⁷ subjected only to uniform in-plane compression will at first remain plane, and carry the applied in-plane load by in-plane forces, with very small deformations in its own plane, and no displacements out of its own plane. When the load reaches the buckling load of the plate⁸ the plate has zero stiffness against out-of-plane movement, and at the slightest disturbance the plate will display out-of-plane displacements (buckling). Such a plate is stable in its post buckling state, and will keep on carrying increasing in-plane load, with increasing out-of-plane displacements as a consequence [51]. This behaviour is illustrated in Figure 6.2(a) by the full-drawn line.

If the plate has a small initial geometric out-of-plane imperfection, this will increase as the in-plane load is applied. This behaviour is illustrated by the dotted line in Figure 6.2(a). As the in-plane load approaches the buckling load for the perfect plate, the out-of-plane deflection will grow faster. After reaching the buckling load, the initial imperfection becomes negligible compared to the increasing out-of-plane deflection, and the behaviour of the imperfect plate will approximate that of the perfect plate.

Out-of-plane load

A plate (see footnote 7) subjected to out-of-plane load (bending action) will at first deflect linearly out of its own plane. As the load and the deflection increase, an in-plane resistance in the plate against out-of-plane deflection arises. This resistance is due to strain in the middle plane of the plate, necessary for the plate to follow the deflected shape [51]. For a plate deflection of more than approximately 0.5 – 1.0 times the plate thickness, this in-plane resistance becomes non-negligible. In the principle sketch shown in Figure 6.2(b),

⁷The plate is plane and of convex, relatively regular, polygonal shape. The plate is supported against translation out of its plane, and is loaded by uniform in-plane compression.

⁸For a plate of regular hexagonal shape the linearized buckling load is determined by $n_{cr} = 0.597 \cdot Et^3 / (a^2(1 - \nu^2))$, where n_{cr} is the uniform line load along the plate boundary (in-plane compression), E is the E-modulus for the plate material, t is the plate thickness, a is the geometric side length and ν is Poisson's ratio for the plate material [61]. In [61] the linearized buckling load for other simple plate shapes can also be found.

this results in an increasing stiffness of the plate as the out-of-plane deflection increase. It is this in-plane stiffening effect which results in the stable post buckling behaviour, referred to above.

In-plane *and* out-of-plane load

A facet in a plate shell is subjected to both in-plane *and* out-of-plane load. Therefore, a stiffening effect will occur when the out-of-plane deflection becomes comparable to the plate thickness, and a softening effect might occur as the in-plane load reaches the linearized buckling load of the plate. The latter will not happen if large plate displacements occur first. The interaction between these effect depends on the ratio between the in-plane and out-of-plane utilization of the plate.

The displacements of a hexagonal facet in a plate shell are shown in Figure 6.3⁹. (The facet is taken from the model **FacC_Perf_Uni.**) The red curve is the vertical displacement of the facet edge mid-point (representing the shell displacement of the structure, see footnote 1 in Chapter 4). The blue curve is the vertical displacement of the facet centre, where the absolute value has been corrected for the edge displacement, so that the shown curve is the plate deflection, relative to its edge mid-points.

The deflection in the plate centre displays an out-of-plane stiffening of the plate for $u/t \gtrsim 1$. The overall stiffness of the structure is continuously lessening, until failure occurs.

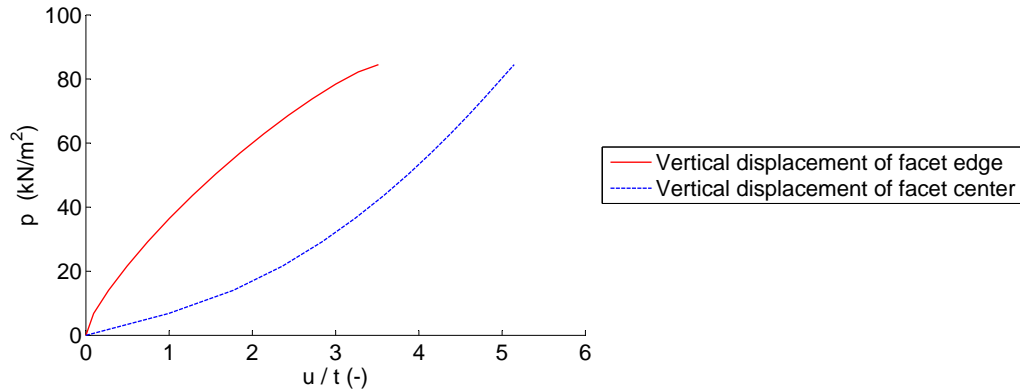


Figure 6.3: Normalized displacements of a hexagonal facet in a plate shell structure.

As the out-of-plane displacement of the facet increases, the in-plane compression forces from the shell action will “move away” from the plate centre, towards the plate edges. At the same time, the large out-of-plane displacements will result in in-plane tension forces in the facet centre, and a surrounding area with in-plane compression forces. As a result of both effects, as the load increases, an in-plane compression ring will develop in the facet,

⁹The linearized buckling load of the plate can be determined as described in footnote 8 in this chapter (– an approximate value, since the geometry is not a regular hexagon). This results in a critical in-plane line load of $n_{cr,plate} = 115N/mm$. When regarding a linear calculation of the plate shell model, the in-plane forces are almost constant over the facets, and an in-plane force of $115N/mm$ corresponds to a load of $p = 22kN/m^2$ on the structure.

and small in-plane tension forces will develop in the facet centre. This redistribution of forces does not in itself cause failure of the structure, because the resulting compression rings behave as frames in the facets' plane.

Failure of the structure may occur when these frames fail due to local buckling. This is the case in all investigations in the present study, as it will be presented in the following sections. Other failure types may become relevant for other plate shell designs (for example global failure of a more shallow dome).

6.2.3 Imperfections

This section studies the influence of imperfections on the non-linear behaviour of plate shells. First, the question of how to impose imperfections to the perfect plate shell geometry is addressed. After this, results of the non-linear FE analysis are presented and discussed.

Using linearized buckling eigenmodes

Typically, when determining the critical load for a *smooth* shell structure, one of the lowest linearized bifurcation buckling modes (or a combination of several) is used as the imperfect geometric shape: one or more of the lowest bifurcation modes is given an amplitude, based on the estimated geometric precision of the physical structure, and geometric non-linear FE analysis is performed on the imperfect geometry.

Such a procedure is not applicable when designing a plate shell, since a large number of the lowest bifurcation modes refers to linearized plate buckling of the facets. In [7] a linear buckling analysis was carried out on a plate shell. The first 50 bifurcation modes were local buckling of facets (individual or a combination of several), and the corresponding eigenvalues were within a 10% range, relative to each other.

If such a bifurcation mode is used for the initial imperfections it will have a very little effect on the results, since such an imperfection is negligible compared to the plate bending deformations that arise as the load increases.

The approach of using linearized buckling modes as initial imperfections is therefore not applicable to a plate shell structure.

Physically realistic imperfections

For a plate shell, the realistic imperfections stemming from production tolerances, erection inaccuracies, creep in connections and interlayer, and support settlements, can be assessed given the special characteristics of this type of structure. Generally, the following conditions apply:

- A *The facets can generally only remain plane if the overall geometry is perfect or almost perfect.* In a point-based system, imprecise bar lengths will result in changes in the shell curvature. In a plane-based system such as a plate shell, overall changes in the shell curvature can generally only happen if the facets become non-plane.

- B The facets are likely to remain plane or almost plane, given their relatively high bending stiffness. Compared to a plate in another context with a similar span and out-of-plane load, the thickness of the facets is relatively large¹⁰.

Items A and B above imply that the plates locally can have small translations and rotations, to the extent that the ensuing geometric deviations can be taken up by the connection tolerances. A plate shell is therefore unlikely to have large geometric imperfections. If the facet production, the placement of the supporting structure, and the erection procedure lacks precision, the structure simply cannot be assembled.

Imperfections implemented in the FE analysis

In the present study, two different types of “imperfection bumps” have been added to the perfect geometry of the three structures in Figure 6.1. The two bump shapes are shown in Figure 6.4. These imperfections are not physically realistic for plate shells as argued above. An implementation of physically realistic imperfections (and the ensuing residual stresses in facets and connections) has not been in focus in the present study. The intent of the analysis is to do an introductory investigation into plate shells’ imperfection sensitivity.

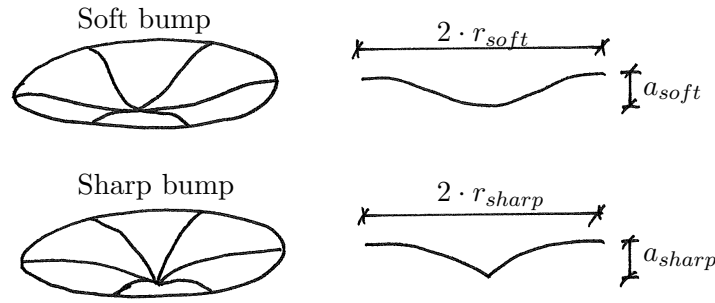


Figure 6.4: Two types of bumps are added to the perfect geometry.

Each type of bump is given an amplitude (a), a radius (r) and a point of origin (location of the maximum value), and the bump value is added to the vertical value of each node of the structure. The soft bump is a cosine surface¹¹, and the radius is chosen relatively large. The sharp bump¹² has been implemented particularly for the faceted shell, to depict a situation where a vertex for some reason is in a lower position than intended. The radius of the sharp bump is chosen so that it is comparable to the side length of the facets.

The imperfection combinations given in Table 6.2 have been applied to the three FE models.

¹⁰The large thickness of the glass facets is due to safety reasons (2-3 layer laminated glass panes), practical reasons regarding the connection detail (see for example the description of the *glued-in plate* connection on page 84), and an aesthetical wish for low plate deflections (they should not be visible in reflections in the facets).

¹¹Soft bump: $f(r, \theta) = f(r) = 0.5a_{soft}(1 + \cos(r\frac{\pi}{r_{soft}}))$

¹²Sharp bump: $f(r, \theta) = f(r) = a_{sharp}(1 - \sin(r\frac{\pi}{2r_{sharp}}))$

| | r_{soft}/m | a_{soft}/mm | r_{sharp}/m | a_{sharp}/mm |
|----------------|--------------|---------------|---------------|----------------|
| Imperfection A | 5 | 50 | 1 | 25 |
| Imperfection B | 5 | 100 | 1 | 50 |
| Imperfection C | 5 | 150 | — | 0 |

Table 6.2: Imperfections added to the perfect shell geometries in Figure 6.1.

When considering the amplitude of the imperfections in Table 6.2, the maximum size of imperfection A corresponds to about $1/150^{th}$ of the total span of the plate shell. Imperfection B is like A, but the amplitude is twice as large, which is an unrealistically large imperfection; B is included to explore the sensitivity of the solution to A. C has the same maximum amplitude as B, but in the shape of a soft bump.

Only imperfection C (where there is no sharp bump) is applied to the smooth shell, see Table 6.1.

Figure 6.5 shows the centre of the bumps on the three analyzed structures.

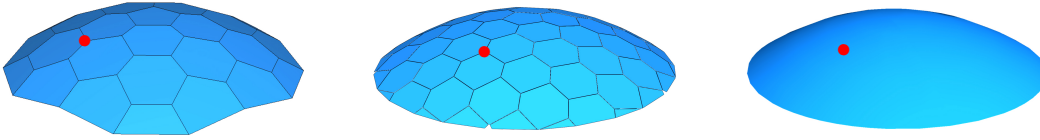


Figure 6.5: Center of the imperfection bumps.

Results

Critical loads of the non-linear models comparing imperfection sensitivity are given in Table 6.3.

| <i>Coarse faceting,</i> FacC | $p_{cr} /$ kN/m^2 | <i>Fine Faceting,</i> FacF | $p_{cr} /$ kN/m^2 | <i>Smooth shell,</i> Smooth | $p_{cr} /$ kN/m^2 |
|----------------------------------------|------------------------|--------------------------------------|------------------------|---------------------------------------|------------------------|
| <i>Perfect geometry</i> | | | | | |
| FacC_Perf_Uni | 84 | FacF_Perf_Uni | 74 | Smooth_Perf_Uni | 107 |
| FacC_Perf_Nonuni | 82 | FacF_Perf_Nonuni | 73 | Smooth_Perf_Nonuni | 80 |
| <i>Imperfection A</i> | | | | | |
| FacC_ImpA_Uni | 78 | FacF_ImpA_Uni | 71 | | |
| FacC_ImpA_Nonuni | 80 | FacF_ImpA_Nonuni | 68 | | |
| <i>Imperfection B</i> | | | | | |
| FacC_ImpB_Uni | 57 | FacF_ImpB_Uni | 64 | | |
| <i>Imperfection C</i> | | | | | |
| FacC_ImpC_Uni | 76 | FacF_ImpC_Uni | 57 | Smooth_ImpC_Uni | 104 |

Table 6.3: Critical loads, comparing imperfection sensitivity. For an overview of non-linear models, see Table 6.1. The imperfections (type A, B and C) are given in Figure 6.4, 6.5 and Table 6.2.

The results in Table 6.3 can be compared from three different perspectives:

- **Geometry.** When comparing the results where *no* imperfections are present, the critical load of the two plate shells is found to be reduced 15 – 25% compared to critical load of the smooth shell. The plate shell with coarse faceting generally has a higher critical load than the plate shell with fine faceting.
- **Imperfections.** The critical load of the perfectly shaped smooth shell is only reduced slightly (3%) by the introduction of a relatively large imperfection. This is most likely due to the relatively large curvature of the shell shape. The plate shells are somewhat more sensitive to imperfections. For imperfection A, the reduction of the critical load is 4 – 8%. Larger imperfections (imp. B and C) result in larger reductions (up to 33%).
- **Load distribution.** The two plate shells seem to be more robust to non-uniform load than the smooth shell. The critical load of the smooth shell is reduced 25% in the non-uniform load case compared to the uniform load case, where as the critical load of the plate shells is almost the same.

In those plate shell analysis where the structure's failure mode is clearly visible from the results, the failure mode is a single sine wave over a facet edge. Figure 6.6 shows a detail of the plate shell model **FacC**, just before and after failure. Figure 6.7 show a similar detail from the plate shell model **FacF**.

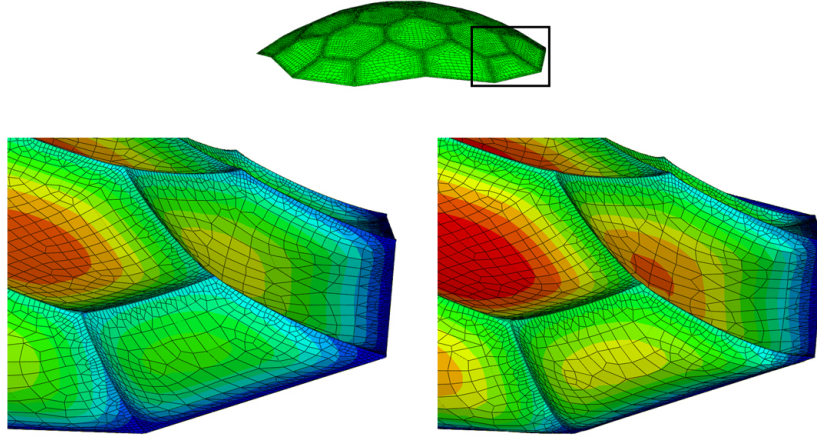


Figure 6.6: Contour deformation plots (detail) of **FacC_Perf_Uni** at the critical load level (before and after failure). The contour scale is consistent in the two images. The difference in load level in the two images is 6%.

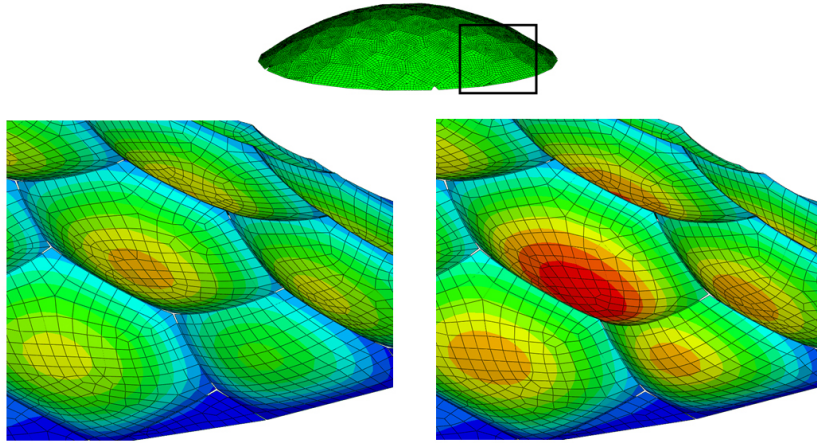


Figure 6.7: Contour deformation plots (detail) of **FacF_Perf_Uni** at the critical load level (before and after failure). The contour scale is consistent in the two images. The difference in load level in the two images is 10%.

6.2.4 Connection stiffness

This section studies the influence of the connection stiffness parameters on the non-linear behaviour of plate shells.

The connection stiffness parameters generally used in the non-linear analysis in this chapter correspond to the *glued-in plate* connection design. In the following study, these parameters have been varied, to investigate the effect on the critical load.

The plate shell with fine faceting has been used, since any effects from the connection stiffness is likely to be enhanced in this model because of the larger number of connections. Imperfection A is added to the perfect geometry, and the load is uniform.

The FE models listed in Table 6.1 under the headline “Connection stiffness” have been analyzed. In two models the rotational stiffness k_m is reduced to 50% and 25% respectively,

and in three models the axial stiffness k_n is reduced to 50%, 25% and 5% respectively. Table 6.4 lists the models, the relevant connection stiffness parameters and the joint parameters used in the models.

The calculated critical load of the models are given in Table 6.5. (The note “standard” indicates that the connection stiffness parameters in this model are the same as used in the other non-linear studies in this chapter.)

| <i>Model</i> | k_m (kN) | k_n (kN/mm ²) | t_j (mm) | E_j (kN/mm ²) |
|--------------------------------------|---------------|--------------------------------|---------------|--------------------------------|
| FacF_ImpA_Uni (standard) | 16 | 5 | 6.15 | 4.07 |
| <i>Reduction of k_m</i> | | | | |
| FacF_ImpA_Uni_kn50 | 8 | 5 | 4.38 | 5.71 |
| FacF_ImpA_Uni_kn25 | 4 | 5 | 3.10 | 8056 |
| <i>Reduction of k_n</i> | | | | |
| FacF_ImpA_Uni_kn50 | 16 | 2.5 | 8.76 | 1.43 |
| FacF_ImpA_Uni_kn25 | 16 | 1.3 | 12.4 | 0.50 |
| FacF_ImpA_Uni_kn05 | 16 | 0.25 | 27.7 | 0.045 |

Table 6.4: Connection stiffness parameters and joint parameters used for modelling, for the models listed in Table 6.1 under “Connection stiffness”. t_j and E_j have been determined as described in Section 3.2.1 (page 27).

| <i>Model</i> | p_{cr} / kN/m ² |
|--------------------------------------|------------------------------|
| FacF_ImpA_Uni (standard) | 71 |
| <i>Reduction of k_m</i> | |
| FacF_ImpA_Uni_kn50 | 68 |
| FacF_ImpA_Uni_kn25 | 69 |
| <i>Reduction of k_n</i> | |
| FacF_ImpA_Uni_kn50 | 67 |
| FacF_ImpA_Uni_kn25 | 52 |
| FacF_ImpA_Uni_kn05 | 25 |

Table 6.5: Critical loads, comparing varying connection stiffness parameters. For an overview of non-linear models, see Table 6.1.

The results in Table 6.5 clearly indicate a correlation between the critical load and the axial stiffness k_n . A reduction of the axial stiffness seems to result in a reduced critical load. This correlation has also been observed in [7] and [8], where a plate shell was subjected to non-linear FE analysis. Those results showed a strong influence of the axial stiffness on the critical load, and almost no influence of the rotational stiffness k_m .¹³ Correspondingly,

¹³The structure that was investigated in [7] and [8] had a different geometry and the axial stiffness k_n

the results in Table 6.5 indicate only a slight reduction of the critical load for a reduced rotational stiffness.

In one model (**FacC_ImpA_Uni_Cor** in Table 6.1 – the plate shell with coarse faceting, imposed by imperfection A, and subjected to the uniform load) the joint elements are modelled so that they connect the full length of the facet edges. In **FacC_ImpA_Uni_Cor** the critical load is increased by 5% compared to **FacC_ImpA_Uni**, which is an identical model apart from the unconnected facet corners (the joint elements end 100mm from the facet corners). The unconnected facet corners thereby appear to be of minor importance to the critical load.

6.2.5 Modelling technique variations

Some variations in the FE modelling technique have been studied:

- The use of a different element type in ABAQUS. In stead of S4 elements, S4R elements have been used. S4R (R for *reduced* integration) has only one integration point, where S4 has four¹⁴.
- Variation of the element size. The same model has been analyzed three times, using three different general element sizes.
- The connection stiffness has been modelled by an isotropic joint material, and (in an otherwise identical model) by an orthotropic joint material. As described in Section 3.2.1 (page 28), when using an isotropic joint material the shear stiffness parameters will not be modelled correctly.

The calculated critical load of the relevant models are given in Table 6.6, 6.7 and 6.8. For an overview of non-linear models, see Table 6.1.

| <i>Model</i> | <i>Element type</i> | <i>p_{cr} / kN/m²</i> |
|--------------------------|---------------------|------------------------------------------|
| FacC_Perf_Uni_S4R | S4R | 77 |
| FacC_Perf_Uni (standard) | S4 | 84 |
| FacF_Perf_Uni_S4R | S4R | 75 |
| FacF_Perf_Uni (standard) | S4 | 74 |

Table 6.6: Critical loads, comparing two element types (S4 and S4R).

The results in Table 6.6 indicate a difference of up to 8% on the critical load when using S4 and S4R elements respectively. The computational time is reduced 20-30% by using

was much lower – about 5% of the values tested here. The rotational stiffness k_m was comparable to the values modelled in the present study.

¹⁴S4R is computationally less expensive than S4. S4 does not have hourglass modes, and generally has a higher solution accuracy [1]. In linear FE analysis of a plate shell in [31] the use of S4R and S8R elements resulted in a few elements with large numerical errors.

| <i>Model</i> | <i>Number of elements per facet edge</i> | <i>p_{cr} / kN/m^2</i> |
|--------------------------|----------------------------------------------|------------------------------------------------------|
| FacF_Perf_Uni_Esmall | 10-13 | 75 |
| FacF_Perf_Uni (standard) | 8-10 | 74 |
| FacF_Perf_Uni_Elarge | 5-7 | 73 |

Table 6.7: Critical loads, comparing varying element sizes.

| <i>Model</i> | <i>Modelled joint material</i> | <i>p_{cr} / kN/m^2</i> |
|-----------------------------|------------------------------------|------------------------------------------------------|
| FacC_ImpA_Nonuni_Ort | Orthotropic | 77 |
| FacC_ImpA_Nonuni (standard) | Isotropic | 80 |

Table 6.8: Critical loads, comparing how accurately the shear stiffness in the connections are modelled.

S4R. For most practical purposes, a feasible approach could be to perform two non-linear analysis on the same structure, using S4 and S4R elements respectively. If the difference in the resulting critical load is negligible, the computationally quicker S4R element may be used for further analysis.

The results in Table 6.7 imply that a mesh density of about 5-7 elements along the facet edges is sufficient for the determination of the structure's critical load. The failure modes for the plate shell structures studied in this chapter is a single wave over a facet edge (see the images in Figures 6.6 and 6.7). For such a failure mode, 5-7 elements along the glass edge is sufficient to describe the structural behaviour with adequate precision. Naturally, the stress peaks in the connection end areas are not determined very well with such a coarse mesh, but the results in Table 6.7 indicate that this has negligible effect on the calculated critical load of the structure.

The results in Table 6.8 indicate a small difference (4%) in the critical load, when the joint material is modelled by an isotropic material, instead of an orthotropic material which reproduces the shear stiffness parameters correctly. As shown previously in a linear FE analysis (page 29 and footnote 3 in Chapter 3), the error on the peak stresses is less than 5% when using an isotropic joint material instead of an orthotropic.

6.2.6 Summary of non-linear study

As the non-linear investigations in Section 6.2 have shown, structural failure due to buckling is not likely to happen for the analyzed structures – the allowable displacements and the ultimate strength of the structural elements is far more critical¹⁵.

The results in Section 6.2 indicate the following tendencies for the non-linear behaviour

¹⁵The allowable displacements and the strength of the structural elements is not elaborated upon in the present study (except briefly in Chapter 7, where the descriptions of possible connection details refer to some experimental results).

of the analyzed plate shells. The critical load of the plate shells is generally comparable to the critical load of the equivalent smooth shell; changing the smooth shell surface into a plane-based faceted surface, and thereby introducing bending moments and connection lines with reduced stiffness, seems to result in a reduction of the critical load of 0-40%. The reduction is larger if the axial stiffness of the connection detail is low. For the analyzed structural shapes, the plate shell is more sensitive to imperfections than the smooth shell, and it is less sensitive to non-uniform load¹⁶.

Since only one overall shell shape is investigated in the present study, the results cannot be used for general conclusions about the non-linear behaviour of plate shells. Other correlations between smooth and faceted shells may exist for other shell shapes – especially if the shell shape is more shallow, and hence more sensitive to imperfections.

¹⁶A smooth shell shape can be shaped so that it is optimal for the predominant load case. The term “optimal” can be understood and implemented in different ways when shaping the structure. Some examples are: shapes where only compressions forces are present (funicular structures [17]), hanging forms (a variant of funicular structures [19]), shapes where the largest stress has been minimized or where the stresses are as uniform as possible [15] [47]. The shape can be optimized using more than one load case, but generally, the optimality of the shape is highly dependant on the load distribution.

Chapter 7

Design of connection detail

The connections between the facets in a plate shell structure are in many ways the *weak link* of the structure. The connections will most likely have less *strength and stiffness* than the facets, and at the same time the largest forces are likely to occur in the connections. *Tolerances* must primarily be taken up in the connections, during assembly of the structure. *Repair work* must be facilitated by the connection design. If the structure is *leaking*, it will be at the connections. If the facets are insulating units, the largest *heat loss* will most likely be at the connections. The connections will be the first part of the structure to *deteriorate*, unless a glass pane is accidentally broken.

A list of functional requirements and wishes for the connection design is set up and discussed in Section 7.1. The list is in prioritized order. These items have served as a basis for the three design suggestions sketched up in sections 7.2 to 7.4.

7.1 Functional requirements for the connection detail

Appearance

The appearance of the connections is of very high importance. The connections should appear slender and light, so that the basic reason for choosing this structural principle becomes clear: the facets *are* the structure – the connections merely transfer loads between the facets. If the connections look large and heavy, they will appear as if carrying the load, and the special meaning of the plate shell principle will be largely lost.

Strength and stiffness

The strength of the connection detail must be sufficient to withstand the loads it attracts, given its stiffness. Details with a high rotational stiffness k_m (see Section 3.1, page 25) are loaded by a relatively large bending moment (depending on the size and thickness of the facets). Details with a very low rotational stiffness k_m and a large axial stiffness k_n may have large in-plane tension forces at the ends of each connection line. (These effects are studied in Chapters 4 and 5.) If the connection detail cannot sustain the loads it attracts via its stiffness, it will fail.

The connection detail should transfer loads between the facets, without causing significant stress concentrations in the glass.

Construction

The connection detail should be as simple as possible to assemble, to ensure connections that are visually homogeneous, and have the desired strength and stiffness.

A key issue in the design of the connection detail is *tolerances*. As previously discussed (Section 6.2.3, page 72), an imperfect geometry can generally only be realized by warping the facets, or by taking up some translations and rotations in the connections. Warping the facets (which have a relatively large bending stiffness, see for example footnote 10 in Chapter 6) may cause large restraining forces in the connections, and they will most likely be difficult to assemble. The connection detail should therefore be able to take up whatever tolerances that may occur.

Solutions with *adhesives* may be difficult to implement on site with optimal quality, due to the possibility of unclean surfaces, and unfavorable temperature and humidity conditions. If possible, work with adhesives should be completed before the facets arrive at the site.

Temperature movements

Temperature movements in the connection detail should not induce significant stresses in the detail or in the glass. This means that materials with a different thermal expansion than the glass must not be fixed too rigidly to the glass.

Failure safety

Given a situation where the load on a connection succeeds the detail's strength, and the detail therefore fails, a certain capacity for *yielding* enables a redistribution of forces, relieving the detail for some of the load. Such a yielding capacity is desirable.

In case of failure in a connection, it should preferably be *visible* by simple visual inspection, so that action can be taken to prevent further damage of the structure.

Also, an extra safety in case of connection failure is desirable. For example, if a friction connection clamped around the facet edges fails, the connected facets could balance against each other, still held together by the otherwise failed detail.

If fracture occurs in the laminated glass facets, the broken facet will remain in one piece, due to the lamination. The connection detail should remain attached to the facet edges, so that the broken facet does not fall out of the structure.

Long term behaviour and wear

If parts of the connection detail display time dependent behaviour, such as *creep*, the consequences must be assessed. Will the creep rate become negligible after a period of time? How does the creep rate respond to fluctuations in temperature and air moisture? What will happen to the forces in the connection, and to the structure as a whole, when

creep occurs?

If the creep rate is load-dependent, this may enable a favorable relaxation of peak stresses at the connection ends, followed by a reduction of the creep rate to a negligible level.

The load-transferring part of the connection should preferably be protected from direct sunlight, rain, ice and physical impact, or have a suitable resistance against these factors. The part of the connection which is directly exposed to weathering should preferably be replaceable, for example a silicone sealant.

The service life of the structure is likely to be governed by the connections, unless these are replaceable.

Water tightness

The connection detail should provide good water tightness, and it should be possible to fix a leak by replacing or adjusting parts of the connection.

Repair work and maintenance

In case a facet needs replacement, it is preferable that the connection detail can be disassembled without harming the surrounding facets, so that the broken facet can be removed, and a new facet can be fastened. The fastening method for the new facet can possibly be different than the original connection detail.

The connection detail should be designed so that water and dirt does not accumulate anywhere, and so that cleaning is as easy as possible.

Insulating properties

In stead of facets of laminated glass, *insulating glass units* (IGU) can be used as facets, thereby greatly improving the insulating properties of the structure.

Only one layer in the IGU should be active in the structural shell action, meaning that the connection detail should only connect one layer in the IGU. This is to avoid the risk of movements and stresses around the spacer that could induce a puncture of the IGU.

The glass layer which is active in the shell action must be laminated glass. A second pane can be supported on a spacer as shown in Figure 7.1 – the connection detail in the illustration is the *glued-in plate* connection described in Section 7.2. The second pane will then be active in the local plate bending (because of the enclosed volume of air), but not in the shell action.

The connection detail should be designed, so that the linear thermal transmission in the connection lines is minimized.

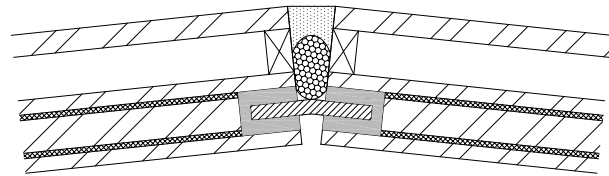


Figure 7.1: IGU in plate shell connection.

7.2 Glued-in plate connection

This section describes the first of three suggested plate shell connection details. Sections 7.3 and 7.4 describe the other two.

The *glued-in plate* connection detail consists of a plate (or another mechanical item), embedded into the glass facet edge using a structural adhesive.

For this connection design, the plate shell facets are built up by three layers of glass, laminated together using SentryGlass®Plus (SGP) interlayer [23].

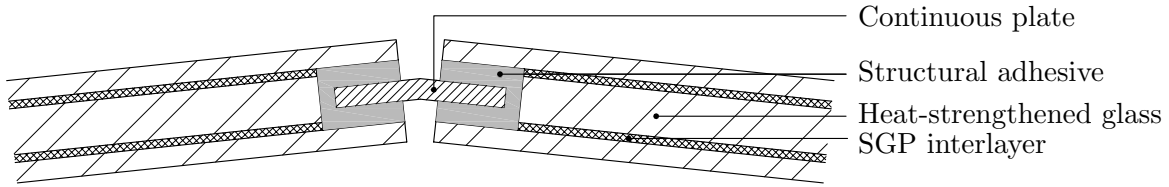


Figure 7.2: Glued-in plate connection.

The sketch in Figure 7.2 is a section perpendicular to the connection line between two facets. As illustrated in the figure, the edge of the middle pane of the three glass layers is offset a small distance from the edge of the two other panes, creating a canal along the facet's circumference. A plate, continuous in the direction of the glass edges, is glued into the edge canal by a structural adhesive, as shown in the figure. The rotational stiffness of the connection can be adjusted by choosing the thickness and material of the glued-in plate appropriately. When choosing the plate thickness, it must be ensured that the thickness is sufficient to sustain the stresses it attracts and, especially for thin plates, that there is no risk that the plate will collapse. The length of the plate is chosen relative to the edges it connects – to allow for uplift of the facet corners, the plate length should be shorter than the connected edges.

In the plate corners, the gaps can be filled with a dark silicone, to maintain the appearance of the dark strip over the entire edge length, and to obtain water tightness in these areas.

The glued-in plate connection design has been tested experimentally at the Technical University of Denmark [32]. In these tests, the edge canal depth is 20mm , the canal's height is 12mm , the free gap between the connected plates are 16mm , and the glued-in plates are 4mm aluminum (alloy 6061-T6), with a width of 50mm . The structural adhesive is DP490 from 3M [6], a two component epoxy adhesive also used for a glued butt joint connection in the glass dome at the Institute for Lightweight Structures and Conceptual Design (ILEK), Stuttgart University [16] (see also Section 7.4). The tests indicate a rotational stiffness of $k_m \approx 40\text{kN}$, and an in-plane shear stiffness of $k_{v,i} \approx 2.5\text{kN}$ (these stiffness parameters are introduced in Section 3.1, page 24). The tests also indicate a slight creep tendency at a relatively high load level, which seems to decrease and become negligible after a few days. Failure has not been attained in in-plane shear (maximum shear force applied: 150N/mm , short term load). Failure was attained in bending for a

bending moment of approximately $700N$ – the failure mode was yielding in the aluminum. Parameters for a glued-in plate connection design have been estimated, prior to the execution of the above-mentioned experiments. These values are used in the conducted FE analysis throughout the thesis. The values are estimated assuming a glued-in aluminum plate with a thickness of $3mm$. The estimated stiffness parameters are as follows:

$$\begin{aligned}
 \text{Rotational stiffness} & \quad k_m = 16kN \\
 \text{Axial stiffness} & \quad k_n = 5kN \\
 \text{In-plane shear stiffness} & \quad k_{v,i} = 1kN \\
 \text{Out-of-plane shear stiffness} & \quad k_{v,o} = 6kN
 \end{aligned} \tag{7.1}$$

Advantages

The glued-in plate connection is deemed the most promising of the suggested connection details for large plate shell structures. Therefore, the advantages and drawbacks of this detail are elaborated in the following.

The connection will appear as a dark strip with a width of $50 - 70mm$. The entire detail is embedded in the glass pane, so no extra height is added to the facet surfaces at the connection, and in the centre line only a strip of $10 - 20mm$ width will be without a glass surface. Its strength considered, it is a slender connection, which will hardly appear as the primary load bearing system.

The above-mentioned ongoing experimental research indicates a high strength of the detail. This could perhaps imply an even smaller total width of the connection than suggested above.

The detail is ductile in bending, as bending failure is in the form of yielding in the aluminum, apparently with no damage to the adhesive.

The connection detail can take up relatively large tolerances in all directions during assembly.

The slight tendency to creep in the adhesive will to some extent reduce the stress peaks at the connection ends. The creep rate appears to reduce quickly and become insignificant.

The load bearing part of the connection can be covered by a replaceable silicone joint, which will protect the detail from weathering.

The laminated glass facets can be extended to become IGU's without increasing the width of the connection noticeably (see Figure 7.1).

Drawbacks

One half of each connection line can be glued in a workshop (so that the aluminum plate protrudes from the edge), but the opposing facet edge must be glued on site.

Failure in the adhesive is unlikely to be visible, unless it causes large dislocations in the structure.

It will be difficult to replace a broken facet.

Other comments

Tests have been made where the adhesive was replaced by a mortar suitable for glass structures, HILTI HIT-HY 70 [30]. To ensure a good load transfer between the mortar and the glass, thin strips of perforated stainless steel were glued to the inner, horizontal surfaces of the edge canal. The stiffness and strength of HIT-HY 70 is comparable to that of DP490, and the mortar shows a higher resistance to increased temperatures during fire. However, because of the mortar's short curing time, it was difficult to position the cast-in plate and achieve a satisfactory appearance of the connection. If an improved production method can be developed, the cast-in solution may be preferable to the glued solution.

The glued-in (or cast-in) plate's material and thickness can be modified to meet specific demands. The plate may also be replaced by other items, which are glued into the edge canal in a similar way. The detail can for example consist of two separate fittings, glued into opposing edge canals in the workshop, and assembled mechanically on site.

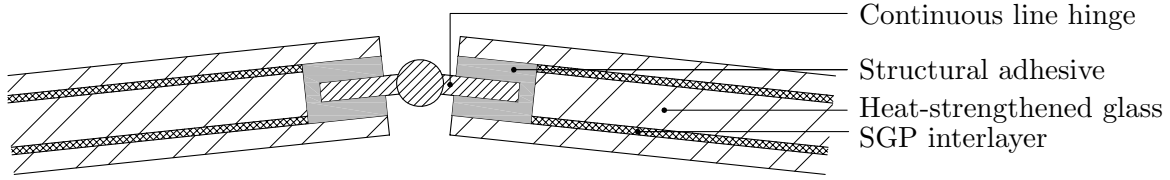


Figure 7.3: Glued-in hinge connection.

Figure 7.3 shows a possible variant where the glued-in item is a line hinge. This connection detail is included as a variant in the FE analysis throughout the thesis, to investigate the structural response when the connection's rotational stiffness is very low and the axial stiffness is relatively high. In Figure 7.3 the detail is sketched as an actual hinge, but it could have a large variety of shapes, with useful characteristics such as an easy mechanical assembly on site.

The estimated stiffness parameters for the glued-in line hinge connection are as follows:

$$\begin{aligned}
 \text{Rotational stiffness} & \quad k_m = 0.6kN \\
 \text{Axial stiffness} & \quad k_n = 5kN \\
 \text{In-plane shear stiffness} & \quad k_{v,i} = 1kN \\
 \text{Out-of-plane shear stiffness} & \quad k_{v,o} = 6kN
 \end{aligned} \tag{7.2}$$

These parameters do not take into account that there may be a small movement in the detail before it starts taking up load. Such a movement may result in smaller stress concentrations at the connection ends.

7.3 Friction connection

Two continuous profiles (aluminum, steel, glass fiber reinforced polymer (GFRP) or another suitable material) are clamped around the edge of a single monolithic sheet of glass. The connection is illustrated in Figure 7.4.

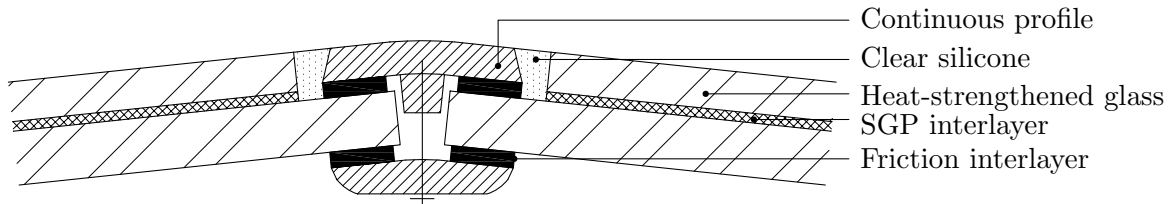


Figure 7.4: Friction connection.

A strip of a softer material serves as interlayer between the profiles and the glass, to secure a good transfer of friction forces, to avoid stress peaks in the glass caused by unevenness in the profiles, to allow for different temperature movements in the glass and the profiles, and possibly to introduce a rotational compliance in the connection. Prestress is applied to the interlayer by tightening the screws that hold the profiles together. A second layer of glass is laminated to the connected layer, so that a smooth outer surface can be attained.

The larger the rotational stiffness in the connection, the larger bending moment in the connection, and thereby the larger the necessary bending strength of the detail. The optimal solution could therefore be an interlayer which is relatively soft, while at the same time ensures a good friction. The problem is, however, that a soft material may not withstand the prestress which is necessary to attain sufficient friction.

The major advantage of the friction connection detail is that it is simple to assemble and, if necessary, disassemble.

The friction connection has been tested experimentally, comparing two different friction transferring interlayers; EPDM and Klingsil® [39]. EPDM is a synthetic rubber with good weather-resistance, used for many purposes, including as friction transferring interlayer. Klingsil [35] is a plate material of carbon fibres embedded in a synthetic rubber, developed for use in gaskets under high pressure and temperature. Klingsil has previously been applied as interlayer in friction connections in glass structures [60]. Like EPDM, Klingsil shows good weather-resistance. The stiffness of Klingsil is significantly higher than that of EPDM¹.

The variant using EPDM as interlayer showed poor strength and a low stiffness in the tests². Additional tests *may* show that the detail is applicable to plate shells where only little strength is needed in the connections. The detail is included in the list of variants used for the FE analysis throughout the thesis, to investigate the structural response when the connections' axial stiffness is very low.

¹An absolute value for the difference in stiffness cannot be given, as the behaviour of especially EPDM is highly dependent on the geometry of the EPDM item, and the stress state. The difference in stiffness is in the range of 20-300.

²A prestress of approximately 5.5N/mm^2 was applied to the 10mm wide EPDM strips. The tests showed an in-plane shear stiffness of $10 - 30\text{N/mm}^2$ and a bending stiffness of $4 - 7\text{kN}$. The force-displacement curve was highly nonlinear, and appeared to be very dependent on the rate with which the load was applied. A relaxation test revealed a 65% reduction of the prestress within the first hour, and a clear tendency to continuing relaxation after that. (No data available for longer load durations.) The in-plane shear strength was $3 - 4\text{N/mm}$ (30 minutes after tightening the screws to the full prestress). The bending strength is irrelevant, as the rotations became very large before the detail failed.

The estimated stiffness parameters for the friction connection using EPDM interlayer are as follows:

$$\begin{aligned}
 \text{Rotational stiffness} & k_m = 5kN \\
 \text{Axial stiffness} & k_n = 0.02kN \\
 \text{In-plane shear stiffness} & k_{v,i} = 0.02kN \\
 \text{Out-of-plane shear stiffness} & k_{v,o} = 0.1kN
 \end{aligned} \tag{7.3}$$

Tests of the friction connection using Klingsil as interlayer showed a higher axial and rotational stiffness³. Since the rotational stiffness is large, the connection will be loaded by relatively large bending moments. The bending capacity of the detail may not be sufficient for the plate shell **FacC**, investigated in Chapters 4 and 5 (see Figure 3.5, page 31). That plate shell structure has facets of roughly $2m$ diameter. A structure with smaller facets will have smaller local bending moments, and the friction connection may in that case be suitable.

The estimated stiffness parameters for the friction connection using Klingsil interlayer are as follows:

$$\begin{aligned}
 \text{Rotational stiffness} & k_m = 100kN \\
 \text{Axial stiffness} & k_n = 0.5kN \\
 \text{In-plane shear stiffness} & k_{v,i} = 0.08kN \\
 \text{Out-of-plane shear stiffness} & k_{v,o} = 1kN
 \end{aligned} \tag{7.4}$$

7.4 Glued butt joint

Ultimate slenderness and transparency could be achieved by connecting the facets with a *glued butt joint*, like the joining method used in the glass dome at ILEK in Stuttgart [16], shown in Figure 1.4 (page 3). The glued butt joint, applied to the plate shell, is illustrated in Figure 7.5.

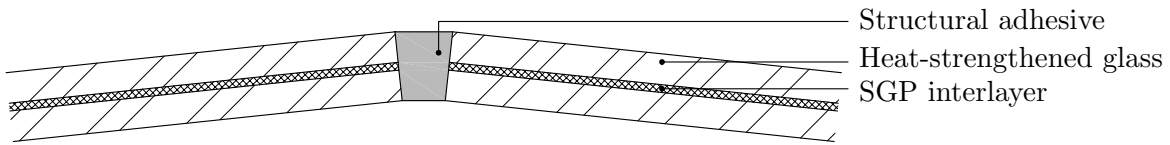


Figure 7.5: Glued butt joint.

Because of the facetted geometry, the plate shell has different forces in the connections than the smooth dome at ILEK. The predominant load in the connections of the ILEK dome are in-plane forces, which lead to a relatively low stress level. In the ILEK dome, the maximum stress in the adhesive is $0.6N/mm^2$, determined by FE analysis [16]. In the

³A prestress of approximately $5.5N/mm^2$ was applied to the $10mm$ wide Klingsil strips. The tests showed an in-plane shear stiffness of $0.5-0.7kN/mm^2$ and a bending stiffness of $70-130kN$. A relaxation test showed a 13% reduction of the prestress within the first 24 hours, and apparently no further relaxation after that (monitoring duration 96 hours). The in-plane shear strength was $12-17N/mm$. The bending strength was more than $250N$ (failure was not achieved, but the stiffness appeared to reduce somewhat at around $200N$).

plate shell, the stress level from in-plane forces is similar, but it is superposed by stresses from local bending in the facets.

In Section 5.1.3 approximate expressions for bending moments in plate shell facets were presented. In Figure 7.6 these expressions are used to investigate the bending stresses in a glued butt joint, for different values of facet size, facet thickness, and E-modulus of the adhesive. Stresses from in-plane forces must be added to determine the maximum stress in the adhesive.

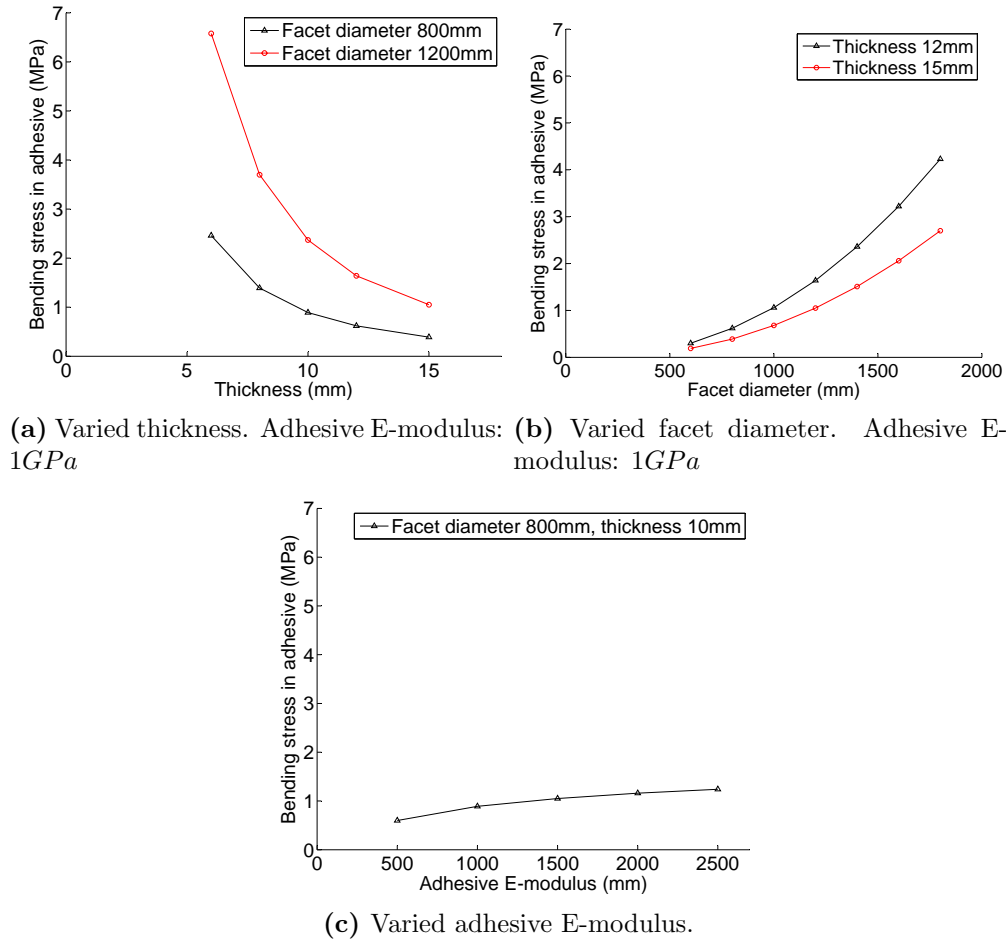


Figure 7.6: Bending stresses in the glued butt joint for varying parameters. “Thickness” denotes the thickness of the joint and the facet.

The load is 1 kN/m^2 perpendicular to the facet. The adhesive is assumed to be linear elastic, and the stress is assumed to vary linearly over the joint thickness. The joint width⁴ is set to 10 mm . The facet thickness and joint thickness are equal. Poisson’s ratio for the adhesive is set to $\nu = 0.45$.

⁴A variation of the joint width is not shown here. Calculations using the approximate expressions from Section 5.1.3 show that the stress level is increased 5 – 10% if the joint thickness is reduced from 10 mm to 7 mm , and that the stress level is reduced 2 – 5% if the joint thickness is increased from 10 mm to 13 mm .

A specific design value for the allowable stress in the adhesive cannot be determined based on available data. Experimental data in [16] indicates that the structural adhesive DP490 from 3M [6] has the most suitable characteristics for the connection, compared to a series of other structural adhesives available at that time (2005)⁵. Before using the glued butt joint in a full scale plate shell structure, the capacity of the joint should be determined through experimental investigations, for varying temperature conditions, air moisture contents and load durations. Based on the above-mentioned data in [16] and the current perfectly intact state of the glass dome at ILEK, the long time strength for DP490 under varying weather conditions is expected to be within the range of $0.5N/mm^2$ to $2N/mm^2$.

Based on that information, and the parameter study in Figure 7.6, a plate shell using the glued butt joint should be a relatively small structure with a span of $3 - 4m$, with relatively thick facets ($15mm$ or more) measuring roughly $0.6 - 0.8m$ in diameter.

The stiffness parameters used in the FE analysis throughout the thesis are based on a joint with thickness $15mm$, width $10mm$, and a constant E-modulus (i.e. *not* time-, load-, temperature and moisture-dependent) of $E_{adh} = 1GPa$ and $E_{adh} = 2.5GPa$ in two variations of the connection respectively. The resulting stiffness parameters are determined using (3.1), (3.2) and (3.3), where E_j is replaced by $\frac{E_{adh}}{1-\nu^2}$ corresponding to a plane strain condition instead of plane stress⁶.

For adhesive E-modulus $E_{adh} = 1GPa$ we get:

$$\begin{aligned}
 \text{Rotational stiffness} & k_m = 71kN \\
 \text{Axial stiffness} & k_n = 3.8kN \\
 \text{In-plane shear stiffness} & k_{v,i} = 1.0kN \\
 \text{Out-of-plane shear stiffness} & k_{v,o} = 1.0kN
 \end{aligned} \tag{7.5}$$

For adhesive E-modulus $E_{adh} = 2.5GPa$ we get:

$$\begin{aligned}
 \text{Rotational stiffness} & k_m = 176kN \\
 \text{Axial stiffness} & k_n = 9.4kN \\
 \text{In-plane shear stiffness} & k_{v,i} = 2.6kN \\
 \text{Out-of-plane shear stiffness} & k_{v,o} = 2.6kN
 \end{aligned} \tag{7.6}$$

⁵Long time tensile tests at $23^\circ C$ on a butt joint measuring $10mm$ by $10mm$ indicated continuous creep after 1200 hours with constant load, where the joint was subjected to a tensile stress of $2.75N/mm^2$. The creep compliance in compression is likely to be smaller than in tension [22].

⁶The three expressions (3.1), (3.2) and (3.3) are derived based on a plane stress distribution in the joint elements, since they are merely a numerical tool to adjust the parameters of the joint elements, so that they represent the stiffness of the actual physical connection detail.

Chapter 8

Guidelines for design of plate shell structures

The aim of this chapter is to propose a set of guidelines for the design of plate shell structures.

The studies done throughout the thesis are summarized, and attention is drawn to the main issues. Some design aspects, which are relevant in a design situation but have not been in focus in the present study, are brought up, together with suggestions for a possible design approach. Also, relevant topics for further research are suggested.

8.1 Geometry

Deciding on a geometry for a plate shell involves two steps: Choosing an overall (smooth) shape, and creating a plane-based faceted approximation to this shape. If glass is used for the facets, the smooth shape should be convex, to avoid concave facet shapes. Areas of very low curvature should be avoided. Generally, the overall structural “soundness” of the final plate shell may, at early stages of the design, be roughly evaluated by analysis of the smooth shape. If the smooth shell has areas with large in-plane stresses and/or large displacements, the corresponding plate shell will most likely have similar problems.

The creation of the plane-based faceted geometry can be carried out using the methods suggested in Section 2.1. Alternatively, other methods can be applied (some possibilities are mentioned on page 11).

8.2 Determining stresses and displacements

In a preliminary design phase, the structural behaviour of a given plate shell design may be estimated by using the methods described in Sections 4.2.3 (shell action) and 5.1.3 (bending action). The methods can be used to determine approximate values for in-plane forces in the connections, bending moments in the connections, bending moments in facets, and the out-of-plane deflection of the facet centres.

It should be noted that only a few different plate shell designs¹ have been used for the development of the methods. It is the author's expectation that the methods will also apply to other plate shell designs – this should be looked into by further research².

At a later stage in the design, a FE model of the plate shell must be created. If the *pyFormex* script presented in Section 2.2 is used for creating the plate shell geometry, this script can also be used for an automatic generation of an ABAQUS model of the structure. If a *pyFormex* generation is not possible, the FE model can be created following the guidelines in Chapter 3. In both cases, the connections between the facets are modelled by a strip of elements, the stiffness of which must be adjusted to the actual connection detail's physical stiffness. Alternatively, other methods for modelling the connection detail's stiffness may be applied.

Based on the FE analysis of the plate shell, the structural behaviour can be assessed, focusing on

- the overall displacements of the structure (the *shell displacements*, see footnote 1 in Chapter 4)
- the local deflection of the facets
- bending moments in the facets
- in-plane forces and bending moments in the connections
- the non-linear behaviour of the structure (in terms of buckling load)

8.2.1 Facets

If the FE analysis shows small shell displacements, this indicates that the plate shell is effective as a shell structure. This means that the bending moments in the facets are *local bending moments*, as described in Section 5.1.

The necessary thickness of the facets is most likely governed by either the local deflection of the plates, or by the local bending moment in the facet middle. If the rotational stiffness of the connection detail is very large, the maximum bending moment may occur at the facet edge.

¹Plate shell models **FacC**, **FacF** and **FacStar** – see Appendix A.

²Further studies must look into the different structural effects (such as the in-plane peak forces at the connection ends) for different shell layouts, i.e. with varying facet diameter, facet thickness, angle between facets, curvature radius for the overall shape of the structure and connection stiffness parameters. The results presented in this thesis cannot explicitly express the balance between the different structural effects for other shell layouts (for example by describing the found results using dimensionless parameters), because the governing correlations depend on the geometrical parameters raised to different exponents. Hence, the deflection of a facet varies with the ratio $\frac{d^4}{t^3}$, whereas the geometric resistance to corner lift varies with the angle between the facets, or $\frac{d}{R}$. The rotational restraint factor varies with $\frac{t^3}{d}$. (d is the facet diameter, t is the facet thickness and R is the curvature radius.) The dimensionless results of one combination of d , t and R can therefore not be reproduced in a different combination of these geometric parameters.

The interlayer in the laminated glass pane may over time loose some of its stiffness. This will reduce the bending stiffness of the facets. In the FE model, the modelled facet thickness can be reduced to an *effective thickness*, representing the facets' reduced bending stiffness by a thinner plate. The procedure for this reduction is described in [46]. Note that stresses in the glass plies will not be correctly reproduced in the model; stresses must be determined using the sectional forces, see [46]. The reduced facet thickness will result in a minor error in the calculated shell deflections.

8.2.2 Connections

The connections are primarily loaded by in-plane forces and bending moments. Generally, the stiffer the connection detail, the larger loads it attracts.

For some combinations of connection stiffness parameters, in-plane stress concentrations may occur at each connection's ends (see Chapter 4). Creep in the connection detail may reduce these stress concentrations. Creep may also reduce the bending moment in the connection, and increase the deflection of the facets. Generally, the consequences of time dependent changes in the connection detail should be evaluated.

It will most likely be necessary to determine the strength and stiffness parameters of the connection detail by experimental testing.

8.2.3 Buckling

As for all thin-walled structures loaded in compression, a critical load, at which the plate shell will collapse due to buckling, must be determined. A geometrically non-linear FE analysis must be carried out, in which the perfect plate shell geometry is imposed by relevant imperfections.

Determining such relevant imperfections has proven troublesome; as described in Chapter 6, a linear buckling analysis is not suitable for defining the imperfection shapes. Because of the nature of the plane-based geometry, the imperfections will most likely be relatively small (see Section 6.2.3). A possible engineering approach, which has been applied in the present study, is to impose relatively large imperfections to the perfect geometry in the shape of a smooth "bump", ignoring the fact that this is not a realistic imperfection shape. A comparison of the critical load of this, imperfect, structure and the critical load of the perfect structure, will indicate whether the structure is sensitive to imperfections. If this is not the case, and/or if the critical load is much larger than the actual load on the structure, no further action needs to be taken.

A relevant subject for further research is the determination of geometrically and structurally possible imperfection shapes, and how to implement these in a FE model of a plate shell.

Non-linear FE analysis of the plate shell structure, where the facet thickness has been reduced corresponding to a softening of the interlayer (as described in Section 8.2.1), will result in slightly conservative results for the critical load.

8.3 Supports

The plate shell structures investigated in connection with this study have all been supported against translations in all three directions, along the entire boundary. (Supports against rotations are not relevant for this type of structure.) Other support conditions may be suitable, if the resulting stiffness of the structure is high enough.

Depending on the overall shape of the structure, the reaction forces will have a horizontal component as well as a vertical. These horizontal forces may be taken up by a tension ring following the boundary of the structure, rather than be taken to the supports. Depending on the shape of the structure, the tension ring may also be loaded by bending moments.

The detail which connects the boundary facets with the supporting structure can be the same as the general connection detail.

8.4 Construction

If the facet production, the supporting structure, and/or the erection procedure lacks precision, then, due to the nature of the plane-based faceted geometry, the plate shell structure simply cannot be assembled (see Section 6.2.3). The facets may locally have small translations and rotations, to the extent that these geometric deviations can be taken up by the connection tolerances.

It is therefore crucial for the realization of a plate shell structure that the connection detail can take up the tolerances that the manufacturer and contractor will produce.

To erect the structure, the facets can be positioned on hydraulic jacks, or on a temporary structure, and adjusted until their position is optimal. In this position, the connection details can be assembled.

An optimal solution could be a connection detail system where the facets are simply “clicked” together, with minimum use of scaffolding. This would require extremely low tolerances in the facet production.

8.5 Fire strategy

A load-bearing glass structure is very vulnerable to heat from a fire. For a building involving load bearing glass elements, a *fire strategy*, which accommodates the special circumstances related to this type of structure, must be integrated into the design.

An increasing number of countries have introduced *performance-based fire safety design* in their building regulations, and now permit construction of extraordinary structures, which are not covered by the traditional classification system. A sufficient safety level may be documented by calculations and experimental testing, instead of the application of prescriptive rules.

Section 8.5.1 deals with the possible elements of a fire strategy, for a building project involving a plate shell structure of glass.

8.5.1 Glass plate shell structures and fire

A standard approach for protecting a load-bearing structure against fire is to cover the structural parts by protective elements, designed to protect the structure from heat developed by the fire, or to design the structural parts with such an excessive load-bearing capacity that a certain loss of strength during a fire is acceptable.

These strategies are not feasible for a glass shell structure. The use of fire resistant glass might to some extent protect the glass sheets, but that would still leave the connections exposed to the fire. It is therefore reasonable to ask the questions “how much heat can the structure tolerate without failing” and “how can the temperature around the structure be kept under a specified limit during a fire”. These questions are discussed in the following.

How much heat

If the glass panels are effected by large temperature gradients, the glass will crack [44]. The interlayer (SGP) will loose most of its stiffness at around 60 degrees Celsius [23]. This will cause the bending stiffness of the facets to decrease about 50-75%, as a decreasing amount of shear will be transferred between the layers. (The structure can be designed so that this decrease in stiffness in itself does not result in failure.) At higher temperatures the interlayer may catch on fire, and leak burning drops of SGP onto the floor area underneath the structure.

If the connection detail involves an adhesive part, this will loose most of its strength and stiffness at around 60-70 degrees.

To sum up, the structure may fail when the temperature exceeds 60-80 degrees, which is a very low temperature in a fire situation. However, by shaping the structure so that the connections mainly transfer axial compression when the structure is loaded by self weight, the connections can be designed so that the facets can “lean” on each other when the adhesive loses its strength. This could be a way of allowing a higher temperature. Experimental testing and FE analysis must be used to show whether this effect can be achieved, and to examine how sensitive such a system would be to small asymmetric loads. This way, an allowable temperature of 100 degrees or more may be possible.

Keeping the temperature down

The temperature underneath the shell structure depends on a series of factors, including

- the nature and amount of materials on fire
- the energy release rate of the fire
- the flame height
- the flow of fresh air to the fire
- the flow of hot gasses away from the fire

When the factors above have been estimated in a given design situation, an approximate state of equilibrium can be found, in which the maximum temperature under the shell structure can be determined [33]. Alternatively, a full computational fluid dynamics (CFD) calculation can be used to find the temperature development.

First of all, direct contact between flames and glass must be avoided, so that high temperature gradients do not occur in the glass. This can be achieved by increasing the room height under the shell structure, and possibly also by setting limits for the allowable amount of combustible material in the room.

The energy release rate of the fire can be kept low by installing a sprinkling system or a water mist system. This reduces the temperature in the approximate state of equilibrium, or in some cases extinguish the fire.

High temperature in a room containing a fire is most often a result of accumulated hot gasses under the ceiling. The temperature can be kept down by fire ventilation, by which the hot gasses are removed by a certain flow rate. The fire ventilation can be either mechanical or natural. Given the very low design temperature in this case, mechanical ventilation will probably be needed, to ensure the necessary air flow rate. The use of fire ventilation might to some degree increase the energy release rate of the fire, since it increases the flow of fresh air to the fire.

In addition to the strategy elements discussed here, it may also, for smaller shells, be of interest to check whether the structure could be classified as a secondary structure, and thereby possibly be allowed to collapse after a certain evacuation period. This way, it would not be the state of equilibrium in a fully developed fire that would determine the necessary fire safety precautions.

8.6 Other design aspects

In the following, issues which are also relevant for the design of a plate shell structure, but have not been brought up in the present study, are mentioned, and some suggestions are given for a possible design approach.

8.6.1 Support settlements

As discussed in Section 6.2.3, an overall shape change in a plane-based geometry can generally only happen if the facets warp out of their own plane. In case of settlements in the supporting structure, such an overall shape change may take place. The consequences in terms of forces in the facets and the connections, should be evaluated. In ABAQUS, support settlements can be applied to the model to determine the structural response.

8.6.2 Temperature movements

As discussed earlier, temperature movements may cause stress concentrations in the glass, if the connection detail is too rigidly fixed to the glass and displays a different thermal expansion.

In addition to this, temperature movements in the structure may cause overall shape changes. As for the support settlements, the consequences for the structure should be evaluated. A temperature load can be applied to the model in ABAQUS. Alternatively, if an analysis of given support settlements have shown negligible consequences for the structure, a comparison of the shape changes may show that forces due to temperature movements are also negligible.

8.6.3 Glass fracture

Fracture in the glass may accidentally happen. Since the glass panes are laminated, a fractured glass facet will remain in position, given that the connection detail remains attached to the facet edges. However, the facet may have lost its stiffness (or parts of it), and therefore it will not be fully active in the load bearing structure. Investigations in [7] and [31] indicate that the structure is still effective as shell structure if a facet is entirely removed. This must be verified for a given design, by performing FE analysis on the structure, where a facet has been removed. Especially, the consequences for the non-linear behaviour of the structure should be investigated.

8.6.4 Final remarks

The plate shell concept opens up for many possible design variations.

If openings in the structure are desired, a number of facets can be replaced by a frame, with an opening panel attached.

Solar cells can be integrated into some of the facets, perhaps serving as sun shade on the south facing part of the structure.

Some facets can have a coloured coating, a partly reflecting film, or other kinds of graphic film, perhaps emphasizing a visual effect in the faceting pattern. Some facets may also be of a different material than glass.

Chapter 9

Conclusion

This chapter summarizes the conclusions of the present thesis, and comments on the applied working methods. Recommendations for future work are given in Section 9.1.

In **Chapter 2** the main characteristics of a plate shell structure are drawn up: a plate shell structure is a piecewise plane (i.e. faceted) structural surface, shaped and supported so that external load can be taken to the supports by in-plane forces distributed in the facets. The faceted geometry is organized so that three facets meet in every vertex. It is this topological characteristic that enables the shell action to be distributed in the facets, instead of acting as concentrated forces in the edges and vertices, as in the case of a triangulated (lattice) shell structure.

The plate shell geometry is termed a plane-based geometry, because it is generated by defining the position of each facet's plane in space, and determining the edges and vertices via the intersection lines and points of these planes. In **Chapter 2**, the author suggests possible methods of generating such a plane-based geometry. All the suggested methods are based on defining a pattern, projecting this pattern onto a convex surface, determining the tangent plane to the surface in the projected points, and creating the plane-based faceted geometry from these tangent planes. In some of the suggested methods, the original pattern is defined on a surface which is not plane, such as a polyhedron or a cone. This enables a smaller distortion of the pattern when it is projected, since the shape difference between the original pattern and the projected pattern is smaller. Also, it enables variations of patterns of rotational symmetry, since a part of the pattern can be cut away, without changing the local topology of the pattern.

Also in **Chapter 2**, a *pyFormex* script for generating plate shell geometry is presented. The script is developed in a cooperation between professor B. Verhegghe, Ghent University, and the author: professor Verhegghe has carried out the actual programming, based on requests from and discussions with the author. The script can generate a plate shell geometry, based on a list of points in space defined by the user. Additional input from the user gives the necessary information to create a full FE model, ready to run in ABAQUS. The *pyFormex* script facilitates a fast and simple generation of both plate shell geometry and FE model.

In **Chapter 3** the author outlines the structural behaviour of plate shells. Based on this description, a method of modelling the structure in FE software is proposed. Focus is upon modelling the structure by as simple means as possible, without losing information which has a non-negligible effect on the results.

A plate shell structure carries load by bending action locally in the facets, and shell action in the structure as a whole. In FE software ABAQUS, the facets are modelled by shell elements, which include both bending and in-plane forces. The connection detail is modelled by a strip of shell elements connecting two facets. The stiffness and geometry of this strip of elements is chosen, so that it reproduces the physical connection detail's resistance against rotations around the joint line (rotation stiffness) and displacements perpendicular to the joint in the facet's own plane (axial stiffness). Comparative results indicate that this simple representation of the joint, which ignores an imprecise representation of the connection detail's shear stiffness, produces negligible errors compared to a joint representation where the shear stiffness parameters are modelled correctly. Time dependent effects are not modelled, but the consequences are discussed in connection with the calculations in Chapters 4 and 5.

As explained above, the author describes the structural behaviour of plate shell structures as a combination of shell action (in-plane forces) and bending action (out-of-plane forces). The two types of action are studied in **Chapters 4 and 5** respectively.

Locally, each facet carries external out-of-plane load by bending, thereby taking the load to the facet edges. At the edges, the out-of-plane shear forces are transformed into in-plane forces, given that the structure is appropriately shaped and supported.

Generally, the shell action in a given plate shell has resemblance to the shell action in a similar smooth shell. However, the in-plane forces in the plate shell are larger, because of the geometric/statical restrictions on the flow of forces.

The local bending action and the shell action in a plate shell couples somewhat, because the facet deflections caused by the bending causes the facet corners to lift. This corner uplift results in in-plane tension forces near the facet corners, which adds to the general in-plane stress state in the structure. The out-of-plane deflection of the facets, and the in-plane tension stresses near the facet corners, depend on a series of geometric and physical circumstances:

- The deflection of the plates increase if the rotational stiffness of the connection detail decreases and if the bending stiffness of the facets decrease.
- The in-plane tension stresses near the facet corners generally increase if the deflection of the facets increase, if the angle between neighbouring facets increases, and if the axial stiffness of the connection detail (i.e. resistance against movements perpendicular to the facet edge) increases.

Hand calculation tools for estimating bending moments and in-plane forces in plate shells are suggested by the author.

The numerical results presented in **Chapters 4 and 5** are found by FE analysis of relatively few plate shell designs. This narrows the applicability of the numerical results down to plate shells which are very similar to the analyzed designs. On the other hand, there is a good accordance between the described physical behaviour of the structures and the numerical FE results, and this strengthens the validity of this physical description.

The same philosophy is behind the developed tools for estimating bending moments and in-plane forces in plate shells: the tools are based on relatively few numerical results and therefore have limited documented applicability, but they express a simplified way of understanding how the plate shell structure works, and therein lies their actual value. By knowing these tools and their origin, the designer can base her or his expectations for a given plate shell design on a physical understanding of the structure, and thereby step outside the domain of documented solutions.

In **Chapter 6** an introductory study of the buckling behaviour of plate shells is carried out. The starting point of the study is the buckling load of a given plate shell structure, and the investigation focuses on how this buckling load varies with changes in the facet size, load distribution, geometric imperfections and connection stiffness. Also, a comparative study is performed on a smooth shell structure of the same span and surface thickness.

The investigated plate shell structure is relatively insensitive to imperfections and facet size. The axial stiffness of the connection detail is seen to have a significant impact on the buckling load, as a reduced axial stiffness results in a lower buckling load. The buckling load of the plate shell is slightly reduced compared to the buckling load of the similar smooth shell, and seems more sensitive to the introduced geometric imperfections. However, none of the models were significantly sensitive to the imperfections. The plate shell models seem less sensitive to the distribution of the load than the smooth shell.

The failure mode of the analyzed plate shell models is a single sine wave over a facet edge, and thereby a local failure mode.

Some variations in the modelling technique have been studied, and these imply that a relatively coarse mesh (with 5 - 7 elements along each facet edge) is sufficient to determine the buckling load of a plate shell with adequate precision.

In the investigated plate shell structures the buckling load greatly exceeds the ultimate strength of the structures, and will therefore not be the cause of failure. However, this is not a general conclusion for plate shells. The buckling load of a more shallow dome will most likely be lower, and the observed low imperfection sensitivity may change.

The design of a suitable connection detail is in focus in **Chapter 7**. The author suggests a list of functional requirements for such a connection detail in prioritized order. Most important are the following elements: a light and slender appearance, sufficient strength, adequate stiffness, and a reasonable constructability. The author proposes three different connection detail layouts: a *glued-in plate connection* (where a plate is glued into a groove in the facet edge), a *friction connection* (a slender profile is clamped around the facet edges), and a *glued butt joint* (similar to a welded butt joint, but using an adhesive).

Experiments and calculated estimates suggests that the *glued-in plate connection* is the most suitable for large span structures (up to 14-16 meter span). Depending on possible production methods, the constructability of this design could be greatly improved by replacing the glued-in plate with a glued-in fitting, prepared for a mechanical assembly on site.

The *friction connection* has its clear advantage because of its easy assembly. This connection detail will suit plate shells with a span of up to 8-10 meters.

The main advantage of the *glued butt joint* is its small visual impact. Because of the large bending moments, which this connection detail attracts given its large rotational stiffness, it is only suited for relatively small plate shells, with a span of 3-4 meters and relatively thick facets.

Based on the studies in this thesis, **Chapter 8** summarizes what a designer must take into account when designing a plate shell structure. Apart from the issues handled throughout the thesis (geometry generation, FE modelling, linear structural behaviour, buckling behaviour and connection design) **Chapter 8** also draws attention to other design aspects, such as support settlements, temperature movements, constructability, fire strategy and glass fracture.

9.1 Future work

This section sums up issues for future work within the research of plate shell structures.

The primary task at hand is to conduct additional FE analysis on various plate shell designs, and thereby expand and consolidate the numerical investigations shown in this thesis. Geometric parameters are to be varied, such as overall diameter of the structure, facet thickness, facet diameter, angle between neighbouring facets and uniformity in facet size. Also, other shell shapes should be investigated, and the possibility of plate shells with free edges should be addressed. For every studied plate shell variant, an equivalent smooth shell should be analyzed and used for comparison of shell displacements and in-plane forces.

Geometric considerations and FE analysis should be used to evaluate plate shells' structural response to support settlements and temperature movements.

Time dependency in the connection detail must be reproduced appropriately in a FE calculation. The question of how much creep/relaxation is needed for in-plane stress concentrations to reduce significantly should be addressed. Also, additional experimental tests on the connection details should be carried out to study the time dependent behaviour of the details. Especially, wear due to possible large fluctuations in moisture and temperature should be evaluated, as well as deterioration due to UV radiation.

The *pyFormex* script should be extended to accommodate an easy definition of wind and

snow load on the modelled plate shell structures. Also, a joint strip between the supports and the supported facets should be implemented, so that the elastic compliance of the supports can be included in the model. The *pyFormex* script could also be extended to accommodate the application of geometric imperfections to the models.

The performed study of the non-linear behaviour of plate shells should be significantly elaborated upon, investigating the influence of span, overall curvature (shallowness), facet thickness, and time dependency in the connection details. Attention should especially be given to plate shell structures, where the load capacity of the equivalent smooth structure is governed by its non-linear behaviour. Also, accidental load cases where one or more facets have lost their stiffness due to severe glass breakage or failing connections, should be investigated in non-linear analysis.

Research could be done in the field of other plate shell shapes than convex. Focus could be on how to generate a non-convex plane-based geometry, and how to deal with the ensuing stress concentrations in the concave corners on the glass facets.

The most important future work, however, is to actually build a plate shell, and learn what is true, what is irrelevant, which issues we have forgotten to address or simply underestimated. At ILEK, Stuttgart University, effort is currently made to raise funding to build a plate shell in the ILEK garden, next to the glass dome shown in Figure 1.4.

Appendix A

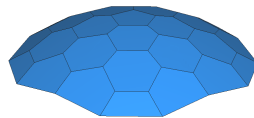
Description of Abaqus models

This appendix contains a detailed description of the ABAQUS models which are referred to in the present work. Input files for all models (generated for ABAQUS v. 6.7-1) can be attained by contacting the author.

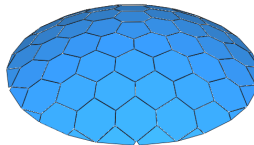
Some models have been analyzed in several variants, in which case these are described.

Five basically different layouts have been used:

FacC



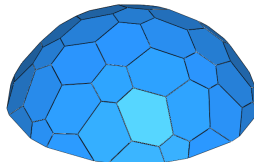
FacF



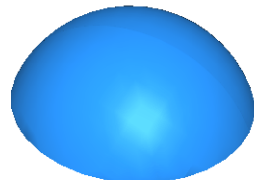
Smooth

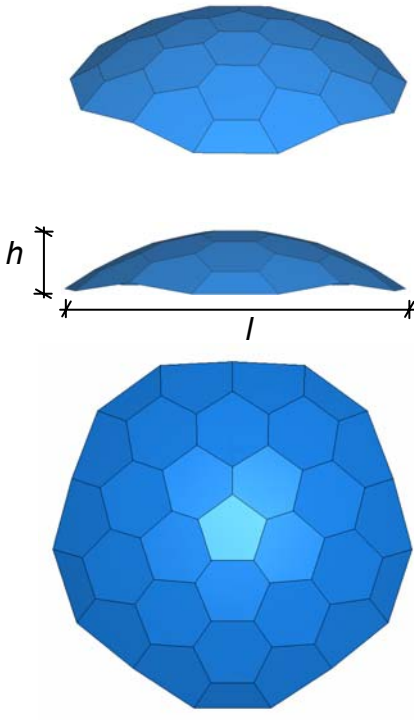
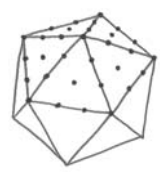


FacStar



Smooth_FacStar



| Model name: FacC (“C” for Coarser faceting pattern) | |
|-------------------------------------------------------------------------------------------------------------|------------------------------------------------------------------------------------------------------------------------------------------------------------------------------------------------------------------------------------------------------------------------------------------------------------------------------------------------------------------------------------------------------------------------------------------------------------------------------------------------------------------------------------------------------------------------------------------------------------------------------------------------------------------------------------------------------------------------------------------------------------------------------------------------------------------------------------------------------------------------------------------------------------------------------------------------------------------------------------------------------------------------------------------------------------------------------------------------------------------------------------------------------------------------------------|
| <p>Structural layout:</p>  | <p>Generation of the geometry:</p>  <p>A regular pattern is defined on an icosahedron (3 subdivisions of each edge.) The pattern points are mapped onto a paraboloid of revolution, using the parametric mapping method described in Section 2.1.1.</p> <p>In the mapped pattern points, the tangent planes to the paraboloid are determined, and brought to intersect with each other.</p> <p>The boundary of the structure is defined by cutting the bottom facets as shown. (As it appears, the boundary is <i>not</i> in a single plane, as is the case for the other models.)</p> <p>The joint strips (see Section 3.2.1) are divided into two parts along the joint centre line, and each half is in the same plane as the adjacent facet. (This separates the FacC model from other models investigated in the study – see e.g. the description of the FacF model.)</p> <p>100 mm of the facet edges are not connected at each facet corner.</p> <p>This plate shell geometry has <i>not</i> been generated by the <i>pyFormex</i> script presented in Section 2.2.</p> |
| Height, h : | 1.9 m |
| Span length, l : | 11.5 m |
| Facet thickness, t : | 15 mm |
| Facet mean diameter, d_{mean} : | ~ 2.0 m |
| Radius of curvature, R : | ~ 9.7 m |
| Angle between adjacent facets, $\gamma \approx d/R$: | ~ 0.21 rad (12 deg) |
| Free part of facet edge, at facet corners: | 100 mm |
| E-modulus, facet material, E : | 70 Gpa |
| Poisson’s ratio, facet material, ν : | 0.22 |
| Width of joint strip elements, w : | 10 mm |
| Other properties of joint strip elements: | See the following description of the FacC model variants. |
| Rotational restraint factor, α : | See the following description of the FacC model variants. |
| Boundary conditions: | The facet edges at the lower boundary are supported against translations in all directions. |
| Loads: | See the following description of the FacC model variants. |
| Mesh | <p>The element size is varying; along the facet edges the element size is 30-40 mm. In the facet centres the element size is 100-150 mm. The mesh is illustrated in Section 3.2.2.</p> <p>The joint strips have 2 elements across the joint width.</p> <p>The Abaqus shell element S4 has been applied.</p> |

Variants of Abaqus model FacC

The FE model **FacC** has been used for both linear analysis and non-linear analysis in Abaqus. In the following, the analyzed variants of the basic model are described.

Linear analysis of the FacC model

In the linear analysis, six different connection details have been modeled in turn, creating six variants of the **FacC** model. The connection details are described in Chapter 7.

The **FacC** model variants used for linear FE analysis are:

- **FacC_plate**: FacC using the glued-in plate connection.
- **FacC_hinge**: FacC using the glued-in hinge connection.
- **FacC_EPDM**: FacC using the friction connection with EPDM interlayer.
- **FacC_EPDM**: FacC using the friction connection with Klingersil interlayer.
- **FacC_adh1**: FacC using the glued butt joint. E-modulus of adhesive: 1.0GPa.
- **FacC_adh2**: FacC using the glued butt joint. E-modulus of adhesive: 2.5GPa.

The input parameters for the joint strip elements are listed in the table below. In all six variants, the joint strip material is isotropic.

| | FacC_plate | FacC_hinge | FacC_EPDM | FacC_Klingersil | FacC_adh1 | FacC_adh2 |
|----------------------------------------------------------------|------------|------------|-----------|-----------------|-----------|-----------|
| <i>Parameters for joint strip elements:</i> | | | | | | |
| Thickness, t_j (mm): | 6.15 | 1.2 | 55 | 49 | 15 | 15 |
| E-modulus, E_j (kN/mm ²): | 4.07 | 20.8 | 0.0018 | 0.051 | 1.0 | 2.5 |
| Poisson's ratio, ν_j : | 0 | 0 | 0 | 0 | 0.45 | 0.45 |
| <i>Resulting stiffness parameters:</i> | | | | | | |
| Rotational stiffness, k_m (kN): | 16 | 0.6 | 5 | 100 | 71 | 176 |
| Axial stiffness, k_n (kN/mm ²): | 5 | 5 | 0.02 | 0.5 | 3.8 | 9.4 |
| In-plane shear stiffness, $k_{v,i}$ (kN/mm ²): | 2.5 | 2.5 | 0.01 | 0.25 | 1.5 | 3.8 |
| Out-of-plane shear stiffness, $k_{v,o}$ (kN/mm ²): | 2.5 | 2.5 | 0.01 | 0.25 | 1.5 | 3.8 |
| Rotational restraint factor, α : | ~ 0.4 | ~ 0.02 | ~ 0.2 | ~ 0.8 | ~ 0.7 | ~ 0.9 |

Two load cases are applied to the six **FacC** model variants, used for linear analysis:

Uniform load case: Uniform pressure of 1.0 kN/m² acting inwards.

Non-uniform load case: Same load, acting on only half of the structure. The orientation of the loaded area relative to the faceting pattern is shown in Section 4.2.1. Contour plots shown in the thesis are oriented so that the load is acting on the *left* half of the structure.

Non-linear analysis of the FacC model

In the non-linear FE investigations, ten different variants of the model **FacC** have been analyzed. All ten models applies the same connection detail: the glued-in plate connection. Therefore, the parameters for the

joint strip elements, and the resulting stiffness parameters, are the same as for the model **FacC_plate** described above. The only exception is the model **FacC_ImpA_Nonuni_Ort** (described below) where the same connection detail is modeled, using an orthotropic joint material to compute the shear stiffness parameters more accurately.

The non-linear **FacC** models apply two different load cases:

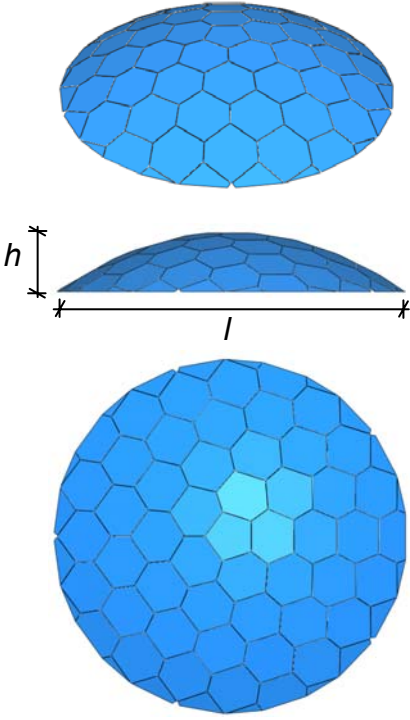
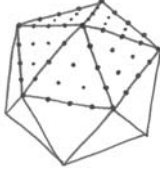
Uniform load case: Uniform distributed vertical load of 100 kN/m^2 acting downwards.

Non-uniform load case: The same load is acting on half of the structure. The other half is loaded by a uniform distributed vertical load of 25 kN/m^2 acting downwards.

The **FacC** model variants used for non-linear FE analysis are:

- **FacC_Perf_Uni:** FacC without imperfections, subjected to the uniform load case.
- **FacC_Perf_Nonuni:** FacC without imperfections, subjected to the non-uniform load case.
- **FacC_ImpA_Uni:** FacC, where the perfect geometry has been superposed by imperfection shape A (described in Section 6.2.3), subjected to the uniform load case.
- **FacC_ImpA_Nonuni:** FacC, where the perfect geometry has been superposed by imperfection shape A, subjected to the non-uniform load case.
- **FacC_ImpB_Uni:** FacC, where the perfect geometry has been superposed by imperfection shape B, subjected to the uniform load case.
- **FacC_ImpC_Uni:** FacC, where the perfect geometry has been superposed by imperfection shape C, subjected to the uniform load case.
- **FacC_ImpA_Uni_Cor:** The same model as **FacC_ImpA_Uni**, but where the joint strips cover the entire length of the facets.
- **FacC_Perf_Uni_S4R:** The same model as **FacC_Perf_Uni**, but applying Abaqus shell element S4R instead of S4.
- **FacC_ImpA_Nonuni_Ort:** The same model as **FacC_ImpA_Nonuni**, but with orthotropic joint material to compute the shear stiffness parameters accurately. Orthotropic joint parameters: $w = 10 \text{ mm}$. $t_j = 6.15 \text{ mm}$. $E_1 = E_2 = E_j = 4.07 \text{ kN/mm}^2$. $G_{12} = 0.81 \text{ N/mm}^2$. $G_{13} = G_{23} = 4.88 \text{ kN/mm}^2$. $\nu_{12} = 0$.

A tabulated overview of these model names can be found in Section 6.2.

| Model name: FacF (“F” for Finer faceting pattern) | |
|-------------------------------------------------------------------------------------------------------------|-------------------------------------------------------------------------------------------------------------------------------------------------------------------------------------------------------------------------------------------------------------------------------------------------------------------------------------------------------------------------------------------------------------------------------------------------------------------------------------------------------------------------------------------------------------------------------------------------------------------------------------------------------------------------------------------------------------------------------------------------------------------------------------------------------------------------------------------------------------------------------------------------------------------------------------------------------------------------------------------------------------|
| <p>Structural layout:</p>  | <p>Generation of the geometry:</p>  <p>A regular pattern is defined on an icosahedron (4 subdivisions of each edge.) The pattern points are mapped onto a paraboloid of revolution, using the parametric mapping method described in Section 2.1.1.</p> <p>In the mapped pattern points, the tangent planes to the paraboloid are determined, and brought to intersect with each other.</p> <p>The boundary of the structure is defined by cutting the geometry by a plane.</p> <p>The joints (see Section 3.2.1) are generated by offsetting the facet edges 5 mm towards the centre of each facet, creating a 10 mm gap between the facet edges. Each joint strip is defined as a plane surface connecting adjacent edges.</p> <p>80 mm of the facet edges are not connected at each facet corner.</p> <p>This plate shell geometry has been generated by the <i>pyFormex</i> script presented in Section 2.2.</p> |
| Height, h : | 1.9 m |
| Span length, l : | 11.5 m |
| Facet thickness, t : | 15 mm |
| Facet mean diameter, d_{mean} : | ~ 1.5 m |
| Radius of curvature, R : | ~ 9.7 m |
| Angle between adjacent facets, $\gamma \approx d/R$: | ~ 0.15 rad (9 deg) |
| Free part of facet edge, at facet corners: | 80 mm |
| E-modulus, facet material, E : | 70 GPa |
| Poisson's ratio, facet material, ν : | 0.22 |
| Width of joint strip elements, w : | 10 mm |
| Thickness of joint strip elements, t_j : | 6.15 mm (varies in some of the non-linear models) |
| E-modulus of joint strip elements, E_j : | 4.07kN/mm ² (varies in some of the non-linear models) |
| Poisson's ratio of joint strip elements, ν_j : | 0 |
| Rotational restraint factor, α : | ~ 0.3 (varies in some of the non-linear models) |
| Boundary conditions: | See the following description of the FacF model variants. |
| Loads: | See the following description of the FacF model variants. |
| Mesh | <p>Unless anything else is mentioned, the element size is constant, with an element side length of approximately 110 mm.</p> <p>Unless anything else is mentioned, there is one element across the joint strip width.</p> <p>The Abaqus shell element S4 has been applied.</p> |

Variants of Abaqus model FacF

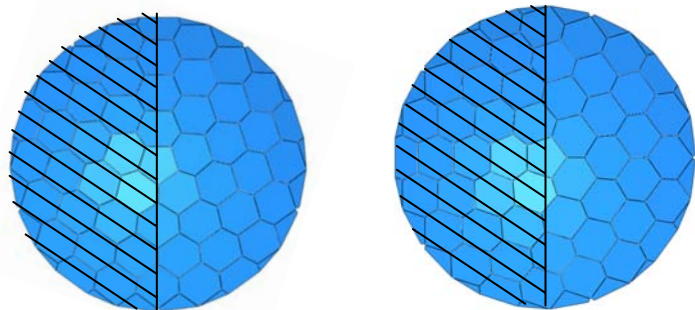
The FE model **FacF** has been used for both linear analysis and non-linear analysis in Abaqus. In the following, the analyzed variants of the basic model are described.

Linear analysis of FacF

Two variants of the **FacF** model have been used for linear analysis in Abaqus. They both apply the same connection detail; the glued-in plate connection. The joint strips are modeled by an isotropic material, and the joint parameters are given in the table above.

The first variant of the **FacF** model for linear analysis (model name: **FacF_plate**) is supported against translations along the entire lower boundary. The model is analyzed for three load cases. A *uniform load case*, where a uniform pressure of 1.0 kN/m^2 is acting inwards on the entire structure, and two *non-uniform load cases*, where the same load is acting on only half of the structure. The difference between the two non-uniform load cases is the orientation of the loaded area relative to the faceting pattern. This orientation of the load is shown in the sketches below (the hatched area is the loaded area).

Orientation of the load in the two non-uniform load cases.



The second of the **FacF** model variants used for linear analysis (model name: **FacF_3points**) is supported in only three points, as illustrated in Section 5.2. This structure is loaded by a uniform pressure of 1.0 kN/m^2 , acting inwards on the entire structure.

Non-linear analysis of FacF

In the non-linear FE investigations, 14 different variants of the model **FacF** have been analyzed. Two different load cases are applied:

Uniform load case: Uniform distributed vertical load of 100 kN/m^2 acting downwards.

Non-uniform load case: The same load is acting on half of the structure. The other half is loaded by a uniform distributed vertical load of 25 kN/m^2 acting downwards.

The **FacF** model variants used for non-linear FE analysis are:

- **FacF_Perf_Uni**: FacF without imperfections, subjected to the uniform load case.
- **FacF_Perf_Nonuni**: FacF without imperfections, subjected to the non-uniform load case.
- **FacF_ImpA_Uni**: FacF, where the perfect geometry has been superposed by imperfection shape A (described in Section 6.2.3), subjected to the uniform load case.
- **FacF_ImpA_Nonuni**: FacF, where the perfect geometry has been superposed by imperfection shape A, subjected to the non-uniform load case.
- **FacF_ImpB_Uni**: FacF, where the perfect geometry has been superposed by imperfection shape B, subjected to the uniform load case.
- **FacF_ImpC_Uni**: FacF, where the perfect geometry has been superposed by imperfection shape C, subjected to the uniform load case.

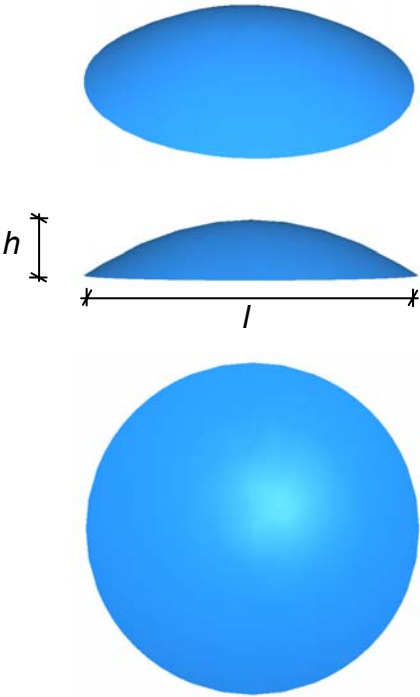
- **FacF_Perf_Uni_S4R**: The same model as **FacF_Perf_Uni**, but applying Abaqus shell element S4R instead of S4.
- **FacF_Perf_Uni_Esmall**: The same model as **FacF_Perf_Uni**, with a general element size of 75 mm, instead of 110 mm.
- **FacF_Perf_Uni_Elarge**: The same model as **FacF_Perf_Uni**, with a general element size of 150 mm, instead of 110 mm.

In addition to the above mentioned 9 model variants, 5 model variants have been investigated where the connection stiffness parameters have been reduced:

- **FacF_ImpA_Uni_km50**: The same model as **FacF_ImpA_Uni**, except k_m is reduced to 50%.
- **FacF_ImpA_Uni_km25**: The same model as **FacF_ImpA_Uni**, except k_m is reduced to 25%.
- **FacF_ImpA_Uni_kn50**: The same model as **FacF_ImpA_Uni**, except k_n is reduced to 50%.
- **FacF_ImpA_Uni_kn25**: The same model as **FacF_ImpA_Uni**, except k_n is reduced to 25%.
- **FacF_ImpA_Uni_kn05**: The same model as **FacF_ImpA_Uni**, except k_n is reduced to 5%.

The relevant joint parameters are listed in Section 6.2.4, and are therefore not repeated here.

A tabulated overview of the models used for non-linear analysis can be found in Section 6.2.

| Model name: Smooth | |
|-------------------------------------------------------------------------------------------------------------|---------------------------------------------------------------------------------------------------------------------------------------------------------------------------------------------------------------------|
| <p>Structural layout:</p>  | <p>Generation of the geometry:</p> <p>The geometry is a symmetric section of a paraboloid of revolution. The geometry is a smooth approximation to the two plate shell geometries, FacC and FacF.</p> |
| Height, h : | 1.9 m |
| Span length, l : | 11.5 m |
| Thickness, t : | 15 mm |
| Radius of curvature, R : | ~ 9.7 m |
| E-modulus, E : | 70 Gpa |
| Poisson's ratio, ν : | 0.22 |
| Boundary conditions: | The boundary is supported against translations. |
| Loads: | See the following description of the Smooth model variants. |
| Mesh | <p>The general element size is 150 mm.</p> <p>The Abaqus shell element S4 has been applied.</p> |

Variants of Abaqus model Smooth

The FE model **Smooth** has been used for both linear analysis and non-linear analysis in Abaqus. In the following, the analyzed variants of the basic model are described.

Linear analysis of Smooth

Only one variant of Smooth has been used for linear analysis. This model is termed **Smooth_linear**.

Two load cases are applied in the linear analysis:

Uniform load case: Uniform pressure of 1.0 kN/m^2 acting inwards.

Non-uniform load case: Same load, acting on only half of the structure. Contour plots shown in the thesis are oriented so that the load is acting on the *left* half of the structure.

Non-linear analysis of Smooth

In the non-linear FE investigations, three variants of the model **Smooth** have been analyzed. Two different load cases are applied:

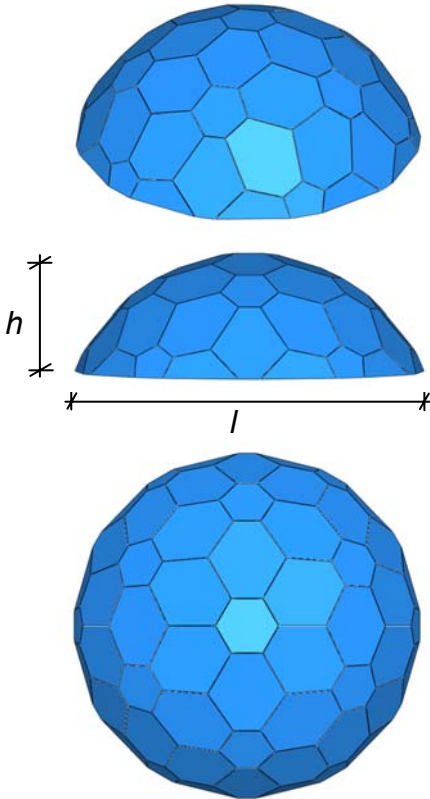
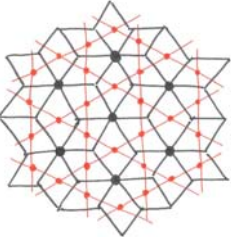
Uniform load case: Uniform distributed vertical load of 100 kN/m^2 acting downwards.

Non-uniform load case: The same load is acting on half of the structure. The other half is loaded by a uniform distributed vertical load of 25 kN/m^2 acting downwards.

The **Smooth** model variants used for non-linear FE analysis are:

- **Smooth_Perf_Uni:** Smooth without imperfections, subjected to the uniform load case.
- **Smooth_Perf_Nonuni:** Smooth without imperfections, subjected to the non-uniform load case.
- **Smooth_ImpC_Uni:** Smooth, where the perfect geometry has been superposed by imperfection shape C (described in Section 6.2.3), subjected to the uniform load case.

A tabulated overview of the models used for non-linear analysis can be found in Section 6.2.

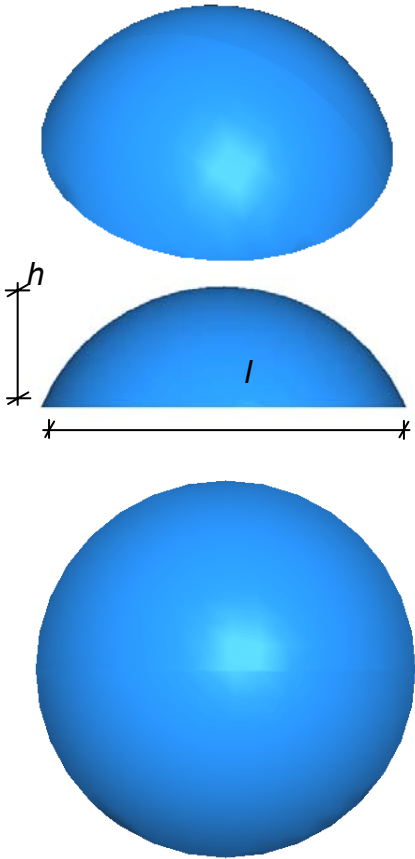
| Model name: FacStar (“Star” for star-formation pattern) | | |
|--------------------------------------------------------------------------------------------------------------|----------------------------------------------------------------------------------------------------------------------------------------------------------------------------------------------------------------------------------------------------------------------------------------------------------------------------------------------------------------------------------------------------------------------------------------------------------------------------------------------------------------------------------------------------------------------------------------------------------------------------------------------------------------------------------------------------------------------------------------------------------------------------------------------------------------------------------------------------------------------------------------------------------------------------------------------------------------------------------------------------------------------------------------------------------------------------------------------------------------------------------------------------------------------------------------------------------------------------|-----------------------|
| <p>Structural layout:</p>  | <p>Generation of the geometry:</p>  <p>The shown pattern is defined in a plane. Two layers of points are created: a layer of points positioned like the red markings (●), and a layer of points positioned like the black markings (●).</p> <p>The two layers of points are each mapped onto a section of a sphere, using the parametric mapping method described in Section 2.1.1. The two spheres have the same centre, and a difference in radius of 13‰.</p> <p>In the mapped pattern points, the tangent planes to the respective spheres are determined, and brought to intersect with each other.</p> <p>The boundary of the structure is defined by cutting the geometry by a plane.</p> <p>The joints (see Section 3.2.1) are generated by offsetting the facet edges 7.5 mm towards the centre of each facet, creating a 15 mm gap between the facet edges. Each joint strip is defined as a plane surface connecting adjacent edges.</p> <p>100 mm of the facet edges are not connected at each facet corner.</p> <p>This plate shell geometry has been generated by the <i>pyFormex</i> script presented in Section 2.2.</p> | |
| Height, h : | 3.3 m | |
| Span length, l : | 10.0 m | |
| Facet thickness, t : | 15 mm | |
| Facet mean diameter, d_{mean} : | small facets: ~ 1.4 m | large facets: ~ 1.9 m |
| Radius of curvature, R : | 5.4 m | |
| Angle between adjacent facets, $\gamma \approx d/R$: | ~ 0.31 rad (18 deg) | |
| Free part of facet edge, at facet corners: | 100 mm | |
| E-modulus, facet material, E : | 70 Gpa | |
| Poisson's ratio, facet material, ν : | 0.22 | |
| Width of joint strip elements, w : | 15 mm | |
| Thickness of joint strip elements, t_j : | 6.15 mm | |
| E-modulus of joint strip elements, E_j : | 6.10 kN/mm ² | |
| Poisson's ratio of joint strip elements, ν_j : | 0 | |
| Rotational restraint factor, α : | 0.3 – 0.4 | |
| Boundary conditions: | The facet edges at the lower boundary are supported against translations in all directions. | |

(The description of model **FacStar** continues on the following page.)

(Description of model **FacStar**, continued:)

| | |
|--------|----------------------------------------------------------------------------------------------------------------------------------------------------------------------------------------------------------------------------------------------------------------------------------------------------------------------|
| Loads: | <p>Uniform load case: Distributed vertical load of 1.0kN/m^2 acting on the entire structure.</p> <p>Non-uniform load case: Same load, on half of the structure.</p> <p>(Contour plots shown in the thesis are oriented so that the load is acting on the <i>left</i> half of the structure.)</p> |
| Mesh | <p>The general element size is constant, with an element side length of approximately 90 mm.</p> <p>There is one element across the joint strip width.</p> <p>The Abaqus shell element S4 has been applied.</p> |

There are no other variants of the **FacStar** model.

| Model name: Smooth_FacStar | |
|------------------------------------------------------------------------------------|-------------------------------------------------------------------------------------------------------------------------------------------------------------------------------------------------------------------------------------------------------------------------------------------------------------------|
| Structural layout: | Generation of the geometry: |
|  | <p>The geometry is a section of a sphere. The geometry is a smooth approximation to the plate shell geometry, FacStar.</p> |
| Height, h : | 3.3 m |
| Span length, l : | 10.0 m |
| Thickness, t : | 15 mm |
| Radius of curvature, R : | 5.4 m |
| E-modulus, E : | 70 Gpa |
| Poisson's ratio, ν : | 0.22 |
| Boundary conditions: | The boundary is supported against translations. |
| Loads: | <p>Uniform load case: Distributed vertical load of 1.0kN/m^2 acting on the entire structure.</p> <p>Non-uniform load case: Same load, on half of the structure. (Contour plots shown in the thesis are oriented so that the load is acting on the <i>left</i> half of the structure.)</p> |
| Mesh | <p>The general element size is 150 mm.</p> <p>The Abaqus shell element S4 has been applied.</p> |

There are no other variants of the **Smooth_FacStar** model.

Appendix B

In-plane forces in three plate shells and their equivalent smooth shells

In this appendix, in-plane forces $n_{22,peak}$, $n_{22,edge}$, $n_{12,peak}$ and $n_{12,peak}$ are listed for three different plate shell models (**FacC**, **FacF_plate** and **FacStar**) at a chosen edge. $n_{ij,peak}$ is the largest value of n_{ij} at the edge. $n_{ij,edge}$ is the value of n_{ij} at the edge mid-point.

The principal in-plane forces in the equivalent smooth shells are also given: $n_{1,smooth}$ and $n_{2,smooth}$ are the principal in-plane forces (maximum and minimum respectively). $n_{12,smooth}$ is the maximum in-plane shear force, determined by $n_{12,smooth} = \frac{n_{1,smooth} - n_{2,smooth}}{2}$.

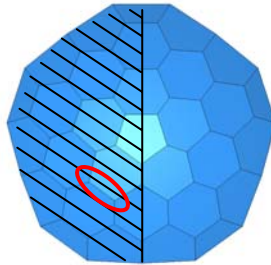
Each force value in a smooth shell is taken at a point which has the same position in the shell's ground plane, as the mid-point of the studied facet edge in the plate shell.

The listed force values for model **FacC** are also given in Section 4.2.2.

Model: **FacC**

Uniform load case: 1kN/m^2 pressure load on the entire structure.

Non-uniform load case: 1kN/m^2 pressure load on the hatched area.



6 variants of model **FacC** have been analyzed; a detailed description of the model and its variants can be found in Appendix A.

The in-plane forces listed below are found at the edge marked in the illustrations above.

The general element size along the edges is 30-40mm.

The forces at the investigated edge have converged for the applied element size, except for the peak values in models **FacC_hinge** and **FacC_plate**.

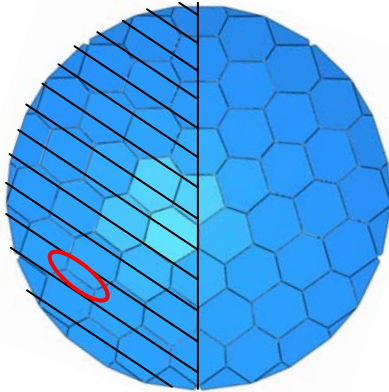
| Model: FacC | | | | |
|---------------------------------------------|-------------------------|-------------------------|---------------------------|---------------------------|
| Load case | $n_{22,peak}$ (N/mm) | $n_{22,edge}$ (N/mm) | $ n_{12,peak} $ (N/mm) | $ n_{12,edge} $ (N/mm) |
| Uniform load case | | | | |
| Glued-in line hinge | 13.1 | -10.0 | 3.1 | 0.1 |
| Glued-in plate | 8.9 | -9.0 | 2.4 | 0.1 |
| Glued butt joint, $E_{adh} = 1\text{GPa}$ | 3.5 | -8.3 | 1.0 | 0.1 |
| Glued butt joint, $E_{adh} = 2.5\text{GPa}$ | 3.4 | -8.0 | 1.5 | 0.1 |
| Friction conn., Klingsil | – | -7.7 | – | 0.1 |
| Friction conn., EPDM | – | -5.7 | – | 0.1 |
| Nonuniform load case | | | | |
| Glued-in line hinge | 13.5 | -10.0 | 5.2 | 3.4 |
| Glued-in plate | 9.5 | -9.2 | 4.9 | 3.4 |
| Glued butt joint, $E_{adh} = 1\text{GPa}$ | 4.4 | -8.6 | 4.4 | 3.3 |
| Glued butt joint, $E_{adh} = 2.5\text{GPa}$ | 4.6 | -8.2 | 4.7 | 3.4 |
| Friction conn., Klingsil | – | -8.0 | – | 3.3 |
| Friction conn., EPDM | – | -5.6 | – | 2.0 |

| Equivalent smooth shell model: Smooth | | | |
|----------------------------------------------|--------------------------|--------------------------|-----------------------------|
| Load case | $n_{1,smooth}$ (N/mm) | $n_{2,smooth}$ (N/mm) | $ n_{12,smooth} $ (N/mm) |
| Uniform load case | -4.7 | -5.0 | 0.2 |
| Nonuniform load case | -2.9 | -5.7 | 1.4 |

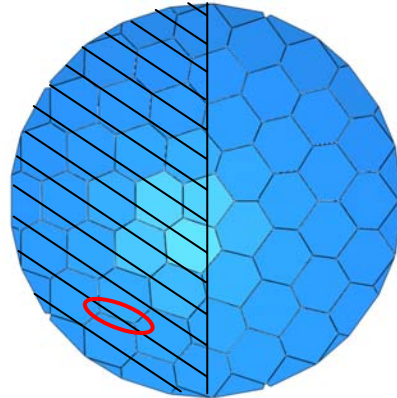
Model: **FacF_plate**

Uniform load case: 1kN/m^2 pressure load on the entire structure.

Non-uniform load case 1:
 1kN/m^2 pressure load on the
hatched area.



Non-uniform load case 2:
 1kN/m^2 pressure load on the
hatched area. (Rotated 18
degrees relative to the faceting
pattern.)



A detailed description of the model can be found in Appendix A.

The in-plane forces listed below are found at the edge marked in the illustrations above.

The general element size is 110mm. At the investigated edge, and in the surrounding facets, the general element size is 10mm.

The forces at the investigated edge have converged for the applied element size.

The given $n_{22,peak}$ force is the maximum $n_{22,peak}$ force value present in the structure.

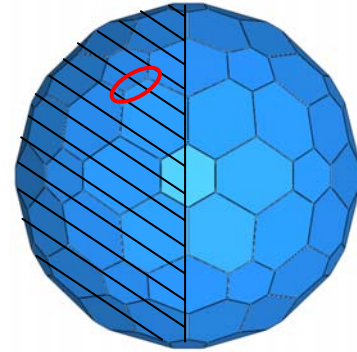
| Model: FacF_plate | | | | |
|--------------------------|-------------------------|-------------------------|---------------------------|---------------------------|
| Load case | $n_{22,peak}$ (N/mm) | $n_{22,edge}$ (N/mm) | $ n_{12,peak} $ (N/mm) | $ n_{12,edge} $ (N/mm) |
| Uniform load case | 7.1 | -10.9 | 1.7 | 1.2 |
| Nonuniform load case 1 | 8.1 | -10.9 | 4.2 | 3.5 |
| Nonuniform load case 2 | 6.8 | -10.9 | 4.5 | 3.8 |

| Equivalent smooth shell model: Smooth | | | |
|----------------------------------------------|--------------------------|--------------------------|-----------------------------|
| Load case | $n_{1,smooth}$ (N/mm) | $n_{2,smooth}$ (N/mm) | $ n_{12,smooth} $ (N/mm) |
| Uniform load case | -4.7 | -5.3 | 0.3 |
| Nonuniform load case 1 | -3.9 | -5.8 | 1.0 |
| Nonuniform load case 2 | -3.6 | -6.2 | 1.3 |

Model: **FacStar**

Uniform load case:
1kN/m² vertical load on the entire structure.

Non-uniform load case:
1kN/m² vertical load on the hatched area.



A detailed description of the model can be found in Appendix A.

The in-plane forces listed below are found at the edge marked in the illustration above.

The general element size is 110mm. At the investigated edge, and in the surrounding facets, the general element size is 10mm.

The forces at the investigated edge have converged at the applied element size.

The maximum $n_{22,peak}$ force present in the structure (located at a different edge than the edge investigated here) is 12N/mm. That value has converged.

| <i>Model: FacStar</i> | | | | |
|------------------------------|-------------------------|-------------------------|---------------------------|---------------------------|
| Load case | $n_{22,peak}$ (N/mm) | $n_{22,edge}$ (N/mm) | $ n_{12,peak} $ (N/mm) | $ n_{12,edge} $ (N/mm) |
| Uniform load case | 6.3 | -4.8 | 1.3 | 0.01 |
| Nonuniform load case | 7.4 | -4.8 | 3.8 | 2.9 |

| <i>Equivalent smooth shell model: Smooth_FacStar</i> | | | |
|-------------------------------------------------------------|--------------------------|--------------------------|-----------------------------|
| Load case | $n_{1,smooth}$ (N/mm) | $n_{2,smooth}$ (N/mm) | $ n_{12,smooth} $ (N/mm) |
| Uniform load case | -1.7 | -3.0 | 0.7 |
| Nonuniform load case | -1.1 | -3.3 | 1.1 |

Appendix C

Test of approximate expressions for plate bending in facets

This appendix presents documentation for the stated precision of the approximate expressions for plate bending in plate shell facets. The approximate expressions are presented in Section 5.1.3.

Approximate calculation

| | d_{mean} / mm | t / mm | $E / N/mm^2$ | ν | $p / kN/m^2$ | k_p / N | k_m / N | α | u / mm | m_j / N | m_m / N | φ |
|----------|-----------------|----------|--------------|-------|--------------|-----------|-----------|----------|----------|-----------|-----------|-----------|
| Facet 1 | 2155 | 15 | 70000 | 0.22 | 1 | 23425 | 600 | 0.02 | 4.7 | -5 | 208 | 0.0079 |
| Facet 2 | 2155 | 15 | 70000 | 0.22 | 1 | 23425 | 5000 | 0.18 | 4.1 | -36 | 194 | 0.0066 |
| Facet 3 | 2155 | 15 | 70000 | 0.22 | 1 | 23425 | 100000 | 0.81 | 1.8 | -165 | 133 | 0.0015 |
| Facet 4 | 2155 | 15 | 70000 | 0.22 | 1 | 23425 | 71000 | 0.75 | 2.0 | -153 | 139 | 0.0020 |
| Facet 5 | 2155 | 15 | 70000 | 0.22 | 1 | 23425 | 176000 | 0.88 | 1.6 | -179 | 126 | 0.0009 |
| Facet 6 | 1769 | 15 | 70000 | 0.22 | 1 | 28536 | 600 | 0.02 | 2.1 | -3 | 140 | 0.0044 |
| Facet 7 | 1769 | 15 | 70000 | 0.22 | 1 | 28536 | 5000 | 0.15 | 1.9 | -20 | 132 | 0.0038 |
| Facet 8 | 1769 | 15 | 70000 | 0.22 | 1 | 28536 | 100000 | 0.78 | 0.9 | -107 | 92 | 0.0010 |
| Facet 9 | 1769 | 15 | 70000 | 0.22 | 1 | 28536 | 71000 | 0.71 | 1.0 | -98 | 96 | 0.0013 |
| Facet 10 | 1769 | 15 | 70000 | 0.22 | 1 | 28536 | 176000 | 0.86 | 0.7 | -118 | 87 | 0.0006 |
| Facet 11 | 1366 | 15 | 70000 | 0.22 | 1 | 36958 | 15780 | 0.30 | 0.6 | -24 | 73 | 0.0014 |
| Facet 12 | 1500 | 15 | 70000 | 0.22 | 1 | 33654 | 15780 | 0.32 | 0.8 | -31 | 87 | 0.0018 |
| Facet 13 | 1554 | 15 | 70000 | 0.22 | 1 | 32484 | 15780 | 0.33 | 1.0 | -35 | 93 | 0.0020 |
| Facet 14 | 1574 | 15 | 70000 | 0.22 | 1 | 32072 | 15780 | 0.33 | 1.0 | -36 | 95 | 0.0021 |
| Facet 15 | 1395 | 15 | 70000 | 0.22 | 1 | 36187 | 60000 | 0.62 | 0.4 | -53 | 63 | 0.0008 |
| Facet 16 | 1915 | 15 | 70000 | 0.22 | 1 | 26361 | 60000 | 0.69 | 1.4 | -111 | 114 | 0.0017 |

Measured using FEM

| | u / mm | % | $m_{j,FEM} / N$ | % | m_m / N | % | φ | % | Origin of facet |
|----------|----------|----|-----------------|-----|-----------|-----|-----------|-----|---------------------------------------|
| Facet 1 | 4.1 | 15 | -3 | 41 | 209 | -1 | 0.0063 | 25 | Hexagonal facet from FacC_hinge |
| Facet 2 | 4.2 | -1 | -28 | 21 | 218 | -11 | 0.0059 | 12 | Hexagonal facet from FacC_EPDM |
| Facet 3 | 2.0 | -9 | -135 | 18 | 126 | 6 | 0.0018 | -15 | Hexagonal facet from FacC_Klingersil |
| Facet 4 | 2.2 | -8 | -125 | 18 | 133 | 4 | 0.0022 | -9 | Hexagonal facet from FacC_adh1 |
| Facet 5 | 1.7 | -9 | -155 | 14 | 113 | 12 | 0.0013 | -27 | Hexagonal facet from FacC_adh2 |
| Facet 6 | 1.9 | 15 | -2 | 29 | 141 | 0 | 0.0034 | 28 | Pentagonal facet from FacC_hinge |
| Facet 7 | 1.7 | 13 | -19 | 7 | 149 | -11 | 0.0030 | 26 | Pentagonal facet from FacC_EPDM |
| Facet 8 | 0.9 | -2 | -108 | -1 | 79 | 16 | 0.0004 | 130 | Pentagonal facet from FacC_Klingersil |
| Facet 9 | 0.9 | 11 | -101 | -3 | 84 | 14 | 0.0009 | 45 | Pentagonal facet from FacC_adh1 |
| Facet 10 | 0.7 | 14 | -127 | -8 | 72 | 20 | 0.0003 | 130 | Pentagonal facet from FacC_adh2 |
| Facet 11 | 0.5 | 10 | -23 | 6 | 73 | 0 | 0.0011 | 31 | Pentagonal facet from FacF_plate |
| Facet 12 | 0.8 | 2 | -35 | -10 | 97 | -10 | 0.0018 | 3 | Hexagonal facet from FacF_plate |
| Facet 13 | 1.0 | -1 | -36 | -4 | 101 | -8 | 0.0019 | 7 | Hexagonal facet from FacF_plate |
| Facet 14 | 1.1 | -5 | -36 | -1 | 102 | -6 | 0.0019 | 11 | Hexagonal facet from FacF_plate |
| Facet 15 | 0.4 | 2 | -49 | 8 | 58 | 10 | 0.0006 | 28 | Hexagonal facet from FacStar |
| Facet 16 | 1.2 | 15 | -74 | 34 | 86 | 32 | 0.0016 | 8 | Octagonal facet from FacStar |

Notes

The deflections of the facets from FacC_EPDM have been adjusted by subtracting the mean deflection of the facet's edge mid-points.

For small φ values: The relative deviation of the values is large, because the values are compared to small numbers. The absolute deviation is not larger than for the other facets.

The octagonal facet (facet 16) is relatively uneven in shape ("oblong"), and the approximate results are therefore more on the safe side than the stated general precision.

Bibliography

- [1] Abaqus Analysis User's Manual (v6.7).
- [2] Abaqus Theory Manual (v6.7).
- [3] Abaqus/CAE User's Manual (v6.7).
- [4] <http://pyformex.org>.
- [5] <http://www.simulia.com>.
- [6] 3M. Scotch-Weld™ EPX™ Adhesive DP490, product data sheet. www.3m.com, 1996.
- [7] Jaap A.M. Aanhaanen. The stability of a glass faceted shell structure. Master's thesis, Delft University of Technology, 2008.
- [8] Jaap A.M. Aanhaanen, Anne Bagger, and Jan N.J.A. Vamberský. The stability of a faceted glass dome structure. In *New Materials and Technologies – New Designs and Innovations*, Acapulco, Mexico, 2008. International Association for Shell and Spatial Structures (IASS).
- [9] Henrik Almegaard. *Skalkonstruktioner - metoder til afklaring af sammenhænge mellem form, stabilitet, stivhed og understøtninger*. PhD thesis, Royal Danish Academy of Fine Arts - School of Architecture, 2003.
- [10] Henrik Almegaard. The curvature coordinate system. In *Shell and Spatial Structures – Structural Architecture: Towards the future looking to the past*, Venice, Italy, 2007. International Association for Shell and Spatial Structures (IASS).
- [11] Henrik Almegaard, Anne Bagger, Jens Gravesen, Bert Jüttler, and Zbynek Sir. Surfaces with piecewise linear support functions over spherical triangulations. In *Proceedings of Mathematics of Surfaces XII*, Sheffield, England, 2007. Springer-Verlag.
- [12] Henrik Almegaard and Klavs Feilberg Hansen. Bygningsstatistiske meddelelser: Skiveskaller – statisk virkemåde og stabilitet. Technical report, Dansk Selskab for Bygningsstatik, June 2007.
- [13] D.J.A. Alsop and R.J. Saunders et al. *Structural use of glass in buildings*. The Institution of Structural Engineers (IStructE).

- [14] Anne Bagger, Benedict Verhegghe, and Kristian Hertz. Modeling plate shell structures using pyFormex. In *Evolution and trends in design analysis and construction of shell and spatial structures*, Valencia, Spain, 2009. International Association for Shell and Spatial Structures (IASS).
- [15] Martin P. Bendsøe and Ole Sigmund. *Topology Optimization – Theory, Methods and Applications*. Springer-Verlag Berlin Heidelberg New York, 2 edition, 2003.
- [16] Lucio Blandini. *Structural use of adhesives in glass shells*. PhD thesis, Institut für Leichtbau Entwerfen und Konstruieren (ILEK), Universität Stuttgart, 2005.
- [17] Philippe Block. *Thrust Network Analysis – Exploring Three-dimensional Equilibrium*. PhD thesis, Massachusetts Institute of Technology, 2009.
- [18] David Bushnell. *Computerized buckling analysis of shells*. Springer Science & Business, 1985.
- [19] John Chilton. *The engineer’s Contribution to Contemporary Architecture – Heinz Isler*. Thomas Telford Publishing, 2000.
- [20] Robert D. Cook, David S. Malkus, and Michael E. Plesha. *Concepts and applications of finite element analysis*. John Wiley & Sons, 3 edition, 1989.
- [21] M.A. Crisfield. A fast incremental/iteration solution procedure that handles snap-through. *Computers and Structures*, 13, 1981.
- [22] G. Dean. Modelling non-linear creep behaviour of an epoxy adhesive. *International journal of adhesion and adhesives*, 27, 2007.
- [23] DuPont. DuPontTM SentryGlas®plus brochure. www2.dupont.com, 2009.
- [24] Wilhelm Flügge. *Stresses in Shells*. Springer-Verlag Berlin Heidelberg New York, 1973.
- [25] Michael John Gorman. *Buckminster Fuller – Designing for Mobility*. Skira, 2005.
- [26] Matthias Haldimann, Andreas Luible, and Mauro Overend. *Structural use of glass*. International Association for Bridge and Structural Engineering (IABSE), 2008.
- [27] Klavs Feilberg Hansen. *Geometrisk modellering til brug i datamat*. Statens Byggeforskningsinstitut, SBI, 1991.
- [28] Klavs Feilberg Hansen. A method for faceting double curved surfaces. *International Journal of Space Structures*, 34(3), 1993.
- [29] Werner Helmet. *From the Arratus Globe to the Zeiss Planetarium*. Gustav Fischer, 1957.
- [30] HILTI. HILTI HIT-HY 70 for structural glass. www.hilti.co.uk, 2008.

- [31] Theis Vielsted Isgreen. Fem-modellering af facetterede skaller i glas. Master's thesis, Department of Civil Engineering, Technical University of Denmark, 2007.
- [32] Stinne Hede Poulsen Jens Zangenberg Hansen. Glued connection in plate shell glass structure. Master's thesis, Department of Civil Engineering, Technical University of Denmark, 2010.
- [33] Björn Karlsson and James G. Quintiere. *Enclosure Fire Dynamics – A first draft of a student textbook*. Lund University, Dept. of Fire Safety Engineering, 1998.
- [34] William Karush. *The crescent dictionary of mathematics*. Dale Seymour Pubn, 1987.
- [35] Klinger. Klingsil® C-4500 product documentation. www.klinger.co.at, 2007.
- [36] Ron Knott. <http://www.mcs.surrey.ac.uk/personal/r.knott/>.
- [37] W.T. Koiter. *Over de Stabiliteit van het Elastisch Evenwicht*. PhD thesis, TH Delft, 1945.
- [38] W.T. Koiter. On the stability of elastic equilibrium, NASA technical translation f10, 833. Technical report, NASA, 1967.
- [39] Helle Krogsgaard. Undersøgelse af en samling til skivebaserede skalkonstruktioner i glas. Master's thesis, Department of Civil Engineering, Technical University of Denmark, 2008.
- [40] W.J. Lewis. *Tension structures – form and behaviour*. Thomas Telford Publishing, 2003.
- [41] Zygmunt Stanislaw Makowski. *Analysis, design and construction of braced domes*. Granada, 1984.
- [42] O.G. McGee, J.W. Kim, and A.W. Leissa. Sharp Corner Functions for Mindlin Plates. *Journal of Applied Mechanics*, 72(1), 2005.
- [43] H. Nooshin. Algebraic representation and processing of structural configurations. *International Journal of Computers and Structures*, 5(2-3), 1975.
- [44] P.J. Pagni and A.A. Joshi. Glass breaking in fires. In *Fire Safety Science – Proceedings, Third International Symposium*, pages 791–802, London, 1991. Elsevier Applied Science.
- [45] H. Pottmann, A. Asperl, M. Hofer, and A. Kilian. *Architectural Geometry*. Bentley Institute Press, 2007.
- [46] prEN13474 3. Glass in building - Determination of the strength of glass panes - Part3: General method of calculation and determination of strength of glass by testing. European Standard, November 2005.

- [47] E. Ramm, K.-U. Bletzinger, and R. Reitinger. Shape optimization of shell structures. *IASS Bulletin of the International Association for Shell and Spatial Structures*, 34(112), 1993.
- [48] C. Schittich, G. Staib, D. Balkow, M. Schuler, and W. Sobek. *Glasbau Atlas*. Birkhäuser, 2006.
- [49] Daniel L. Schodek and Martin Bechthold. *Structures*. Pearson Prentice Hall, 6 edition, 2008.
- [50] Semra Arslan Selcuk, Al J. Fisher, and Chris J.K. Williams. Biomimesis and the geometric definition of shell structures in architecture. In *www.generativeart.com*, Milano, Italy, 2005. 8th Genrative Art Conference.
- [51] Stephen P. Timoshenko and James M. Gere. *Theory of Elastic Stability*. McGraw-Hill Book Company, 1963.
- [52] Stephen P. Timoshenko and S. Woinowsky-Krieger. *Theory of Plates and Shells*. McGraw-Hill Book Company, 1959.
- [53] Ole Vanggaard and Einar Thorsteinn. *TRANS-SPACE structures*. Luna Tryk, 1995.
- [54] Benedict Verhegghe. pyFormex Manual, Release 0.8-a1. Technical report, Ghent University, 2009.
- [55] Ture Wester. *Structural Order in Space - the plate-lattice dualism*. Smed Grafik, The Royal Danish Academy of Fine Arts, School of Architecture, 1984.
- [56] Ture Wester. *Dualisme og Syntese for Kræfter og Former*. Skivelaboratoriet, Kunstakademiets Arkitektskole, The Royal Danish Academy of Fine Arts, School of Architecture, 1987.
- [57] Ture Wester. A geodesic dome-type based on pure plate action. *International Journal of Space Structures*, 5(3), 1990.
- [58] Ture Wester. Structural morphology and natural structures. In M. Hilliges, editor, *Proceedings of the 3rd International Symposium of the Sonderforschungsbereich 230: Evolution of Natural Structures, Principles, Strategies, and Models in Architecture and Nature*, pages 137–142, Stuttgart, 1994.
- [59] Ture Wester. Nature teaching structures. *International Journal of Space Structures*, 17(2), 2002.
- [60] Jan Wurm. *Glass structures – design and construction of self-supporting skins*. Birkhäuser, 2007.
- [61] Warren C. Young and Richard G. Budynas. *Roark’s formulas for stress and strain*. McGraw-Hill, 7 edition, 2002.

List of Symbols

| | |
|---------------|--------------------------------------------------------|
| E | Modulus of elasticity |
| G | Shear modulus |
| D | Flexural rigidity of plate |
| ν | Poisson's ratio |
| q | Distributed load |
| u | Displacement |
| κ_{ij} | Plate curvature |
| φ | Rotation of plate edge |
| σ | Stress |
| m_{ij} | Bending moment |
| n_{ij} | Sectional in-plane force |
| N_{ij} | Sectional in-plane force, integrated over a facet edge |
| h | Height of structure |
| l | Span of structure |
| t | Thickness |
| d | Diameter |
| R | Curvature radius |
| γ | Angle between neighbouring facets |
| w | Width of joint strip |
| r, θ | Polar coordinates |
| x, y, z | Cartesian coordinates |

List of Symbols

| | |
|-------------|---------------------------------------------------------------------|
| k_m | Rotational stiffness of connection detail |
| k_n | In-plane axial stiffness of connection detail |
| $k_{v,i}$ | In-plane shear stiffness of connection detail |
| $k_{v,o}$ | Out-of-plane shear stiffness of connection detail |
| $k_1 - k_4$ | Dimensionless factor in approximate expressions for in-plane forces |
| α | Rotational restraint factor |
| β | Difference in scale between surfaces for multi-layer pattern |
| r | Radius of imperfection |
| r | Amplitude of imperfection |

List of Figures

| | | |
|-----|-----------------------------------------------------------------------------------------------------------------------------------------------------------------------------------------------------------------------------------------------|----|
| 1.1 | Examples of shell structures. | 2 |
| 1.2 | Examples of facettted shell structures with triangulated geometry. | 2 |
| 1.3 | Load bearing glass columns at the headquarters of Danfoss, Denmark, by Schmidt, Hammer & Lassen. Each column carries a vertical load of $250kN$. Photo: Rambøll. | 3 |
| 1.4 | Glass dome at ILEK [16]. The glass segments are doubly curved laminated glass with a total thickness of $10mm$, connected by glued butt joints with a width of $10mm$. The diameter of the shell structure is $8.5m$. Photo: ILEK. | 3 |
| 1.5 | Dual facettted systems. Left: triangulated system. Right: plate shell system. Illustration from [56]. | 4 |
| 1.6 | Plate shell structures in nature. | 5 |
| 1.7 | Full scale model of plate shell structure in $19mm$ plywood, located at the Danish Building Research Institute, Denmark. Designed by Henrik Almgaard. Illustration from [9]. | 5 |
| 1.8 | Visualization of a plate shell structure with glass facets. Prepared by M. Rippman, ILEK. | 6 |
| 2.1 | The two basic types of facettted convex geometry. (Illustration: Ture Wester.) | 9 |
| 2.2 | Three examples of a plane-based facettted geometry, generated by mapping a plane pattern onto a section of a sphere, and determining the tangent planes to the sphere in these points. | 13 |
| 2.3 | A plane regular pattern is adjusted to outline a butterfly, and used to produce a plane-based facettted geometry. | 14 |
| 2.4 | Construction of the Zeiss Planetarium in Jena, Germany, designed by Walther Bauersfeld in 1923 [29]. | 15 |
| 2.5 | Geodesic triangulation of sphere (left), and the dual plane-based geometry (right). Illustration from [55]. | 15 |
| 2.6 | Three examples of plane-based geodesic domes, based on a tetrahedron, an octahedron and an icosahedron respectively. Illustrations from [55]. | 16 |
| 2.7 | Generation of a plane-based facettted geometry from a pattern on a cone. | 16 |

| | | |
|------|------------------------------------------------------------------------------------------------------------------------------------------------------------------------------------------------------------------------------------------------------------------------------------------|----|
| 2.8 | Mapping of two different patterns defined in a cone. To the left a regular pattern with 3 principal directions. To the right a Penrose pattern. | 17 |
| 2.9 | Principle sketch of the multiple layer patterns. | 18 |
| 2.10 | Four examples of the use of two layers of points. β refers to the applied difference in scale between the two surfaces. | 18 |
| 2.11 | Illustration of the stepwise plate shell geometry generation in the <i>pyFormex</i> script. | 22 |
| 3.1 | Definition of the two most significant stiffness components in the connection; rotational stiffness k_m and axial stiffness k_n . The red block represents the physical connection detail. The terms refer to <i>local directions</i> , relative to the regarded facet edge. | 24 |
| 3.2 | The distance between the facet edges change when the edge deforms out of the facet's plane. | 26 |
| 3.3 | Three connection details suggested in Chapter 7. | 27 |
| 3.4 | Section perpendicular to a joint line. | 28 |
| 3.5 | Plate shell model FacC , modelled in ABAQUS. | 31 |
| 3.6 | Stress distribution in a detail of a model, for varying element sizes. Stress component: Largest principal stress $S1$ in the upper surface. The stress contour scale is identical in the three plots. | 33 |
| 4.1 | Deformed plot of a vertex in a plate shell. In-plane stress concentrations will develop at the ends of the connections. | 38 |
| 4.2 | In-plane forces are examined along the marked (red) glass edge. Model: FacC | 39 |
| 4.3 | Comparison of axial and shear in-plane forces along the glass edge marked in Figure 4.2, for six different connection details. | 40 |
| 4.4 | Vector plots of in-plane forces near a corner of the studied facet. | 43 |
| 4.5 | Left: Model FacC_plate . Right: the equivalent smooth shell, model Smooth . Minimum principal stress (i.e. largest compression) in the surface mid-plane (units: $N/m^2 = 10^{-6}N/mm^2$). The contour scale is identical in the two plots. | 46 |
| 4.6 | Model FacF_plate . Minimum (left) and maximum (right) principal stress in the surface mid-plane (units: $N/m^2 = 10^{-6}N/mm^2$). | 46 |
| 4.7 | Model FacF_plate . Minimum (left) and maximum (right) principal stress in the surface mid-plane (units: $N/m^2 = 10^{-6}N/mm^2$). The load is rotated 18 degrees relative to the load case in Figure 4.6. | 46 |
| 4.8 | Plate shell model FacStar and its equivalent smooth shell, model FacStar_Smooth . The contour scale is the same in (c) and (d) (units: $N/m^2 = 10^{-6}N/mm^2$). | 48 |

| | | |
|-----|------------------------------------------------------------------------------------------------------------------------------------------------------------------------------------------------------------------------------------------------|----|
| 4.9 | Illustration of the terms in (4.1). | 50 |
| 5.1 | Deformed plot of plate shell, showing three types of areas on a facet where bending moments are in focus. | 52 |
| 5.2 | Local orientation of bending moment terms at a facet edge. | 52 |
| 5.3 | Deformed facet from the plate shell models FacC_EPDM , FacC_hinge , FacC_adh1 and FacC_plate respectively. | 54 |
| 5.4 | Bending response in the plate shell FE model described in Section 4.2.1, for the uniform load case. | 55 |
| 5.5 | Section through centre of a circular plate, for three different support conditions. Top sketches: displacements. Bottom sketches: bending moment m_r . Illustration from [39]. | 58 |
| 5.6 | Two plate shells models: FacF_plate and FacF_3points . The models are identical except for their support conditions, see Appendix A. Scaled deformed plots, and details showing principle stresses in the upper surface. | 63 |
| 6.1 | The three analyzed structures. The span of all three structures is 11.5m. | 67 |
| 6.2 | Principle sketches of non-linear out-of-plane deflection of plate. | 70 |
| 6.3 | Normalized displacements of a hexagonal facet in a plate shell structure. | 71 |
| 6.4 | Two types of bumps are added to the perfect geometry. | 73 |
| 6.5 | Center of the imperfection bumps. | 74 |
| 6.6 | Contour deformation plots (detail) of FacC_Perf_Uni at the critical load level (before and after failure). The contour scale is consistent in the two images. The difference in load level in the two images is 6%. | 76 |
| 6.7 | Contour deformation plots (detail) of FacF_Perf_Uni at the critical load level (before and after failure). The contour scale is consistent in the two images. The difference in load level in the two images is 10%. | 76 |
| 7.1 | IGU in plate shell connection. | 83 |
| 7.2 | Glued-in plate connection. | 84 |
| 7.3 | Glued-in hinge connection. | 86 |
| 7.4 | Friction connection. | 87 |
| 7.5 | Glued butt joint. | 88 |
| 7.6 | Bending stresses in the glued butt joint for varying parameters. “Thickness” denotes the thickness of the joint and the facet. | 89 |

List of Tables

| | | |
|-----|-------------------------------------------------------------------------------------------------------------------------------------------------------------------------------------------------------------------------------------|----|
| 2.1 | Three methods used to map a regular pattern onto a section of a sphere. . . | 12 |
| 2.2 | User defined input to the <i>pyFormex</i> script. | 20 |
| 2.3 | Output of the <i>pyFormex</i> script. | 21 |
| 3.1 | Estimated stiffness parameters for six variants of connection details, plus a pure glass joint. The values are summarized from Chapter 7. | 26 |
| 3.2 | Values to be used in a FE model of a plate shell, to model the connection stiffness parameters summarized in Table 3.1 (page 26). w and t_j are defined in Figure 3.4. | 30 |
| 4.1 | Transformation of external load into shell action in a plate shell. | 37 |
| 4.2 | In-plane force resultants N_{22} and N_{12} , found by integration of the in-plane forces n_{22} and n_{12} plotted in Figure 4.3. | 41 |
| 4.3 | In-plane forces at a glass edge in model FacC . The glass edge is marked in Figure 4.2. The used terms are defined in the text above. * This peak value has not converged in the FE model (see page 41). ** No peak value. . | 44 |
| 4.4 | In-plane principal forces in model Smooth (equivalent smooth shell to model FacC). | 45 |
| 5.1 | Comparison of maximum bending moments at the studied edge in model FacC | 57 |
| 5.2 | Analytical expressions for u , m_{edge} , m_{mid} and φ for a circular plate. | 58 |
| 5.3 | Approximate expressions for u , m_{edge} , m_{mid} and φ for a plate shell facet, for $k_m = 0$ and $k_m \rightarrow \infty$ respectively. | 60 |
| 6.1 | Overview of geometrically non-linear FE models. | 68 |
| 6.2 | Imperfections added to the perfect shell geometries in Figure 6.1. | 74 |
| 6.3 | Critical loads, comparing imperfection sensitivity. For an overview of non-linear models, see Table 6.1. The imperfections (type A, B and C) are given in Figure 6.4, 6.5 and Table 6.2. | 75 |

| | | |
|-----|---------------------------------------------------------------------------------------------------------------------------------------------------------------------------------------------------------------------------------|----|
| 6.4 | Connection stiffness parameters and joint parameters used for modelling, for the models listed in Table 6.1 under “Connection stiffness”. t_j and E_j have been determined as described in Section 3.2.1 (page 27). | 77 |
| 6.5 | Critical loads, comparing varying connection stiffness parameters. For an overview of non-linear models, see Table 6.1. | 77 |
| 6.6 | Critical loads, comparing two element types (S4 and S4R). | 78 |
| 6.7 | Critical loads, comparing varying element sizes. | 79 |
| 6.8 | Critical loads, comparing how accurately the shear stiffness in the connections are modelled. | 79 |

A shell structure of glass combines a highly effective structural principle - the shell - with a material of unique aesthetic qualities - glass. Glass is often used as cladding material in lattice shell structures, where a spatial grid of bars and nodes constitutes the primary load bearing structure. Research at the Royal Danish Academy of Fine Arts, School of Architecture, has shown the existence of a type of faceted shell structure, where the facets themselves constitute the load bearing system - the plate shell structure.

The present study, done at the Technical University of Denmark, looks at the structural behaviour of plate shell structures, particularly with facets of glass. The aim is to draw up guidelines for the structural design of plate shells.

DTU Civil Engineering
Department of Civil Engineering
Technical University of Denmark

Brovej, Building 118
2800 Kgs. Lyngby
Telephone 45 25 17 00

www.byg.dtu.dk

ISBN: 9788778773005
ISSN: 1601-2917